Source separation analysis of visual cortical dynamics revealed by voltage sensitive dye imaging

Esin Yavuz

UNIVERSITE PIERRE & MARIE CURIE
LA SCIENCE A PARIS

THÈSE DE DOCTORAT DE l'UNIVERSITÉ PIERRE ET MARIE CURIE

Spécialité :Neurosciences
École doctorale Cerveau, Cognition et Comportement (Paris)

Présentée par

Esin YAVUZ

Pour obtenir le grade de

DOCTEUR de l'UNIVERSITÉ PIERRE ET MARIE CURIE

Source separation analysis of visual cortical dynamics revealed by voltage sensitive dye imaging

Date de soutenance : 19 Octobre 2012

devant le jury composé de :

Dr. Frédéric CHAVANE	Rapporteur
Dr. Dirk JANCKE	Rapporteur
Pr. Gilles LAURENT	Examinateur
Pr. Régis LAMBERT	Président du jury
Dr. Yves FRÉGNAC	Directeur de thèse
Dr. Cyril MONIER	Co-directeur de thèse

Laboratoire UNIC, CNRS - 1 Avenue de la Terrasse, 91198 Gif-sur-Yvette, France

Summary

Voltage Sensitive Dye (VSD) imaging is a new and powerful multi-channel recording tool that provides the optimal spatial and temporal resolution range to date for investigating mesoscopic dynamics of neural population activity. However, extracting the neural-related response despite the weak signal-to-noise ratio of the fluorescence measurements remains a major issue. Conventional denoising strategies such as blank subtraction entail averaging of multiple trials and neglect the importance of the non-repetitive response components present in each trial of the evoked and spontaneous activity. Moreover, this method relies heavily on the hypothesis that the artefact-related components are always synchronized, which may not always be the case.

Another complexity for interpretation of the signal recorded by VSD imaging is the multi-channel nature of the data. VSD imaging provides simultaneous recording of thousands of different channels, each of them recording from several hundred micrometer squares of cortical sheet. Understanding how different modules of cortex interact requires development of adequate methods that provide analysis of complex spatio-temporal patterns of activity rather than individual pixels.

The work presented in this thesis consists of a statistical source separation analysis of VSD imaging recordings in order to 1) separate the neural-related signal from the artefacts, and 2) investigate the dynamics of the spatio-temporal patterns of activity created by populations of cells that share common statistics. For this purpose, we performed VSD imaging of areas 17 and 18 in the anaesthetized and paralyzed cat. Full field sinusoidal luminance grating stimulations whose orientation was chosen among 4 or 6 cardinal values were presented moving each at two opposite directions. The choice of these stimuli is justified by the fact that the functional architecture of the visual cortex is well established on the basis of independent measures, such as electrophysiological recordings.

For the denoising aspect, we developed a hybrid approach that benefits from the advantages of both model-based and data-driven strategies for source separation. As a first step, we adapted to our data the general linear model (GLM) regressor

basis which was developed by Reynaud et al. (2010) in order to denoise awake monkey recordings. As a second step, model-based GLM denoising was followed by data-driven temporal principal components analysis (PCA). This two-step approach was more efficient than blank subtraction (BS) to remove artefacts on single trials.

Once the recordings were denoised, we analyzed the artefact-free signal by using PCA which could successfully decompose the neural-related signal into functional groups of populations, revealing the single-trial feature-selective assembly dynamics corresponding to each grating orientation. The principal component with highest energy corresponded to the global activation process of the cortical network independently of the orientation content of the stimulus. Orientation selectivity was revealed in the latter two components: all the possible orientations were represented respectively on a ring on the two orientation-selective principal components.

This representation led us to investigate dynamics of orientation selectivity in a state space of reduced dimensionality (3D). The main results show that:

1. Trajectories in the principal component space converged rapidly to the attractor state defined by the orientation and stayed around the attractor until the offset of the stimulation;
2. Single trials of evoked responses to drifting gratings stayed in the vicinity of the mean trajectory corresponding to the stimulus orientation during visual response plateau, and the clusters of time points grouped by orientation remained separable;
3. The orientation selectivity was detectable right at the onset of the transient visual response;
4. Trajectories triggered by the onset of the visual response exhibited a higher selectivity to orientation than triggered from the offset;
5. Horizontal orientation was more separable than the other orientations, supporting the existence of an “oblique or anisotropy effect” previously observed in behavioral and electrophysiological studies;
6. Two opposite directions corresponding to the same orientation projected to nearby but still differentiable points on the orientation-selective ring. Independent component analysis (ICA) could distinguish different directions, showing that higher order statistics are needed in order to discriminate populations responding to different directions.

We also adapted our source separation method to analyze VSD imaging data for a larger spectrum of stimuli used to investigate input statistics dependence of trial-to-trial variability of visually evoked responses. These stimuli were previously used

in the lab combined with intracellular recordings. For each cell recorded intracellularly, a prototypical set of four types of stimuli of increasing complexity was used: drifting grating, grating and natural image animated by a modeled eye-movement sequence and dense binary white noise. A stimulus-locked frequency-time wavelet analysis showed that noise and temporal reliability of neural activity depend on visual input statistics (Baudot et al., submitted; Frégnac et al., 2005; Marre et al., 2009; El Boustani et al., 2009). Natural scene animation evoked temporally precise sparse spike response and large and highly reproducible irregular fluctuations in the sub-threshold membrane potential, while classical simple stimuli such as drifting gratings evoke highly variable responses. In order to adapt this protocol to VSD imaging, longer recording times are required to obtain an adequate temporal frequency resolution. During longer recording epochs (>1 sec), however, the intrinsic signal contaminates the fluorescence signal. We modified our GLM regression basis in order to include signals that are involved in longer response time scales. We could obtain a clear denoising that should permit more sophisticated analysis of single-trial responses to non-classical stimulation with longer recording times.

In summary, we developed an analysis method for VSD imaging that separates the neural response from the artefacts on single trials, and extracts the spatio-temporal patterns of activity that are related to functionally differentiable populations. Our method relies on the hypothesis that the artefactual and neuronal sources that contribute to VSD imaging recordings are linearly separable by their common statistics. Our denoising method permits to perform single trial analysis, for instance to study trial-to-trial variability of signal-to-noise ratio in neuronal population activity. Furthermore, neuronal populations themselves are also separable by their stimulus preference and response dynamics. We could separate neural populations that show different response profiles to orientation and/or to direction of the drifting grating stimuli by using PCA and ICA. The compression and projection of V1 maps in response to drifting gratings on three spatiotemporally structured components allowed us to investigate cortical state dynamics and demonstrate the separation of state trajectories as a function of orientation. The sensitivity of our method appears much higher than that gained with conventional analysis of time courses of individual pixels. Our results indicate that neuronal coding of orientation preference at the population level rather than individual channels is more efficient. We hope in the future to provide a measurement framework to quantify and interpret the responses to more naturalistic stimuli.

Résumé

L'imagerie par colorants sensibles au potentiel (VSD) est une technique d'enregistrement multi-canal récente. Son principal avantage est de combiner une forte résolution spatiale à une forte résolution temporelle ce qui en fait un outil optimal pour l'étude de la dynamique de l'activité de populations neuronales à l'échelle mésoscopique. Toutefois, l'extraction de la réponse neuronale reste un problème majeur dû au faible rapport signal sur bruit des mesures de fluorescence. Les stratégies traditionnelles de débruitage telle que la soustraction du blanc repose sur le moyennage de plusieurs enregistrements VSD en réponse aux mêmes conditions de stimulation visuelle et négligent l'importance des composantes de réponse non répétées présentes dans chaque essai de l'activité évoquée et spontanée. En outre, cette méthode repose en grande partie sur l'hypothèse que les composantes artefactuelles sont toujours synchronisées, ce qui n'est pas toujours le cas.

Une autre difficulté pour interpréter le signal enregistré par l'imagerie VSD provient de la nature multi-canale des données. L'imagerie VSD permet d'enregistrer simultanément de plusieurs milliers de canaux différents, chacun d'entre eux reflétant l'activité neuronale de plusieurs centaines de micromètres carrés de surface corticale. Afin de comprendre comment les différents modules du cortex interagissent, il est nécessaire de développer des méthodes adéquates permettant l'analyse des motifs spatio-temporels complexes plutôt que des pixels individuels.

Le travail présenté dans cette thèse consiste en une analyse statistique de séparation des sources des enregistrements d'imagerie VSD afin de 1) séparer le signal neuronal des artefacts, et 2) d'étudier la dynamique des motifs spatio-temporels de l'activité créés par les populations de cellules qui partagent des statistiques communes. À cette fin, nous avons effectué des enregistrements en imagerie VSD des zones 17 et 18 du cortex du chat anesthésié et paralysé. Des réseaux sinusoïdaux de luminance en mouvement et en plein champ dont l'orientation a été choisie parmi les 4 ou 6 valeurs cardinales ont été présentés dans les deux directions. Le choix de ces stimuli est justifié par le fait que l'architecture fonctionnelle du cortex visuel est bien établie sur la base de mesures indépendantes, telles que des enregistrements électrophysiologiques.

Pour le débruitage, nous avons développé une approche hybride exploitant à la fois la nature des données et un modèle numérique des sources des enregistrements. Dans un premier temps, nous avons adapté un modèle linéaire général (GLM) à nos données qui a été initialement développé par Reynaud et al. (2010) pour débruiter des enregistrements chez le singe éveillé. Le débruitage GLM a par la suite été complété par une analyse en composantes principales (PCA) dans le domaine temporel. Cette approche en deux étapes est plus efficace que la soustraction du blanc (BS) pour enlever des artefacts sur les essais unitaires.

Une fois les enregistrements débruités, nous avons analysé le signal sans artefact à l'aide de la PCA afin de décomposer le signal neuronal provenant de différents groupes de neurones fonctionnels, révélant ainsi la dynamique spécifique à chaque essai pour chaque orientation des réseaux sinusoïdaux de luminance en mouvement. La composante principale avec l'énergie la plus élevée correspondait à l'activation globale du réseau cortical indépendamment de l'orientation des stimuli. La sélectivité à l'orientation a été révélée dans les deux composantes suivantes : les attracteurs correspondants à toutes les orientations possibles ont été représentés respectivement sur un anneau défini par les deux axes respectifs de ces deux composantes.

Cette représentation nous a permis d'étudier la dynamique de la sélectivité à l'orientation dans un espace d'état réduit en trois dimensions. Les principaux résultats montrent que:

1. Les trajectoires dans l'espace des composantes principales convergent rapidement vers un état attracteur défini par l'orientation de la stimulation et restent autour de cet attracteur jusqu'à la fin de la stimulation;

2. Les réponses évoquées par chacun des essais unitaires résident au voisinage de la trajectoire moyenne correspondant à l'orientation de la stimulation pendant le plateau de la réponse visuelle, et les points temporels sont groupés par orientation restent séparables;

3. La sélectivité à l'orientation est détectable dès le début de la réponse visuelle transitoire;

4. Les trajectoires déclenchées par l'apparition de la réponse visuelle montrent une plus forte sélectivité à l'orientation par rapport aux trajectoires de retour;

5. L'orientation horizontale est davantage séparable que les autres orientations, ce qui soutient l'existence d'un ńăeffet de l'oblique ou d'anisotropieăż déjà observé dans des études comportementales et électrophysiologiques;

6. Deux directions opposées correspondant à la même orientation projettent à proximité mais restent toujours distinguables sur l'anneau de sélectivité à l'orientation. L'analyse en composantes indépendantes (ICA) a permis de distinguer les deux directions différentes, montrant que des statistiques d'ordre supérieur sont nécessaires afin de discriminer les populations qui préfèrent des directions différentes.

Nous avons également adapté notre méthode de séparation des sources pour l'analyse de données d'imagerie VSD sur un plus large spectre de stimuli afin d'étudier la dépendance des statistiques d'entrée sur la variabilité des réponses évoquées pour chaque essai unitaire. Ces stimuli ont été utilisés précédemment dans le cadre d'enregistrements intracellulaires dans le laboratoire. Pour chaque cellule enregistrée au niveau intracellulaire, un ensemble de quatre types de stimuli de complexité croissante a été utilisé : un stimulus contrôle dont la luminance est uniforme ('blank'), des réseaux de luminance sinusoïdaux en mouvement, une image naturelle dont l'animation reflète les mouvements oculaires naturels du chat pendant l'exploration et un bruit blanc dense binaire. Une analyse fréquence-temps en ondelettes clampées aux stimulations visuelles a montré que le bruit et la fiabilité temporelle de l'activité neuronale dépend des statistiques de l'entrée visuelle (Baudot et al, soumis;. Frégnac et al, 2005;. Marre et al, 2009;. El Boustani et al. , 2009). L'image naturelle animée par des mouvements oculaires modélisés a quant à elle évoqué des réponses précises avec peu de potentiels d'action associé à de larges fluctuations irrégulières du potentiel membranaire sous-liminaire hautement reproductibles. Au contraire, les stimuli classiques plus simples tels que les réseaux de luminance sinusoïdaux en mouvement ont provoqué des réponses très variables. Afin d'adapter ce protocole d'imagerie VSD, des durées d'enregistrement plus longues ont été nécessaires pour obtenir une résolution de fréquence temporelle adéquate. Pour ces enregistrements plus longs (> 1 s), le signal intrinsèque à la réponse contamine le signal de fluorescence. Nous avons modifié notre base de régression GLM afin d'inclure des signaux qui sont impliqués dans des échelles de temps plus longues qui sont adaptées à ces réponses. Nous avons obtenu un débruitage clair qui devrait permettre une analyse plus sophistiquée des réponses aux stimulations unitaires non-classiques avec des durées d'enregistrement plus longues.

En résumé, nous avons développé une méthode d'analyse pour l'imagerie VSD qui sépare la réponse neuronale à partir des artefacts sur les essais simples, et extrait les motifs spatio-temporels de l'activité qui sont fonctionnellement liés à des populations différentiables. Notre méthode repose sur l'hypothèse que les sources artefactuelles et neuronales qui contribuent aux enregistrements d'imagerie VSD sont linéairement séparables par leurs statistiques communes. Notre méthode de

débruitage permet d'effectuer des analyses sur des essais unitaires, par exemple pour étudier la variabilité intrinsèque de chaque réponse de la population neuronale enregistrée pour une même stimulation. En outre, les populations neuronales sont aussi séparées selon leur préférence aux stimuli et la dynamique de leur réponse. Nous avons pu séparer des populations de neurones qui montrent différents profils de réponse à l'orientation et / ou à la direction des réseaux de luminance sinusoïdaux en mouvement à l'aide de la PCA et de l'ICA. La compression et la projection des cartes V1 en réponse aux réseaux de luminance sinusoïdaux en mouvement sur trois axes de composantes principales nous a permis d'étudier la dynamique des états corticaux et démontrer la séparabilité des trajectoires d'état en fonction de l'orientation. La sensibilité de notre méthode semble beaucoup plus élevée que celle obtenue avec l'analyse classique des réponses temporelles des pixels individuels. Nos résultats indiquent que le codage neuronal de préférence à l'orientation au niveau de la population plutôt que des canaux individuels est plus efficace. Nous espérons à l'avenir fournir un cadre de mesure pour la quantification et l'interprétation des réponses aux stimuli plus naturels.

Contents

List of Abbreviations

2-DG 2-deoxy-D-glucose

BOLD Blood oxygen level dependent

ECG electrocardiogram

EEG Electroencephalography

fMRI Functional magnetic resonance imaging

GLM General linear model

ICA Independent components analysis

LFP Local field potential

LGN Lateral geniculate nucleus

MEG Magnetoencephalography

PCA Principal components analysis

PET Positron emission tomography

PTV postero-temporal visual cortex

RF Receptive field

SC superior colliculus

SNR signal-to-noise ratio

V1 Primary visual cortex

VSD Voltage sensitive dye

Part I

Introduction

Brain is the most complex structure known to us, consisting of up to 100 billion of neurons, each neuron making up to 10^4 connections, and each of them firing one to several hundred times per second. In the need of extracting useful information from the unpredictable and unstable environment, nervous systems have evolved to feature both hierarchical and parallel structures and developed efficient coding strategies. Information is processed in parallel structures each responsible of a particular task. Meanwhile, each structure is organized in several levels of organization, each modulated both by the feed-forward emergent properties of the inferior level, and the top down immergent influence of the higher level.

The visual system is intensively studied in both experimental and modeling aspects, as a result of its importance for human perception. Importance of vision in perception hints that the most complex circuitry in the brain is the visual system. Even though our knowledge about its functioning is considerably widened, the most important and basic questions are not clearly answered yet: How do the neurons and hence different structures in the brain coordinate in response to the visual input? How does the brain encode the information coming from the dynamic environment?

Efficient interpretation of the dynamic sensory input is crucial for survival of the animal in its natural environment. Anatomical organization of the cortex has evolved in order to successfully process signals coming from external world, and to interpret the incoming signal in an appropriate context. The perceptive task is shared among different structures in different levels of organization, which are combined at the end to obtain an adequate interpretation of the whole.

Mammalian Brain as a Complex Adaptive System

A complex system is a collection of a number of building blocks interacting nonlinearly and giving rise to properties as a whole that are not evident from the properties of the individual parts. Some basic characteristics of complex systems are summarized in Figure 1. Complex systems emerge from self-organization of the coordinative behavior of simple units in order to maintain energy optimization. Even though the building blocks seem to be fairly simple, nonlinear interactions between them may change the state of the whole. Smooth changes of the parameters that define the interaction between single units may change the behavior of the whole in a drastic way.

The brain is a “complex temporally and spatially multiscale structure that gives rise to elaborate molecular, cellular, and neuronal phenomena that together form the physical and biological basis of cognition” (Bassett and Gazzaniga, 2011). As any complex system, the nervous system is organized at several levels of organization,

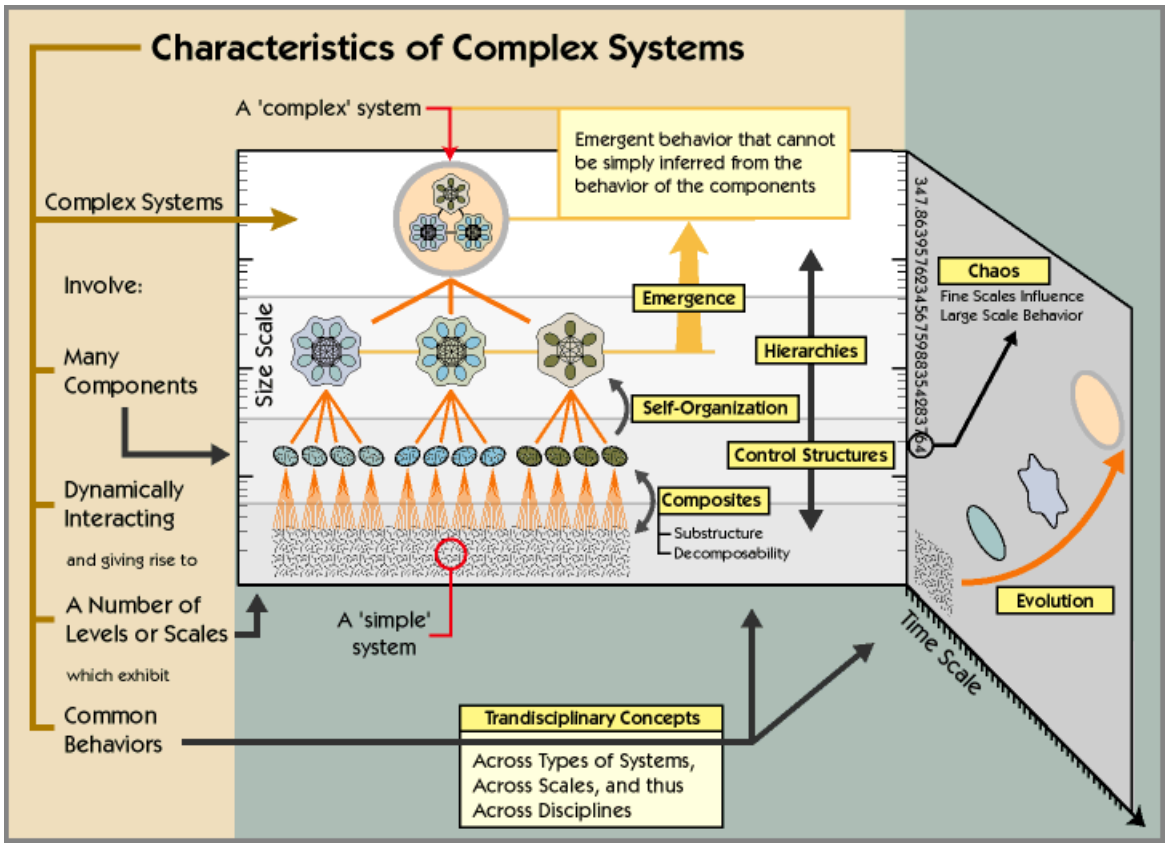

Figure 1 – Characteristics of adaptive complex systems. Dynamically interacting "simple" systems self-organize and give rise to a number of scales which then form the complex system. This organization evolves in time, resulting in different behaviors as a whole. Image created by Marshall Clemens.

which are "separable conceptually but not detachable physically" (Churchland and Sejnowski, 1988). Still, the brain is much more "complex" than any other classically studied "complex system". This complexity is a result of the vast number of different levels of organization, and the very rich nature of the emergent and immergent properties. Our limited knowledge about each level obstructs the "simplification" of building blocks, which is necessary in order to study the brain with the tools provided by the complex systems literature.

Brain is also an adaptive system. One of the biggest difficulties for brain functioning arises from the unpredictability of the nature. Brains have to retrieve the information collected from the dynamic and often "noisy" environment, in the sense that the information is not always present the same way in the same context. This requires the brain to act by adapting the organism to the new state of the environment. Structure of the brain is plastic, hence not only the behavior, but also the material adapts to the environment in order to increase efficiency. Therefore, every brain has its own structure, as a function of both its own properties and the natural

environment in which the structure is shaped (Koch and Laurent, 1999).

The levels of organization in the brain include molecules, synapses, single neurons, columns, hypercolumns, maps, cortical areas, sensory systems, and finally, the whole central nervous system (see Figure 1.1, which will be explained more in details in Section 1). Organization at each level emerges from the interactions between the micro-level "agents" of the inferior level. Once the structure is stable, the whole is insensitive to the individual activities of the members of the inferior level (Wolf and Geisel, 2003).

Figure 2 – Archimboldo's painting of Rudolf II represented as *Vertumnus*, the Roman god of the seasons. When the painting is seen from a short distance, the image is a collection of fruits, vegetables and flowers. If the painting is seen from a longer distance, the image of a person appears as a result of the good continuation of the forms of the individual parts.

The concept of "Perception" can be thought as an emergent property arising from the central nervous system, even though there is no physical layer corresponding to this level of organization. Self-organization at the perceptual level is revealed by the *Gestalt* psychology. Gestalt principles indicate that the sole interpretation of individual parts is not enough to explain the whole. In this sense, if the individual parts are not linked by the Gestalt laws, there is no information provided by a single part that would change the interpretation of the whole. The works of the medieval artist Archimboldo are good examples. For instance in the painting presented in Figure 2, Emperor Rudolf II is presented as the Roman god of seasons. The image is

a collection of fruits, vegetables and flowers; which form the portrait of the emperor as a result of the Gestalt law of good continuation of the forms. In mental disorders such as schizophrenia or visual agnosia, this nice organization may be deteriorated, resulting in the loss of the concept of the whole, and a perception that is affected by the inner abnormal activity of the brain (hallucinations).

Perception emerges as the neuronal circuits are shaped by the information received from the natural environment. The organization schemes that will be explained in the following chapters are dependent on the initial training of the genetically-predefined neuronal networks. For example, development of the cortical maps can be explained by a self-organizing neural network trained by retinal waves and the natural environment (Mikkulainen, 2005), and animals that grow up in a different natural environment show biases in cortical map development (Tanaka et al., 2006).

As functionality of each brain is shaped by its own experience in the natural environment, individual experiences can be subjective. Different emergent properties of each individual brain may hence lead to the philosophical notion of *qualia*, i.e. how a certain mental state is felt or perceived by an individual. Mainzer (2007) argued that the qualia emerge by the interaction of the individual with the environment, and that this interaction can be explained by the nonlinear dynamics of complex systems. Understanding the limits of variability in how the brain respond to a particular stimulation may help us to understand the objective limits of qualia, and study of the dynamics of the brain activity involving a single experience may give a quantitative measure of a certain quale.

In summary, a complex systems approach to study the brain would be useful to understand how individual units at a certain level (for example ion channels, single cells or columns) interact in order to give rise to the properties observed at the higher level. An illustration of levels of organization (or levels of abstraction) in the visual system is shown in Figure 3. Mesoscale level can be further divided into local and global population levels. Each level has a particular connectivity and coding strategy in order to solve a certain goal that would link the levels.

The work presented in this thesis is focused on population level processing in primary visual cortex: We investigate how small groups of neurons coordinate in order to perform a common task that would give rise to global activity patterns. Understanding of a particular level requires an intuition of what is done in inferior and superior levels. In our case, inferior level corresponds to the cellular level: each neuron has a way of handling the incoming information. Superior level can be considered as the system level: we are studying the primary visual cortex (V1) which has a particular task of local information extraction, but which acts also as a read-out buffer of the whole visual system (Lee and Mumford, 2003). We will

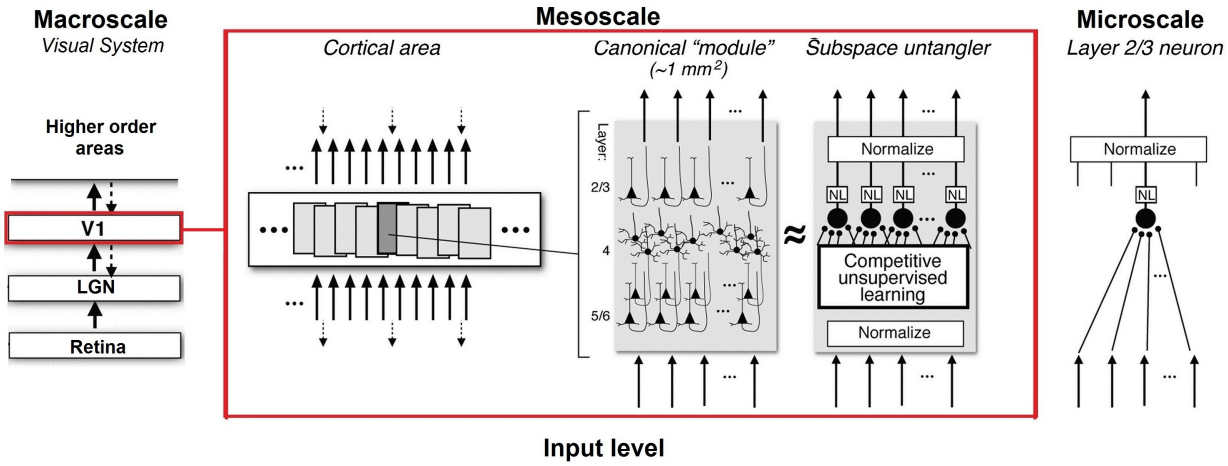

Figure 3 – Levels of organization in the visual system, and their potential links. The region indicated by the red frame is the scale of interest of this thesis. Modified from DiCarlo et al. (2012).

first explain the basic properties of neurons that involve *microscopic scale* activity in the brain. Then, we will introduce the *macroscopic scale* organization of the visual system, which corresponds to the regions and pathways. For each region, we will explain the region-specific characteristics of the microscopic organization which corresponds to the individual neurons. Finally, we will elaborate the *mesoscopic scale* organization which emerges from the interactions between individual neurons, corresponding to the population level. Before explaining the anatomy and physiology of the visual system, it is convenient to remind available tools which help us investigate the neuronal activity in different levels of organization.

Chapter 1

Measures of neuronal activity at different scales

Our knowledge of the function of the brain has evolved very fast since the first observations of Santiago Ramón y Cajal, Camillo Golgi and Heinrich Wilhelm Gottfried von Waldeyer-Hart at the end of the 19th century about the existence, structure and connectivity of neurons. Early studies were mostly based on anatomical investigations of the neuronal tissue. The beginning of recordings with electrodes made a revolutionary contribution to the field, permitting to study real-time electrical activities of the neurons. Since several decades, multichannel recordings and techniques that provide recording of the brain at various scales were developed. Combination of all these tools now will hopefully let us investigate the brain activity in all the aspects. In this chapter, we will briefly explain techniques used in neuroscience to study the function of the brain at different scales.

Neuronal tissues can be studied *in-vitro,* or *in-vivo*. *In-vitro* studies often involve working on slices of brain and are useful to determine the individual properties of isolated neurons independent of the interactions with other brain regions. However, in most cases, slicing procedures destroy most of the axons and dendritic trees, isolating the individual cell from the local network but it is still possible to study physical properties of the cellular membrane by injecting ionic solutions.

In order to understand the function of the living tissue in its context, network interactions need to be taken into account. If we want to study how the local and global activities interact together, *in-vivo* studies are more suitable. *In-vivo* studies involve working on intact animal, taken into account ethical considerations which may involve working with anesthetizers.

These two approaches combined may allow one to understand how brain tissue function at different scales and bridge together multiple levels of organization. The-

oretical, computational, or hardware models of the neuronal systems permit deeper but more speculative investigations of the neuronal theories without the complications of working with the living tissue. Modeling is especially useful for investigating parameter scales not reachable with *in-vitro* or *in-vivo* studies, or to bridge various studies performed at different scales. It is generally fruitful to combine analytical and computational tools with classical *in-vitro* and *in-vivo* studies in order to verify the consequences and limits of experimental findings.

Levels of organization in the nervous system and the spatio-temporal limits of the most well-known tools available in neuroscience are shown in Figure 1.1. The classification of levels is based on the spatial scale. However, it should be noted that in the lower levels dynamics are faster than in the higher levels. It is important to choose an appropriate method that provides information about the level of organization of interest.

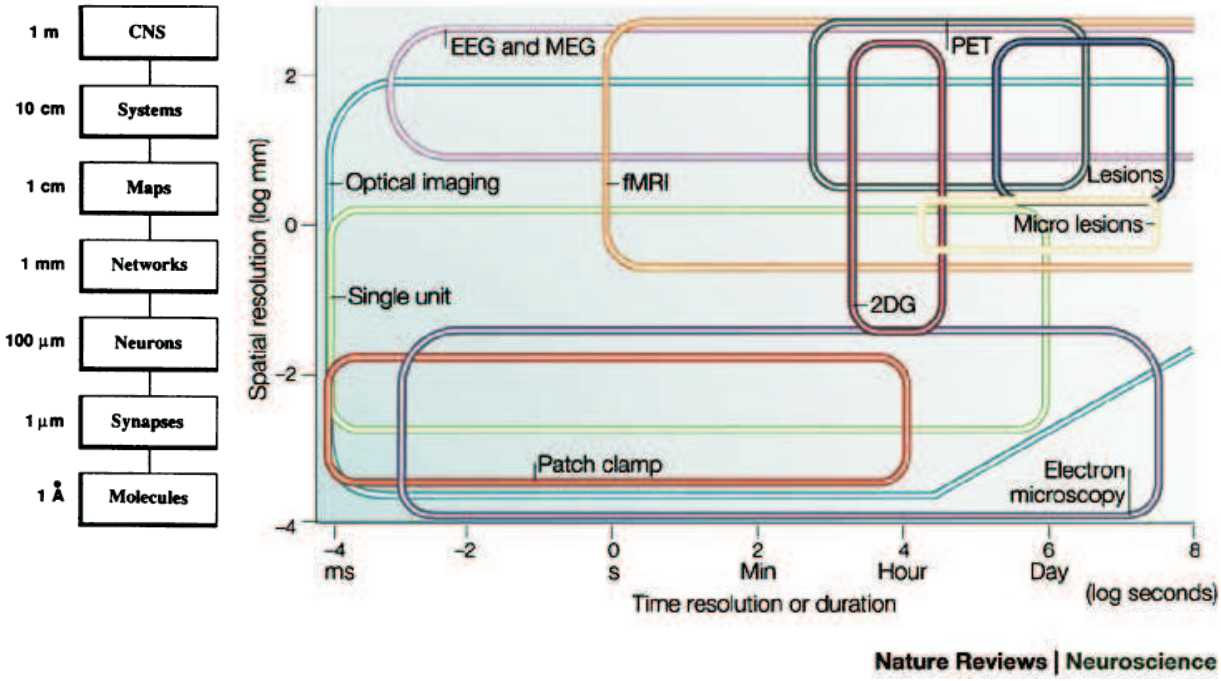

Figure 1.1 – Levels of organization in the brain, and available methods to investigate the dynamics at each level. Adapted from Churchland and Sejnowski (1988) and Grinvald and Hildesheim (2004).

1.1 Electrophysiology

Most of our knowledge today about the brain is based on electrophysiological studies. Depending on the type of recording, electrophysiological studies provide information about the electrical activity in a certain level using electrodes. More

conventional techniques involve single unit recordings. For intracellular studies, recordings are done with different types of electrodes. Micropipette electrodes in patch clamp provide recording of single or multiple channels, and sharp electrodes provide a measure of the voltage or current across the membrane. With these techniques, it is possible to record action potentials created by the neuron in a millisecond range. These recordings provide also the measures of the fluctuations of the sub-threshold membrane potential that reflects more mesoscopic interactions in the local network.

Transmembrane currents can also be observed on the extracellular medium. Single unit activities revealed as action potentials and local field potentials (LFP) created by multiple neurons in a small volume can be recorded with microelectrodes placed in the extracellular space. LFP is a measure of the potential between two nearby but sufficiently apart electrodes, which gives information about the local current flow in the extracellular medium. Any activity of any excitable tissue around the recording site contributes to the LFP signal. The raw signal obtained by the recording electrode is low-pass filtered around a cut-off about 200 Hz for analysis. This process eliminates any fast events such as action potentials, and consequently the resulting signal reflects a more mesoscopic activity rather than fast individual activation of nearby neurons.

Even though the extracellular field provides a pooling of the activation of multiple neurons in the area, biases in sampling may arise from a number of reasons such as the geometry of the neurons, distance of a neuron from the electrode, and packing density (Buzsáki et al., 2012). Moreover, the reference electrode should be placed nearby in the brain, and this area often has very similar properties as the recording region. It is very difficult to choose a reference region that does not have any dominant local activity. Therefore, placement of the reference electrode introduces a second bias in LFP measurements.

In the last decades, development of multielectrode arrays provided means to record activity from a grid of multiple channels simultaneously. These improvements opened the way to study spatial arrangement of the cortical tissue at a mesoscopic scale. Multichannel recordings provide means to record spatiotemporal patterns of activity in the brain by sampling from multiple sites. Advances in recording and computation devices opens the way to record the data simultaneously from a high number of channels, however analysis of the large datasets provided by multichannel recordings require development of appropriate algorithms that optimize computation. This is a common problem with neuroimaging techniques which may also be considered as multichannel recordings.

Strong extracellular potentials originate mostly from correlated activity of the neu-

rons, as any uncorrelated activity will result in a flat profile. Correlated activity on an even more global scale can be observed with electrocorticography, which corresponds to the recording of the electrical activity using subdural surface electrodes. On the most global end of electrophysiology, we find electroencephalography (EEG). This is the oldest and the only noninvasive electrophysiological technique, which involves recording the activity filtered by the skull using scalp electrodes. Modern EEG caps provide up to 256 channels of recording.

1.2 Neuroimaging

Alternative methods to electrophysiology involve indirect measures of the neuronal activity. In the last decades, development of various neuroimaging techniques provided noninvasive measures of the brain activity. Especially fMRI become very popular as a result of the high-resolution non-invasive dynamic measurements provided by the method. fMRI is a special case of magnetic resonance imaging. It benefits the different relaxation times of magnetization between oxygenated and non-oxygenated tissue. As the neural populations get activated, local blood volume, oxyhemoglobin and deoxyhemoglobin concentrations change, giving rise to the blood oxygen level dependent (BOLD) signal. Time scales of activation and dynamics of the BOLD signal is relatively very slow with respect to the electrical activity. The time constant of the hemodynamic transfer function is in the order of a few seconds while electrophysiological activity may occur at a range of milliseconds. BOLD signal reflects the metabolic changes that result from oxygenation and energy consumption of the tissue, therefore not only neurons but also glial cells and neurovascular coupling contribute to this signal (Logothetis and Wandell, 2004). fMRI method provides a three dimensional recording of the brain activity with high spatial resolution and sampling. High spatial resolution up to tens of micrometers may be obtained using stronger magnetic field (>7 Tesla) using external contrast agents and smaller scanners, while human recordings can be done up to a millimeter range using 3-4 Tesla magnetic field.

Other indirect measures of the macroscale brain activity are positron emission tomography (PET), Magnetoencephalography (MEG) and 2-deoxy-D-glucose (2-DG) method. PET was the most popular tool before the invention of the fMRI and is still used in neuroimaging. It involves usage of radioactive tracers which either stay in blood vessels or bind to receptors. These tracers emit gamma rays which are then detected by the PET scanner, reflecting the dynamics of the binding sites. MEG provides measure of the magnetic field created by the brain activity at high temporal but low spatial resolution. 2-DG method provides a metabolic measure of

active brain areas. Using 2DG marking, it is then possible to perform post-mortem visualization of active brain areas, networks or single cells. This method has been very useful in order to image the functional architecture of the cortex before optical imaging methods were developed. However, real-time observation of the dynamics is not possible with this technique. 2-DG can also be used as a tracer for in-vivo functional near infrared imaging, similar to the radioactive agents used in PET scan.

1.3 Optical Imaging

As we see in Figure 1.1, optical imaging covers the widest spatial and temporal bandwidth for recording the brain activity. In reality, spatio-temporal resolution that is available while doing optical imaging is not limited by the nature of the interactions that are reflected by optical imaging, but the recording devices often limit the resolution of the recordings to a certain degree.

Optical imaging is less invasive than the other electrophysiological tools available in the micro and mesoscales. Recordings can be repeated over years on the same animal. The method also provides the possibility to work on behaving animals.

Optical imaging can be divided into two subcategories: intrinsic and extrinsic imaging. Intrinsic imaging involves recording of the metabolic changes of the tissue only by optical techniques. In extrinsic imaging, contrast agents that are sensitive to a particular change in the neuronal activity are used. Voltage Sensitive Dye (VSD) imaging falls into the extrinsic imaging category. Optical imaging is also a neuroimaging tool, and VSD imaging can be considered as both neuroimaging and electrophysiological recording technique. Good reviews of the optical imaging technique are available (see Grinvald et al. (1999) for a general overview, Grinvald and Hildesheim (2004) and Chemla and Chavane (2010b) for VSD imaging). Here we will briefly introduce the basic principles of optical imaging, but the nature of the VSD signal and the important bibliography will be further detailed in the text.

Intrinsic imaging is a measure of metabolic changes due to neuronal activity. The underlying mechanism in intrinsic imaging is the BOLD signal, as it is for fMRI. When light is shed on the brain, these metabolic changes result in scattering and absorption of the light reflected by the tissue.

Optical signal observed by intrinsic imaging follows the BOLD signal activation range. Following the sensory stimulation, deoxyhemoglobin concentration increases in active regions as a result of initial oxygen consumption, resulting in darkening of the cortex. This signal is equivalent to the “initial dip” observed in the fMRI recordings. Following this signal, delayed blood supply arrives in the tissue, decreasing he

deoxyhemoglobin concentration and increasing oxyhemoglobin concentration. On a more precise time resolution, highly localized oxygen delivery to the active neuronal tissue occurs 200-400 ms after stimulus onset. This oxygen delivery is followed by the increase in blood volume 300-400 ms later, and finally oxyhemoglobin concentration starts to increase after 1000 ms (Frostig et al., 1990). The last contribution to the intrinsic signal is the light scattering that arises from the ion and water movement, volume changes of extracellular space, capillary expansion and neurotransmitter release (Grinvald et al., 1999).

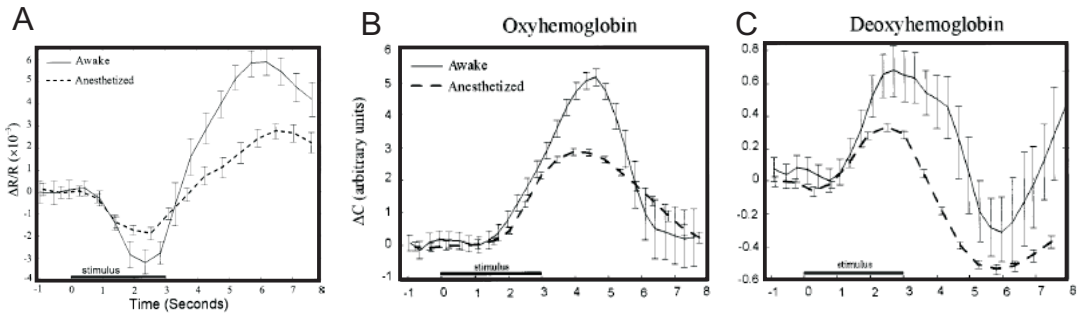

Figure 1.2 – Time courses of intrinsic signal compared to oxyhemoglobin and deoxyhemoglobin concentrations. A: Time course of the global intrinsic signal on awake (solid line) and anesthetized (dashed line) monkey B: Oxyhemoglobin concentration and C: Deoxyhemoglobin concentration on awake monkey (solid lines) and anesthetized cat (dashed lines). Modified from Shtoyerman et al. (2000).

The relationship between the intrinsic signal and hemodynamic changes can be measured by image spectroscopy (Malonek and Grinvald, 1996; Vanzetta and Grinvald, 1999; Shtoyerman et al., 2000). This method is based on the differences of reflection resulting from the amount of absorption by capillaries, small arterioles, and venules at different wavelengths. Time courses of the intrinsic signal and oxyhemoglobin and deoxyhemoglobin concentrations observed by Shtoyerman and colleagues are shown in Figure 1.2. Following these observations, Vanzetta and Grinvald (1999) measured the oxygenation level in the tissue directly by phosphorescence and showed that the global intrinsic signal can be predicted by a linear combination of the oxyhemoglobin and deoxyhemoglobin concentrations (Vanzetta and Grinvald, 1999).

VSD imaging provides a more direct and temporally precise measurement of the neuronal activity. Voltage sensitive dyes are molecules that bind to the external surface of membranes of neurons. The dye's sensitivity to voltage changes can be explained by a direct electro-chromic effect or the motion of the dye molecule in and out of the membrane. These effects reflect the changing electric field across the membrane and result in an increase of fluorescence. The blue dye (RH 1691, Optical Imaging, Rehovoth, Israel) filters out most of the hemodynamic artefacts

because of the wavelength of light that is recorded (Shoham et al., 1999). Fluorescence is captured by exciting the tissue on the peak of the optimum wavelength for the dye (~630nm), and then by filtering the emitted light above the peak of the optimum response range (~665nm). For intrinsic imaging, the cortex is illuminated at 605nm wavelength light and no other filter is used. The use of the second filter in VSD imaging is one of the major differences between VSD imaging and intrinsic imaging: in VSD imaging, only the fluorescent light is recorded while in intrinsic imaging the reflected light is recorded at all wavelengths. This provides filtering of an important amount of blood flow related artefacts.

Dyes provide information about the local change of the membrane potential. Fluorescence that is reflected by the dye can be captured over different levels of organization with a good choice of recording equipment. Therefore, the resolution indicated in Figure 1.1 represents the limitation of the dye technology only, but the recording limitations should also be taken into account.

In order to record population activity from V1, the dye which is diluted in an appropriate solvent is applied on the cortical surface in a glass-covered chamber mounted on the skull opened over the areas to be recorded, and washed out after 2-3 hours of staining. This provides the dye to penetrate the cortical surface. In rodents, it is possible to stain the cortex without removing the dura (Lippert et al., 2007).

Due to the limit of penetration in the six layered cortex and filtering out of the signal coming from the deep layers, VSD signal reflects mostly the activity from layer II/III (Ferezou et al., 2006). However, dendritic trees of the neurons in different layers spread over other layers. A recent modeling study suggested that the 45% of the VSD signal originates from layer II/III activity, 20% from layer IV and 35% from layer V (Chemla and Chavane, 2010a).

Population recordings pool activity of tens of neurons under a single pixel. This single pixel reflects the activation of all the dye molecules under the recorded area (plus the light scattering from the nearby neurons) in a millisecond resolution. As the action potentials are very fast events that move very locally on the axon, and as the dendritic surface is very large compared to axonal surface, action potentials are filtered out in VSD recordings and the origin of the signal is mostly dendritic (Ferezou et al., 2006). Nevertheless, Chemla and Chavane (2010a) estimated the contribution of the pure spiking activity on the axons in VSD signal to be around 14%.

In contrast to multielectrode arrays, VSD imaging at population level provides pooling of multiple neurons under a pixel. Extracellular electrodes are sensitive to single unit activities over a region, but the recordings are biased as a result of the geometry and electrode placement (see the previous section). Instead, VSD imaging

provides a more even pooling of all the excitable membrane surfaces under a pixel, which reflects direct intracellular membrane potential including the fine structure of the dendrites and axons. Chemla and Chavane (2010a) estimated the different contributions to this signal. They showed that the VSD imaging reflects mostly the dendritic signals (77%) of excitatory neurons (83%). Glial cells also contribute to the signal. However,e glial cells have very slow activation dynamics; hence their contribution is not present during the first seconds of recording.

As a result of this rich pooling, synchronous activity of nearby neurons is essential in order to obtain a high quality recording. As we will see in the following chapters, modular organization of the cortex provides packing of functionally similar neurons in nearby regions. This is the crucial mechanism that makes VSD imaging possible in the population level. One other consequence of the pooling of all excitable membranes under a pixel is the over-representation of dendritic activities over the activities going on the somata and the axons. This is a result of the greater volume of dendrites compared to somata and axons in the cortex, especially on the layers 2/3 where horizontal connections between cells are prominent.

Even though the same cameras are often used for VSD imaging and intrinsic imaging, lower temporal resolution of intrinsic imaging permits sacrificing the temporal resolution for higher spatial resolution. Lower temporal resolution is also a factor that increases the signal-to-noise ratio in intrinsic imaging. As we go to higher temporal resolutions, the number of photons detected per frame will decrease, increasing the shot noise detected by the camera.

VSD imaging provides the optimal spatial and temporal resolution range to date for investigating mesoscopic dynamics of neural population activity. Extracellular recordings via multichannel arrays and two-photon imaging of calcium signal are the other techniques that offer comparable resolution. Multielectrode arrays provide fast and direct recording of electrical activity in the brain, however the spatial sampling is low compared to VSD imaging. Moreover, multielectrode arrays record the activity on the extracellular media, and adequate methods are needed in order to extract single cell responses. The advantage over VSD imaging is the temporal resolution and the possibility to record supra-threshold activity.

Calcium imaging is another method that is comparable to the VSD imaging spectrum. This method measures the calcium in the cells by using chemical or genetically encoded indicators, which bind to calcium ions. When this binding occurs, a fluorescence change which permits visualization of intracellular calcium concentration takes place. When combined with 2-photon microscopy, calcium imaging provides very good spatial resolution that make observation of single cell activity possible. However, calcium dynamics are relatively slow with respect to membrane

potential measures. Calcium signal is also biased towards supra-threshold activity (Peterka et al., 2011).

Berger et al. (2007) performed simultaneous recording of VSD and calcium imaging in order to quantify the differences between the measures provided by these methods. They showed that calcium signal is slower than membrane potential revealed by VSD to return to baseline, and calcium signal filters fast fluctuations of the membrane potential. Moreover, the VSD signal spread more than the calcium signal, which is expected from the differences between subthreshold and suprathreshold activities revealed by VSD and calcium imaging respectively. It should be noted that as it is the case for VSD imaging, calcium signal itself offers a high resolution measure (it occupies the lower two-thirds of the optical imaging resolution in Figure1.1 (Grinvald, 2005)), but the main restriction is the recording and staining technology.

Overall, VSD imaging overcomes the low temporal dynamics of intrinsic and calcium imaging, while providing a much higher spatial sampling than multielectrode arrays. Moreover, subthreshold potential recorded by VSD imaging reflects local neuronal interactions avoiding the bias of individual cell spiking, which provides a better measure of mesoscopic activity in the brain.

Chapter 2

Visual Cortical Network: Functional Organization of the Visual Cortex

2.1 Neuron as a Basic Processing Unit

The fundamental cornerstone of information processing in the brain is a neuron. Each neuron in the cortex makes connections with a number of cells (several thousands in case of pyramidal neurons) via synapses. Neurons make usually more than one synapse and many of them make and receive hundreds or thousands of synapses. Dendritic trees can differ in the degree of convergence of the signals that they receive: all or many of the synapses on a dendritic tree can come from different neurons, or from only a few.

Neurons are excitable cells which communicate via electrical signals created by the potential difference between the intracellular and extracellular media. When membrane potential of a neuron exceeds a certain threshold, it fires action potentials which provide digital information transfer between neurons. This is done by the neurotransmitter release in the synaptic cleft by the presynaptic neuron, which will be detected by the postsynaptic neuron.

Firing of action potentials is not the only way that neurons communicate. Fluctuations of the membrane potentials are also important for modulation of the information transfer, even if the action potential threshold may not have been exceeded. A recent study showed that the ephaptic coupling between adjacent nerve fibers also alters network activity, showing that the synaptic coupling is not the only communication channel between neurons (Fröhlich and McCormick, 2010).

Neurons that modulate the neuronal activity by diminishing the membrane potential of the post-synaptic neuron rather than transmitting the discharge are called inhibitory neurons. The ratio of inhibitory to excitatory neurons in the brain is 1/4; a ratio that is conserved across species and cortical regions.

Neurons in the visual system extract local information by processing the information that falls into their receptive fields (RF). Part of the visual scene falling on the RF of a cell may evoke ON or OFF response. RFs constitute of subregions that code for ON and OFF responses. A visual response is called ON when a stimulus with a positive local luminance is present on the field. A stimulus on the OFF region creates a response after a positive luminance stimulus disappears from the region, or when a negative luminance stimulus appears.

As we go higher in the cortical hierarchy, RFs of neurons become larger and selective to more complex structures. On the lowest end of this hierarchy, in retina and Lateral Geniculate Nucleus (LGN) neurons possess concentric on center-off surround or off center-on surround RFs. We will explain RF properties in each area in details in the following of the text.

2.2 Overview of the Visual System

Vision is amongst the most complex tasks that we humans are capable to perform, involving almost one-fourth of the whole brain. Even though vision is the one which is the most studied among all brain functions, our knowledge about the functioning of visual processing is still limited.

Vision in humans employs a highly connected network of a high number of brain regions. Nevertheless, there are very primitive animals with much smaller brains consisting of much less neurons that are capable of detecting light and extracting relevant information from the light. As we go lower in the evolutionary tree, number of specified cortical regions decrease, giving more elaborate functions to earlier visual structures. Therefore, studies done on different species should be considered in the framework of the species-specific visual system organization. The study presented in this thesis is based on cat, a species which possesses a highly developed visual system that has been studied extensively in the past and now.

In cat brain, there are 22 regions that are involved in visual processing. 17 of these regions are classically visual and 5 of them are limbic structures. This 22 node graph includes 224 connections, of which 168 are reciprocal (Scannell et al., 1995) (see Figure 2.1A). Extrinsic connections from a single area constitutes only for a small portion of synapses of their target area. More precisely, the strongest single

cortico-cortical connection contributes only 15% of extrinsic input and the strongest single thalamo-cortical input contributes only 20% of total extrinsic input (Scannell and Young, 2002). This indicates that the rest of the synaptic connections are maintained by the input from other cortical areas, and by the parallel connections within the area.

Information flow for visual processing is mostly based on the studies on primates. Here we will explain the pathways based on primate studies, and we will give the cat homologue of the corresponding areas where available.

Major visual areas and their role in perception are shown in Figure 2.1B. The sensory information flow in this complex hierarchy is hypothetically considered in two parallel streams: Dorsal (or where) pathway, and Ventral (or what) pathway (Mishkin et al., 1983). The distinction between these two pathways starts early in the retina, with the parasol ganglion cells that give rise to the magnocellular stream in LGN, and the midget cells that converge to the parvocellular stream of the LGN (reviewed by Nassi and Callaway (2009)). Two streams project to different layers of V1 and then to different subregions of V2. After V2 and V3, those pathways project to distinct cortical areas.

Although the two visual streams are considered to be completely independent, in fact they are strongly connected. The high connectivity between different areas shown in Figure 2.1A reveals that the information flow is not only hierarchical: Feedback and parallel connections are also very important in visual processing. This means that even though every neuron in each region is responsible of a particular task, each of them receive information from other regions that are responsible of processing other types of information. Neurons also communicate with the other neurons in the same area that are processing other specific aspects of the visual stimulus. Moreover, it is difficult to determine a strict hierarchy in such a densely connected network. Hilgetag et al. (1996) used connectivity algorithms and showed that there is no optimal hierarchy between the brain regions.

The RF of the neurons in each structure gets bigger as we go higher in the hierarchy. This indicates that emergent feed-forward activity helps shaping the global response, and immergent feedback activity provides the modulation of the local response by more global features. Likewise, in higher areas, neurons become selective to more complex structures while early areas extract information about the local structure of the visual input (for a review, see Van Essen and Gallant (1994)).

Hierarchies and parallelism in the visual system may vary from species to species. In cat, areas 17 and 18 are parallel while in primates they are hierarchical.

Now we will present briefly the role of visual areas in vision, going from low to high order structures in the hierarchy.

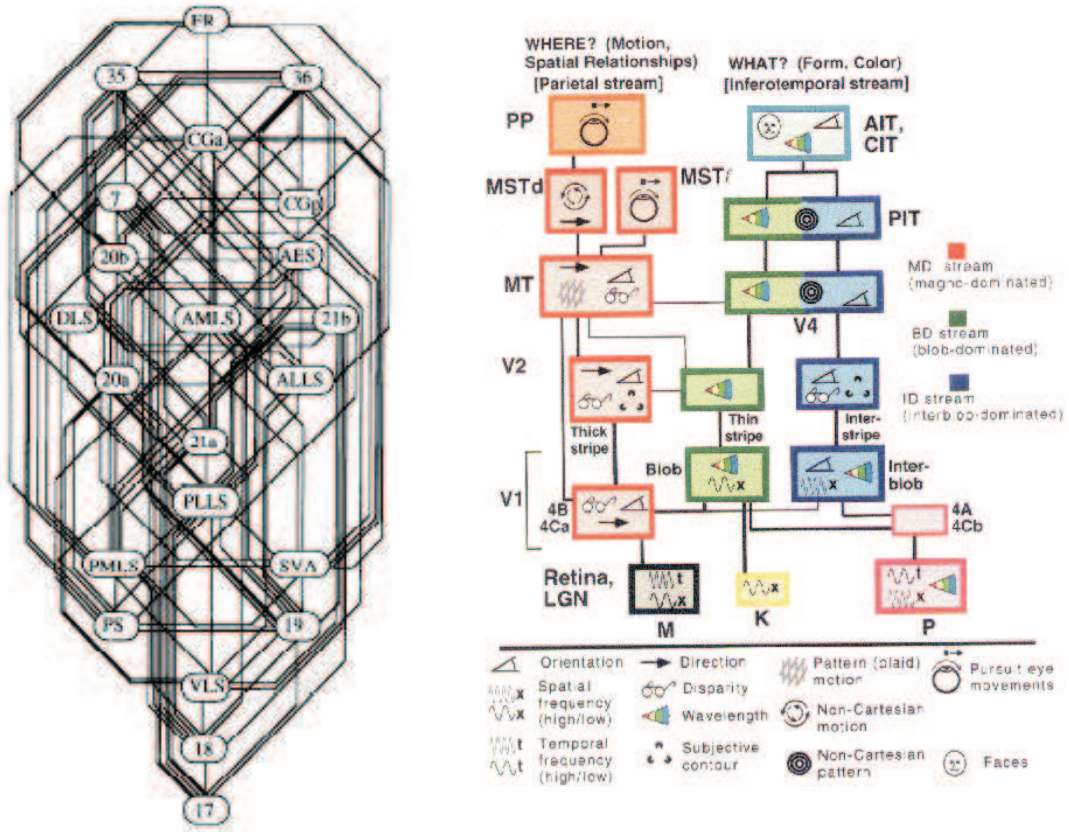

Figure 2.1 – Connectivity of the visual system. A: Hierarchy of the anatomical connectivity of the cat visual system (reprinted from Scannell et al. (1995)). B: Hierarchy of the functional connectivity of the macaque visual system and processing streams (reprinted from Van Essen and Gallant (1994)).

2.2.1 Early Visual System

The Retina

The information flow through the brain for visual processing is initiated when the light hits the photoreceptors in the retina. When a photon excites a photoreceptor, the membrane potential of the cell changes and triggers the depolarization in ganglion cells that will be transmitted through the visual system.

Retina is considered to maintain light adaptation and lateral inhibition in addition to the primary light detection task. Atick and Redlich (1992) suggested that the retina performs a "whitening" of the visual scene by removing the redundancies in order to optimize the channel capacity of the optic nerve.

Retina is a complex neural circuitry which consists of about 80 different cell types, partitioned over three functional layers. Even though the tasks maintained by the retina seems to be simple, necessity of such a complex circuitry is still not clearly

understood. Gollisch and Meister (2010) argued that many visual tasks such as motion discrimination and extrapolation, and saccadic suppression start in the retina, even for higher mammals. Understanding the functional properties of retinal cells will surely shed light to the future of the vision research.

The cells that do the essential and final processing in the retina and send the output to the LGN are the ganglion cells. They have concentric center-surround ON-OFF RFs (Kuffler, 1953), with an increasing size from fovea to the periphery, smaller than a degree in average. On the other hand, the density of cells in the fovea is higher than in the periphery, providing a much denser overlap of RFs. This controversy of RF size and cell density indicates that in the fovea more detailed features of the visual field are extracted in cellular level with a higher sampling at the population level.

Two main types of ganglion cells are present in the retina: center-ON surround-OFF and center-OFF surround-ON. In reality, there are much more ganglion cell types that we will not elaborate here (in monkey, there are 17 ganglion cell types discovered so far (Field and Chichilnisky, 2007)). Ganglion cell RFs are assumed to be circular. Nevertheless, Hammond (1974) showed that in cat retina, ganglion cell RFs tend to have slightly elliptic shape with an average ratio of 1.23 of major to minor axis, and that more than half of all the RFs they analyzed were oriented within 20° of horizontal orientation.

Neurons in the retina (and in other areas of the brain as well) are organized in a way that when one gets activated, it suppresses the activity of nearby neurons. This property helps sharpening the response of the neuron by increasing local contrast. This property partially rises from the ON-OFF receptive fields. Pioneered by Hartline in his Nobel-Prize winning study, discovery of lateral inhibition could later explain very important features of the brain activity such as map development that will be explained later in this text.

Anatomical separation of ventral and dorsal processing streams starts with ganglion cell type differentiation. Retinal ganglion cells are classified as Parasol (α) cells, Midget (β) cells, and bistrafied (γ) cells based on their morphology (Polyak, 1941). These calls are also referred to as Y, X and W based on the functional differences. We will retain the second notation, as it also corresponds the naming of corresponding pathways initiated by the cells in the retina.

X cells have small cell bodies, small dendritic trees and narrow RFs (0.2° to 1°). They exhibit color-opponent contrast sensitivity, low luminance contrast and temporal frequency selectivity. Y cells have large dendritic trees and large RFs (0.5° to 2.5°), and they prefer stimuli with high luminance contrast, low spatial frequency, high temporal frequency. They do not respond to color contrast. W cells are more

heterogeneous and less common, and differently than the two main cell types, they project to superior colliculus (SC) along with the LGN.

The axons of the retinal ganglion cells bundle together and provide the transmission of sensory information from retina to the thalamus via the optic tract.

The Thalamus

The retinal signal coming from the optic tract has three main targets: SC, the pretectum, and the LGN. Among these, the relay structure to the visual cortex is the LGN.

LGN is a six layered structure in cats and primates, with a distinction of magnocellular, parvocellular and koniocellular regions that are targeted by X, Y, and W cells respectively. Hence, the functional distinction that originates from different cell types in the retina is preserved in the LGN to be later projected to distinct layers of V1 (see Chapter 2.5 for more details). Each layer in LGN receives afferents coding only for either ipsilateral or contralateral visual field. No binocular information is extracted by neurons of the LGN.

Ganglion cells in the retina and relay cells in the LGN are often considered to be the preprocessing subunits of the visual system. Cells in the early visual system are considered to possess RFs that detect and enhance local contrast of the image of the external world. The circular shape and ON-OFF structure of receptive fields in the retina are also common in LGN cells. One different RF property of LGN neurons is the lagged response: X and Y cells that respond to a stimulus with a lag are called *lagged cells*. X and Y cells that respond with a normal temporal profile are called *non-lagged cells*.

X pathway projects to area 17, Y pathway projects to areas 17 and 18, and W pathway projects to areas 17, 18 and 19 in the cat. LGN receives a strong cortical feedback that shapes continuously the thalamic responses.

2.2.2 The Primary Visual Cortex

The earliest visual cortical area is the primary visual cortex. This area is often considered as the local feature extractor, with a very well defined representation of the visual space. It occupies the largest cortical surface among all visual areas even in primates, and performs an important part of the perceptive task. V1 is reciprocally connected with LGN, and receives feedback from most of the higher order areas. Lee and Mumford (2003) suggested that the main role of V1 in visual processing is to act as a geometric “buffer” to transmit the best guesses from the

higher areas to LGN, in order to modify the local computations in the most plausible global context.

In cat, areas 17 and 18 are accepted as primary visual cortices as both areas receive and process the information coming from the LGN in parallel (Payne and Peters, 2002)[1]. Still, they process different information: Area 17 is more selective to low temporal and high spatial frequency, while area 18 is more selective to high temporal and low spatial frequency stimulation. Even though these are parallel structures, RFs in area 18 are bigger than those in area 17, which may point out also a hierarchical order. Difference of hierarchy in two species may be a result of the evolutionary principles that shaped the brains: primates need to process fine details of the visual world, while cats need to discriminate the fine details of movement such as binocular vision for a good estimation of distance and acute detection of speed in order to chase preys, which would require accurate cortical mechanism in addition to the classically accepted subcortical mechanisms. Indeed, cats can discriminate speed of a moving object better than primates (Geisler and Albrecht, 1997). Another possibility is that the cat visual cortex can be thought as an intermediary step in separation of V2 from V1.

The functionally distinct input which is preserved in the LGN with the magnocellular and parvocellular pathways projects to distinct non-overlapping areas in different layers of the primary visual cortex. Inputs from magnocellular and parvocellular pathway are integrated for the first time in the pyramidal cells that span all the layers of the primary visual cortex (Payne and Peters, 2002). Similarly, signals from both eyes are also integrated in the V1 for the first time.

V1 neurons have elongated RFs, which gives rise to the orientation selectivity (Hubel and Wiesel, 1959). Orientation selectivity is the most striking property of the neurons in the primary visual cortex. Visual cortical neurons are also known to be selective to other visual features such as direction of motion, spatial frequency, temporal frequency and color. A single neuron is not selective only to one feature, but to a number of features (Leventhal et al., 1995).

Hubel and Wiesel (1959; 1962) were the first to describe the RF properties of cortical neurons. They classified the neurons they observed as “simple” or “complex” with respect to the response characteristics.

Simple cells possess distinct excitatory and inhibitory subdivisions (ON and OFF regions respectively) that exhibit an antagonism and linear summation in space and time within those two parts. With this linear summation, responses to static

[1]It should be noted that area 19 also receives direct input from the LGN, via the W pathway. However, the number of neurons in this pathway is very small and this connection is very weak (Payne and Peters, 2002).

or moving stimuli are predictable. Simple cells receive *push-pull inhibition*, which implies that the OFF regions receive inhibition from the on response, and vice versa. 70% of the neurons in area 17 are simple cells.

Other cells that have more intricate and nonlinear properties are called complex cells. Complex cells are considered to perform a summation of the output of simple cells with similar tuning properties on different positions and phases, resulting in a nonlinear spatial summation of the local contrast.

Hubel and Wiesel suggested that the LGN afferents contact simple cells. Outputs of single cells are then integrated by complex cells. Later, Tanaka (1983) showed that both simple and complex cells receive LGN input with a bias from X and Y pathways. His observations indicate that functional discrimination of V1 connectivity may be more complex than thought.

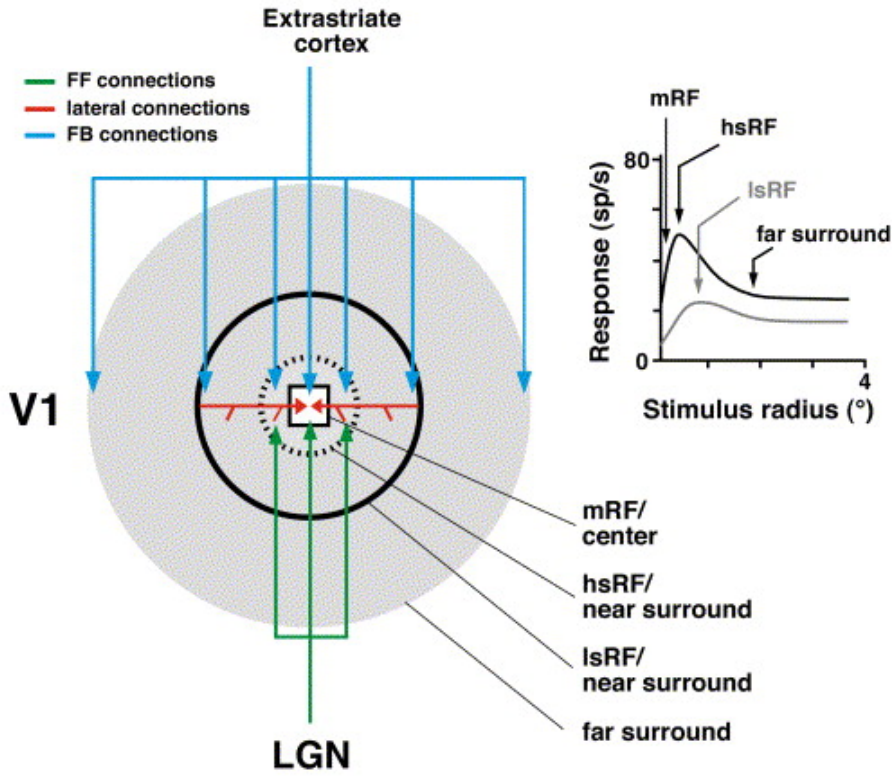

Figure 2.2 – Modulation of the RF size of a neuron in V1 by feed-forward input from LGN, short range or long range lateral connections in V1, and the feedback from the higher cortical areas. White square in the center stands for the RF center and the gray area is the surround of V1 neurons. Response of a cell as a function of contrast and stimulus size is shown in the inset on the right. Adapted from Angelucci and Bressloff (2006).

Anatomically, LGN afferents which exhibit strong surround suppression (Jones et al., 2000) project to a region that is comparable to the minimum discharge re-

ceptive field (mRF) of the V1 cells. This corresponds to the classically accepted RF size of V1 neurons. In reality, RF size of a neuron is modulated by a set of interactions between the feed-forward input from LGN, short range or long range lateral connections in V1, and the feedback from the higher cortical areas (Angelucci and Bressloff, 2006). Therefore, the non-classical RF size gives information about how big is the area that a cell sees in the whole network. Figure 2.2 demonstrates the relationship between the RF size and the network connectivity. It should be noted that this Figure summarizes the surround modulation in primates, and the receptive field sizes given in the inset are bigger in cat. Moreover, surround suppression in cat is weaker than in monkey (Jones et al., 2001). mRF is the region in which the high contrast small stimulation with optimal selectivity for the cell evokes spikes. Projection size of the LGN afferents taken into account the surround matches the high contrast summation receptive field (hsRF) size in primates (Angelucci and Sainsbury, 2006). In this region, high contrast gratings at the same orientation as in the center facilitate the response of the cell. Besides, the low-summation RF size is proportionate to the monosynaptic spread of neuronal activity inside V1 and the feed-back size from higher visual areas (Angelucci et al., 2002). Gratings presented in this region facilitate or suppress the response of the cell at the center depending on the contrast. The region surrounding the lsRF is called the far surround, which is modulated by feedback connections. Gratings presented in the far surround usually suppress the response of the cell at the center. Facilitation or suppression as a function of the contrast is shown in Figure 2.2 inset on the right.

Most of the cells in V1 are subject to center-surround modulation. The nature of the surround modulation depends on multiple features such as contrast, level of anesthetizer, cortical adaptation, position of the cell in the network, type of the surround stimulation, and the species (for a review, see Seriès et al. (2003); Angelucci and Bressloff (2006)). Center-surround modulation of the cells can explain psychophysical observations such as emergence of Gestalt laws in visual perception (reviewed by Seriès et al. (2003)). Subthreshold activity that extends to a larger region than the spiking activity in the superficial layers of V1 is an important factor that modulates the firing and subthreshold activity of a cell, extending the network influence further than the firing-dependent RF definitions (Bringuier et al., 1999).

Receptive fields of V1 neurons and their role in contextual integration is illustrated in Figure 2.3 (image from Dakin and Frith (2005)). Co-alignment of similar receptive fields facilitate contextual grouping of features with similar orientation, which gives rise to the good continuation law of Gestalt. Nature of the horizontal connectivity that gives rise to contextual modulation will be discussed in details in Chapter 2.3.3.

Orientation selectivity is one of the most important characteristics for V1 neurons. As the LGN neurons do not share the same profile, the question of how the orientation selectivity occurs in V1 has been a debate. Thalamic input and the center-surround modulation are the two major contributors to the orientation selectivity in the visual cortex.

Originally, Hubel and Wiesel (1962) suggested that the orientation selectivity emerges from solely the thalamic input to simple cells in layer IV. They argued that the ON-center of the cortical RFs arise from the specificity of the spatial arrangement of the ON-centers of the RFs of the neurons in LGN, and the OFF-center RFs to be derived from the spatial arrangement of the OFF-center RFs of LGN neurons. This model explains the development of orientation selectivity by a purely feed-forward way. However, this model cannot explain the center-surround modulation and contrast invariance of orientation selectivity. Contrast invariance of orientation tuning problem can be solved by considering the *push-pull model*. Following the stimulus presentation, thalamic input initiates the *push* to the ON field, which is then enhanced by intra-cortical excitation. This excitation is then followed by the *pull* created by the intra-cortical inhibition, which suppresses the response. Troyer et al. (1998) predicted that in order to obtain contrast invariant tuning, neurons should receive anti-phase inhibition stronger than the feed-forward input. Hirsch et al. (1998) and Borg-Graham et al. (1998) showed that the neurons receive cortical OFF inhibition on the ON subfields and strong ON inhibition on the ON subfields. Monier et al. (2003) showed that the conductances are also tuned to the orientation of the input, which can be accepted as a direct proof of intra-cortical contribution to orientation tuning.

The “ring model” (Ben-Yishai et al., 1995) aims to explain emergence of orientation maps by network connectivity. In this model, connection weights vary as a function of distance and orientation selectivity between pre-synaptic and post-synaptic cells. Nearby cells make excitatory connections while distant neurons make inhibitory connections. The model can explain emergence of orientation selectivity and contrast invariance of orientation tuning. If only inhibitory connections are considered in the model, contrast invariance cannot be explained. Ring model claims that there is a symmetry breaking and line attractor dynamics. Line attractor dynamics indicate reduction of dimension, collapsing the cortical response into the two-dimensional ring attractor.

Primary visual cortex is an exhaustively studied area in the brain, and yet our knowledge about its functioning is still limited. Olshausen and Field (2005) stated that even though long years of neuroscientific research could explain a considerable amount of the functioning of V1, our knowledge is biased because of experimental and theoretical restrictions. Taken into account the variance explained by the the-

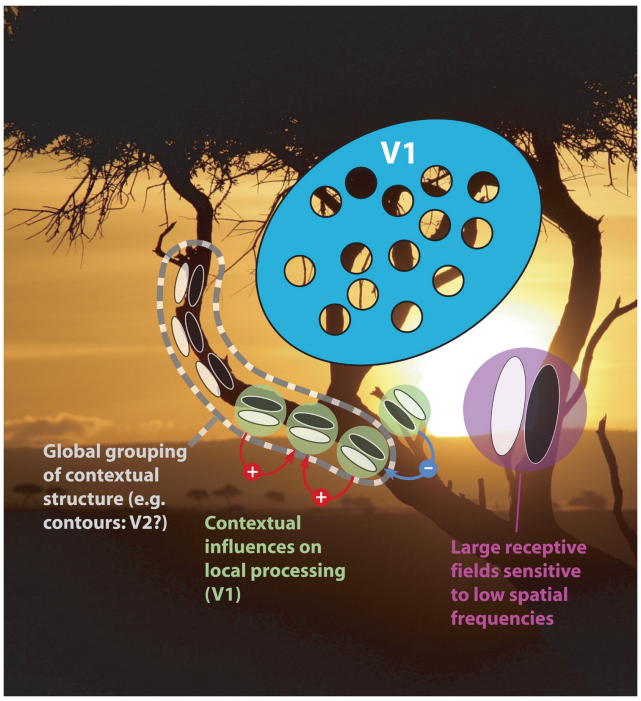

Figure 2.3 – Receptive fields in V1 and their role in contextual grouping. Small receptive fields permit extraction of local information in the local scene. Contextual grouping arises from the local processing in V1 that provides either facilitation (+) or suppression (-) that permits to extract coherent information. Global grouping is considered to be achieved in higher areas, but the mechanisms are still not well known. Reprinted from Dakin and Frith (2005).

ory and the proportion of the cells studied, they concluded that 85% of V1 function is not understood. They suggested that development of multichannel recordings and more ecologically relevant protocols may help to extend our knowledge about primary visual cortex, and to explain how this region responds in a naturalistic context.

2.2.3 Higher Visual Areas

V1 projects to a number of higher cortical areas that process more global features of visual scenes. A good review of the processing streams in visual system is written by Van Essen and Gallant (1994). Areas involved in the what and where pathways in cat are shown in Figure 2.4. In cat, area 17 accepted to be primarily involved with the 'what' pathway, while area 18 is more involved in 'where' pathway.

V1 first projects to V2 and V3 (area 19) which are considered to be the "association cortices". These regions are also called *extrastriate cortex* because of the lack of the myelin stripes in V1 that originates from thalamic input. V2 is thought to be responsible for contour completion, as the cells in V2 prefer angles between lines

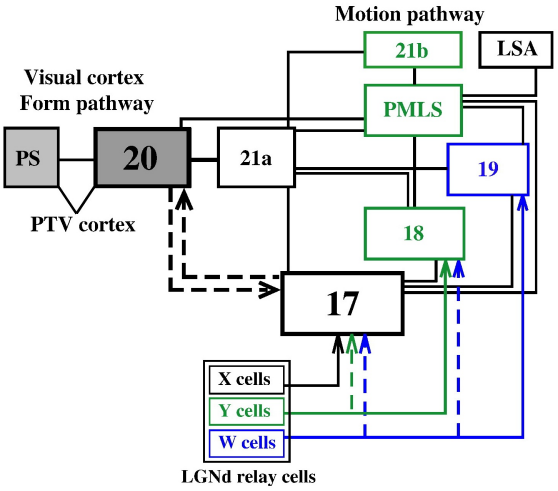

Figure 2.4 – Connectivity of the pathways in the cat visual cortex. Reprinted from Huang et al. (2007).

rather than local orientations. After this step, the two pathways project to different cortical regions.

Dorsal pathway continues with the projections to MT/V5 (Area 21), which extract information about the global direction of movements, as in case of plaid motion (Movshon et al., 1985). In cat, homologue of MT is the posteromedial lateral suprasylvian area (PMLS). The information about the direction of global motion is then segregated into the two subregions of the MT that are responsible to distinguish whether the movement is related to navigation in the environment or to eye movements. These regions then project to MSTd and MSTℓ. After that, connections are made with the Posterior Parietal (PP) cortex which combines the input from different sensory, limbic and motor output areas.

Ventral pathway continues with V4 (area 20), a region that is responsible for identification of more complex non-Cartesian shapes. The ventral pathway includes two substreams that follow blob-dominated or interblob-dominated regions. This information is further sent to IT that recognizes even more complex 3D shapes like faces, or any useful shape information that was learned by the animal (Gross et al., 1972). The cat homologue of IT is the postero-temporal visual cortex (PTV).

Feedback to V1

V1 activity is continuously shaped by the feedback from higher areas. In rat visual cortex, 97-98% of the postsynaptic cells of the feedback connections to V1 are excitatory neurons (Johnson and Burkhalter, 1996). Feedback from V2 and V3 are patchy except in layer 1A (Angelucci and Bressloff, 2006). This patchiness

corresponds to a functionally-selective feedback depending thanks to the modular architecture of the cortex (see the following Chapter).

Feedback from higher areas modulates V1 neurons by controlling their response gain. Inactivation of higher areas results in decrease of the response amplitude, and tuning width (Wang et al., 2000; Galuske et al., 2002; Wang et al., 2010). However, at least a small number of neurons in V1 have different RF properties under inactivation of higher areas. Huang et al. (2007) showed that cooling down of PTV cortex results in modification of response magnitude (mostly reduction) and receptive field properties of neurons in V1. Their results indicate that the function of V1 cannot be studied completely independent of higher visual areas. Another consequence of this relationship is the difficulty of studying a region with system identification methods using unnatural stimuli. In a context outside natural statistics, even if the individual cells in a particular region in the brain are tuned to the particular local structure of the stimulus, if the stimulus does not have a natural structure there would be no top-down information telling the cells what they should see, which may diminish the efficiency of coding.

2.3 Mesoscale Organization at the Population Level in V1

In the previous chapters, we presented the functional properties of individual neurons and the gross structure of the visual system. Here we will focus on the connectivity of the neurons that gives rise to the patterns of activity produced at the mesoscopic level, which then will be transmitted to the higher order structures in the macroscopic hierarchy.

2.3.1 Columnar organization of the cortex

Modularity is a property of network connectivity that favors strong connections among small groups of agents that are specialized to perform a common task. Cell populations in the brain exhibit a modular organization that favors tight connections between a small group of neurons that process similar information. Bullinaria (2007) has shown that the modular structure in neural networks provide more efficient processing than non-modular architectures for multiple discrimination task, given that the connection length is limited. Another advantageous implication of the modular organization in a hierarchical network would be the generation of the output “patterns” of activity that will be detected by the higher-order structure in the hierarchy.

The modular structure in the brain was first pointed out by Lorente de No (1938), introducing the idea that the cortex is built of small cylinders of vertical chains of neurons. He proposed that these cylindrical units constitute elementary units of operation in the cortex. This idea was then developed by Mountcastle (1957), who introduced the concept of *minicolumn*.

Minicolumns are accepted to be the smallest anatomical populations in the cortex consisting of cells that share a common function. After the first observations in the somatosensory cortex, minicolumns were reported in diverse areas of the cortex, with a highly similar structure and connectivity despite the variety of the tasks that are done in different cortical regions. Nevertheless, a certain level of heterogeneity is also present (Buxhoeveden and Casanova, 2002; DeFelipe et al., 2002). Microcolumns are considered to be related to the migration of neurons through radial glial fibers into radial columns during development (Rakic, 1988). A minicolumn consists of about 150 neurons that receive same input and have similar RFs, covering about 40 μm of cortical sheet in monkey and about 56 μm in cat (Mountcastle, 1997).

Following the studies of Mountcastle, Hubel and Wiesel showed that columnar organization exists also in primary visual cortex. They recorded the activity of neurons by a tangential penetration and showed that RF properties are continuous and systematic changes of orientation and ocular selectivity are observed as the electrode advanced (Hubel and Wiesel, 1977, 1963). In these preliminary studies, they reported 12 orientation column sites over a 180° complete cycle. However, in their future work they observed orientation columns to be quantal, without physical borders.

Cortical columns further give rise to *macrocolumns* that contain 60 to 80 minicolumns that are connected via very short range horizontal connections (Mountcastle, 1997). In the visual cortex, notion of a macrocolumn is ambiguous, as anatomically functional organization is rather continuous than discrete. A more widely used term is *hypercolumn*, a term originally used by Hubel and Wiesel (1977). A hypercolumn is a local patch that contains a set of all necessary units that code for a maximum number of features on a specific retinotopic region. Hubel and Wiesel argued that 2 mm x 2 mm patch of cortical surface is necessary and sufficient to analyze all the features of a small region of the visual field (following studies retained 1mm^2 surface as hypercolumn size). If we consider the network influence on functional integration performed by a single vertical column, we arrive to the definition of a *metacolumn*, which should be considered as a complete functional entity (Frégnac et al., 2006)

The notion of hypercolumns as primary processing units in the population layer

was suggested by Hubel and Wiesel with the ice-cube model of cortical organization (Hubel and Wiesel, 1962, 1968). Hypercolumn hypothesis was the first attempt to explain how different features in the primary visual cortex are interconnected.

Although earlier recordings reported that neurons that exhibit same RF properties are sharply clustered on radial columns of the cortex, latter studies found that RF properties are rather continuous than sharp distinct patches (Albus, 1975; DeAngelis et al., 1999, reviewed by Horton and Adams, 2005). DeAngelis et al. (1999) recorded nearby pairs of neurons by a single electrode, and showed that nearby neurons in the visual cortex do not always share exactly same RF properties. They showed that some response properties such as orientation selectivity and retinotopy are well clustered, while others such as spatial phase preference are not. These findings call the existence of the anatomical substrate for functional columns in the visual cortex into question. This view may be true and the cortical column concept can be thought as an abstract notion that provides a passage from the cellular level to cortical maps, rather than having an anatomical identity. In this manuscript, the term "column" will be used as an abstract functional unit, and should not be considered as an anatomically distinct structure in the visual cortex.

2.3.2 Connectivity inside a column: Spanning the layers of the cortex

Historically, the laminar structure of the neocortex is subdivided into six layers. These layers were originally defined with respect to the axon packing density of the laminar sections of the cortex. As more advanced methods became available in the last decades, this classification has slightly changed. In the visual cortex, layer IV is divided into three sublayers as IVA, IVB and IVC which is further divided into two as IVCα and IVCβ in primates, and layers II and III are often considered together. Roughly speaking, laminar organization of the cortex can be considered in three gross subdivisions: Input level (Layer IV), feedback and motor output level (layers V and VI), and association level (layers I, II and III, and to a lesser extent layer VI in the cat) (Figure 2.5A). Association level corresponds also to the feed-forward output level: The information processed here is sent to the layer IV of the next higher order area in the hierarchy and the same laminar organization is applied.

It should be noted that the six-layered structure of the cortex is not universal. Fine structure of the connectivity between layers may differ among cortical areas and species. Moreover, some simpler animals may perform cortical tasks similar to that of highly developed animals with less layers. For instance, turtle visual cortex has only three layers and despite that cortical activity codes for some basic features of visual stimulation such as position and speed. Furthermore, number of cells and cell subtypes in a column may also differ among species (DeFelipe et al., 2002;

Buxhoeveden and Casanova, 2002), pointing out that columns differ in organization in order to meet the functional requirements of the system that they belong to. The difference in innervations of areas 17 and 18 in cat is a good example (Figure2.5B). Even though both areas receive thalamic input and hence considered as primary visual cortices, there are important differences of input types and the way they are processed. Area 18 does not receive any X input (or a little (LeVay and Voigt, 1990)); therefore this region does not respond to high spatial frequency and low temporal frequency visual stimuli. This property is employed to distinguish the two cortical areas in imaging experiments.

Thalamic input arrives mostly in the layer IVC, and partially in the layer VIA of the primary visual cortex. First projection from here is made to layer IVB and to layer III by the stellate cells. Simple cells are most often found in layer IV and VI, in accordance with Hubel and Wiesel's hypothesis that the first target of the thalamic input to cortex is simple cells. After the thalamic projection arrives at the spiny stellate cells, synapses made with the dendrites of the pyramidal cells provide spanning all the length of the column.

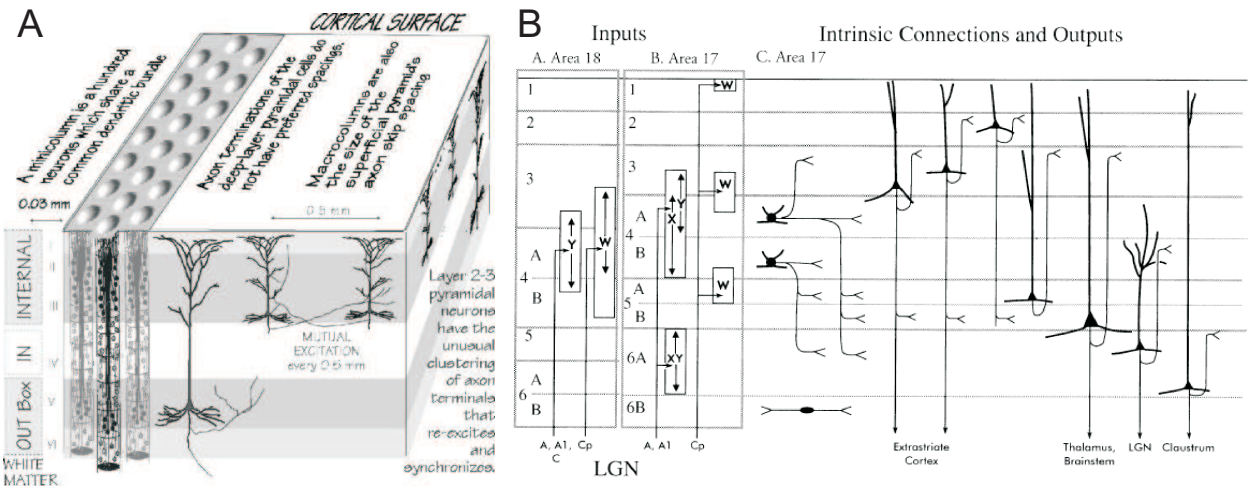

Figure 2.5 – Laminar organization of the cortex. A: Some basic properties of columns and their laminar organization (reprinted from Calvin (1996)). B: Innervations in areas 17 and 18 of cat cortex (reprinted from Payne and Peters, 2002).

The utmost important task in the visual cortex is performed on layers II/III: Cells in these layers permit the extraction of spatially coherent information among different columns via horizontal connections. Unlike other layers, cells in layer II/III are strongly connected with the cells of other columns with similar preferences. This connectivity provides an important support to the modular architecture of the cortex. The work presented in this thesis conducted on recordings in the superficial layers of the cortex, therefore layer II/III is of importance for us.

The information processed by layer II/III is then sent to higher cortical areas. Layer

II/III cells also send their output to the layers V and VI. Layer VI sends the feedback to the thalamus, and layer V projects to deep brain structures, mostly related to the motor output.

2.3.3 Connectivity between columns: Horizontal connections

Neurons in layer II/III have very large dendritic trees, extending over several hypercolumns. Spatial profile of the functional connectivity of a neuron is often described as a "Mexican hat": Nearby neurons (in a diameter of a size of a column) receive a strong excitation, medium distance neurons receive inhibition, farther neurons up to a certain distance receive excitation. This type of connectivity gives raise to emergence of the very particular organization of the cortical maps, and also to the emergence of the RF properties of the neurons (Mikkulainen, 2005).

Another important consequence of the lateral excitation is the association of the local information with the global activity. While the first models of visual cortex restricted the visual activity to point-to-point mapping regions of the visual field to the visual cortex, it was shown that visual stimulation triggers a spread of activity on the cortex that travels 0.05-0.5 meters per second. (Grinvald et al., 1994; Bringuier et al., 1999; Benucci et al., 2007, see Muller and Destexhe (2012) for a review). This phenomenon is partly related to the horizontal connections in layer II/III that are made by pyramidal and spiny stellate cells in order to integrate information over several millimeter squares of cortical sheet.

Horizontal long-range connections in the cat visual areas 17 and 18 are patchy: they tend to link neurons in the columns with similar functional properties. Pioneering studies showed that lateral connections are strongest between the cells with co-axially aligned RFs (Gilbert and Wiesel, 1989; Bosking et al., 1997; Schmidt et al., 1997). Horizontal connections tend also to link either blob-to-blob regions, or interblob-to-interblob regions in primate cortex (Yabuta and Callaway, 1998; Yoshioka et al., 1996). On the other hand, Kisvarday et al. (1997) showed that the connections are not systematically orientation-specific although iso-orientation connections are the most common. While middle range connections (1 to 3 mm) prefer similar functional properties, long range connections (>3mm) and short range connections (<1mm) innervate regions that have much diverse functionalities. All these evidences show that there is a functional relationship between the cells that are interconnected via horizontal connections, and a certain degree of anisotropy is kept in order to explore all possible interpretations of the local input in a global context (Douglas and Martin, 2004).

The preferential linkage of the functionally similar neurons in the cortex can explain a number of phenomena. First, emergence of cortical maps may be related to the

preferential functional attachment (Mikkulainen, 2005). Second, implementation of Gestalt laws in the visual cortex is possibly partially modulated by horizontal connections. Finally, visual illusions such as filling-in and apparent motion can be explained by sequential activation of functionally connected regions (Jancke et al., 2004).

Preferential attachment results in global clustering of neurons with same RF properties. These global clusters can be observed by recording population responses to a set of possible arrangements of a RF property, while fixing the other properties to one common value. This would provide observation of "cortical map" organization of a receptive field property.

2.3.4 Cortical Maps

A more global way to see the clustering of neurons that have similar RF properties is to look at how these regions are organized on the cortical sheet. Nearby neurons of the sensory and motor cortices express a continuity of RF properties, giving rise to the spatial functional maps in the cortex.

Visual system is one of the most striking examples to functional organization of nearby neurons, by virtue of the number of different features provided by single neurons. DeAngelis et al. (1999) quantified the similarities among the RF properties of nearby simple cells in the area 17 of cat. Orientation selectivity was followed by RF width, spatial frequency, peak response latency, response duration and temporal frequency respectively by means of clustering. They could not find an obvious clustering for spatial and temporal phase and direction selectivity. Development of optical imaging methods provided a better visualization of the spatial continuity of RF properties at population level (Blasdel and Salama, 1986; Bonhoeffer et al., 1995), proving or disproving map properties discovered by other electrophysiological recordings.

Each separable RF property exhibits a spatially periodic organization which defines a cortical map, with a periodicity of 0.5 to 1 mm. These maps are superimposed on the cortical sheet and they provide uniform coverage (Swindale et al., 2000). Uniform coverage suggests minimization of the cortical surface that is needed to represent a maximum of features. Cat and primate cortices contain maps for retinotopy, ocular dominance, orientation, direction of motion, and spatial frequency preference. Primate cortex contains a color selectivity map in addition to these others. Other maps that have not been discovered yet may also exist. Swindale (2000) suggested the number of cortical maps to be six or seven (upper limit of nine or ten) in order to optimize uniform coverage. For a recent review about the functional maps and related models, see Issa et al. (2008).

Retinotopy

Most universal feature of the functional organization of the cortex is the orderly topographical organization of the projection of the external world on the cortical surface. In case of vision, this property is called *retinotopy*: left visual hemi-field projects to the right hemisphere, and right visual hemi-field to the left hemisphere, where the visual field is mapped in a continuous way with a logarithmic scaling (Schwartz, 1977; Tusa et al., 1978). This means that the foveal region is represented in a larger cortical area than the periphery, with a smooth spatial displacement.

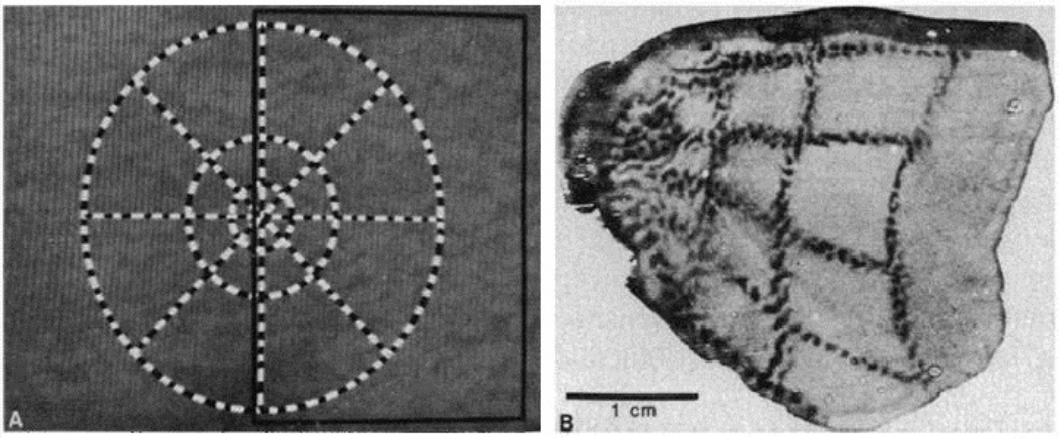

Figure 2.6 – Retinotopy in macaque visual cortex revealed by 2-DG method. Figure from Tootell et al. (1988b)

One of the very striking examples of the retinotopy is shown in Figure 2.6 (Tootell et al., 1988b). Tootel and colleagues showed the anesthetized monkey the pattern on Figure 2.6A after the 2-DG injection, while one eye is closed. The active regions on the flattened cortex marked with 2-DG are shown in Figure 2.6B. These results confirm logarithmic mapping and foveal magnification in retinotopic arrangement.

Retinotopic organization implies that nearby regions in the visual field are represented nearby in the retina, LGN and in the cortex. Hence, connections from retina to LGN to cortex are also topographically organized. Mapping is organized as partially shifted overlaps and there is no strict point-to-point mapping, which may also be considered partially as a result of receptive field scatter at cellular level (Albus, 1975). While retinotopic map is rather regular in area 17 of the cat cortex (Tusa et al., 1978), asymmetries start to occur in areas 18 and 19 (Tusa et al., 1979). Higher order areas also exhibit retinotopic organization, but as a result of increasing RF sizes, these maps are much less precise (Tusa and Palmer, 1980).

The inverse problem of receptive field of neurons would be to determine the patch of cortex that respond to a point stimulus, which is referred to as the *cortical spread function*. Grinvald et al. (1994) addressed this problem using VSD imaging, and

showed that this area is small first, but it grows rapidly much larger than what is predicted from the receptive field sizes of individual neurons. The size of the spread they observed was consistent with the size of long range horizontal connections.

Orientation Map

The most striking RF property of neurons in the primary visual cortex is orientation selectivity. When Hubel and Wiesel observed that neurons in the primary visual cortex exhibit a preference to a particular orientation of elongated bars, they also reported that this property is continuous in space (Hubel and Wiesel, 1977). This hypothesis is later confirmed with intrinsic imaging, revealing also the patterns of orientation preference in the primary visual cortex (Blasdel, 1992b).

In most of the higher mammal species, neurons with similar orientation preference are clustered together and form orientation columns which are further organized in a crystal-like orientation maps in the primary visual cortex. An example from area 18 obtained by intrinsic imaging by Bonhoeffer and Grinvald (1993) is shown in Figure 2.7. Orientation columns are continuous in orientation and together they form "linear zones", which are segregated by discontinuity regions. Discontinuity zones occur either as one dimensional "fractures" if the discontinuity is smaller than 90°, or as zero-dimensional singularities called "pinwheels" if the discontinuity is greater than 90° (Bonhoeffer and Grinvald, 1991; Blasdel, 1992b). Orientation domains rotate around pinwheels and make a full 180° turn that provide uniform coverage of orientation selectivity around the pinwheel. Recently, fine detailed clustering of this organization is shown using 2-photon calcium imaging (Ohki et al., 2005). The authors showed that the neurons that are selective to different orientations are clearly segregated even at the very center of the pinwheels.

Relationship between the tuning profile of a neuron and its localization on the orientation map has been a debate. Earlier studies reported that the neurons that are located on the center of pinwheels are as selective to orientation as the cells found in the iso-orientation domains at least by means of spiking activity (Maldonado et al., 1997), but they are more broadly tuned than the neurons in iso-orientation domains by means of membrane potential (Schummers et al., 2002, 2007). Ohki et al., 2006 showed the precise organization of the orientation selectivity of neurons around pinwheels using calcium imaging. They showed that the tuning width of neurons at the pinwheel centers was slightly larger than in iso-orientation domains. Nauhaus et al. (2008) used combined multielectrode recordings and VSD imaging to test whether there is a relationship between the map location and orientation selectivity. They showed that the orientation tuning is sharper in the iso-orientation domains. They showed that the tuning width is correlated with the local

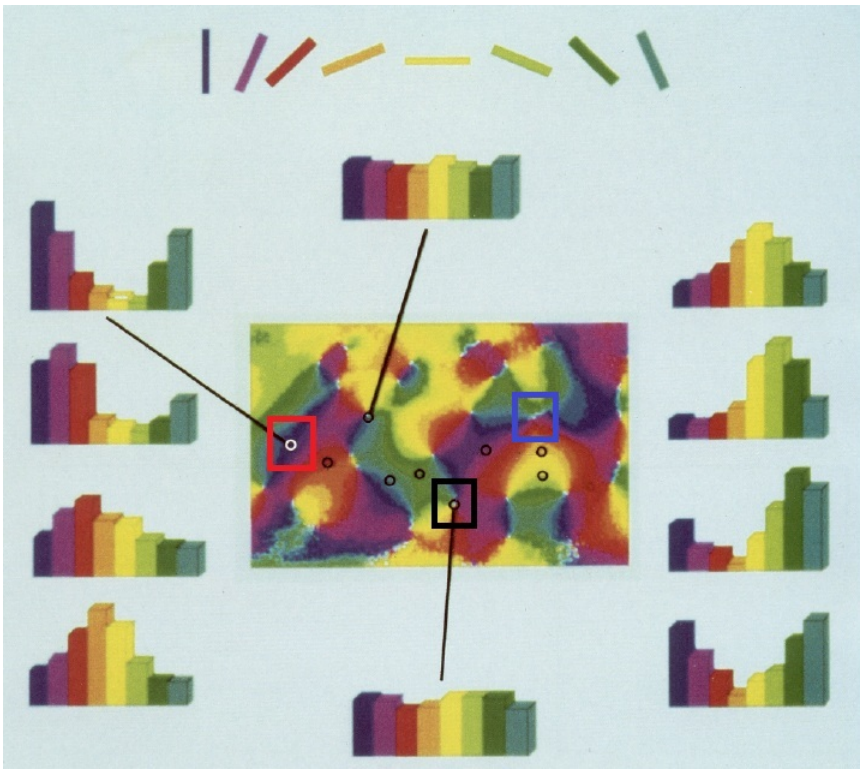

Figure 2.7 – Orientation map of cat area 18. Histograms depict the tuning curves of the points indicated on the map. Black square is an example of pinwheel, red a linear zone, and blue a fracture. Adapted from Bonhoeffer and Grinvald (1993).

homogeneity of orientation selectivity, which explains why the neurons in cat cortex are more sharply tuned than in monkey cortex, in which orientation domains are smaller. They argued that because of the same reason orientation tuning is broader in rodents where there is no orientation map; hence the map is completely inhomogeneous. The contradictions in the literature may be a result of the difficulties of detecting the electrode placement on the orientation map, and the low resolution of orientation sampling in imaging, as pointed out in the latter paper. It should be noted that the differences in tuning width reported in Nauhaus et al. (2008) are present but even at pinwheel centers tuning width is not that large in cat (~25° around pinwheels, 10° around iso-orientation centers). This may be another reason for different interpretations.

While the existence of orientation and direction selective neurons in the primary visual cortex is confirmed for most of the mammals (primates, canines, rodents and birds), spatial smooth gradient of orientation preference in the laminar plane of the cortex is not a universal property.

There are some differences between the areas 17 and 18 of the cat cortex in terms of orientation-selective organization. The pinwheel density in area 17 is almost 1.7-

fold higher than in area 18 (Bonhoeffer et al., 1995). Average orientation domain width and RF size in area 18 is larger than in area 17 (Issa et al., 2008). Moreover, in area 18, linear zones of orientation selectivity are also observed embedded in the radial organization domains around pinwheels (Shmuel and Grinvald, 2000). Higher density of pinwheels in area 17 may be a result of all these evidences. Linear zones are common at the border between areas 17 and 18 (Bonhoeffer et al., 1995). These linear zones tend to be aligned perpendicular to the area 17/18 border (Swindale, 1996).

Direction Map

Existence of a clustering of the direction preference in the primary visual cortex has been more controversial than the existence of other receptive field properties. Earlier studies have reported that the direction selective cells are not clustered in the cortex (Bonhoeffer et al., 1995; DeAngelis et al., 1999). Proceeding studies could succeed to show that a weak clustering of direction selectivity exists in the primary visual cortex (Swindale et al., 1987; Shmuel and Grinvald, 1996; Weliky et al., 1996).

In the direction map, regions that are selective to two opposite directions are separated by sharp direction fractures (Figure 2.8). These fractures pass through the peak of the iso-orientation domain selective to the orientation orthogonal to the direction of movement, and tend to terminate next to the orientation singularities. An important level of separation of counter-selective regions was observed near the direction fractures: Ohki et al. (2005) observed that in cat area 18, direction selectivity boundaries are as sharp as one or two cells apart.

The fact that only one fourth of neurons in macaque V1 is selective to direction of motion may be a reason for why direction selectivity clustering is not easy to detect. Another reason is the analysis method that is used to generate direction maps: Vector summation method may lead to erroneous results where the selectivity is poor (Swindale et al., 2003). Gaussian fitting gives more accurate maps of direction selectivity. However, one has to use a good sampling of the orientation domain, which is mandatory for a good fitting of the tuning curve.

Direction selectivity in V1 neurons are accepted to arise from the organization of the input from lagged and non-lagged cells of the LGN. Galuske et al. (2002) showed that inactivation of higher areas that are involved in motion-processing abolished the structure of the direction maps. Their result indicate that the clustering of direction selectivity, and possibly the mechanism of direction selectivity of individual neurons are mostly shaped from feed-back from higher areas.

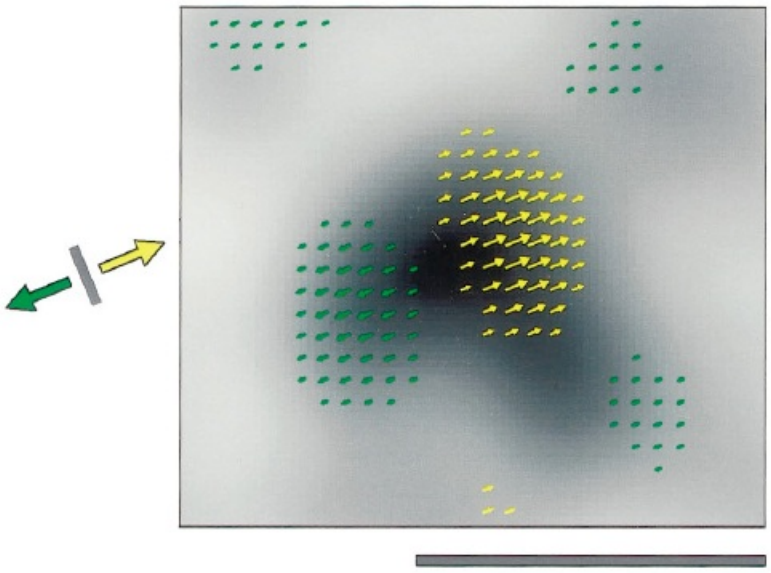

Figure 2.8 – Organization of direction selectivity on an iso-orientation domain. Reprinted from Shmuel and Grinvald (1996).

Ocular Dominance Map

One of the first observations about clustering of the functional domains in the visual cortex was the discovery of ocular dominance columns. Existence of ocular selectivity was first observed by Hubel and Wiesel along with orientation selectivity (Hubel and Wiesel, 1959). They showed that while most of the cells are binocular, most of the cells preferred stimulus from one eye to the other. Furthermore, in layer IV they found cells that respond only to one eye. Later on, Hubel and Wiesel (1969) showed that ocular dominance has columnar organization in the visual cortex by recording cells with perpendicular penetration to the surface. The columnar organization of ocular dominance selectivity was further supported by 2-DG recordings (Tootell et al., 1988a) and intrinsic imaging (Ts'o et al., 1990).

Similar to orientation maps, ocular dominance columns are also not present in all species. Moreover, species-specific anomalies may also exist, as in the case of squirrel monkey (Adams and Horton, 2003), which is an animal that may or may not have ocular dominance columns. In monkey cortex, ocular dominance patterns are very regular elongated stripes which sometimes branch or terminate, similar to the patterns on the skin of a zebra. In cat, ocular dominance patterns are less regular. Comparison of an example from macaque and cat brains is shown in Figure 2.9.

Clustering of ocular dominance in the layer II/III was reported to be three-fold weaker than clustering of orientation-selective domains (Bonhoeffer et al., 1995). This may be a result of the ocular dominance columns to be stronger in layer IV.

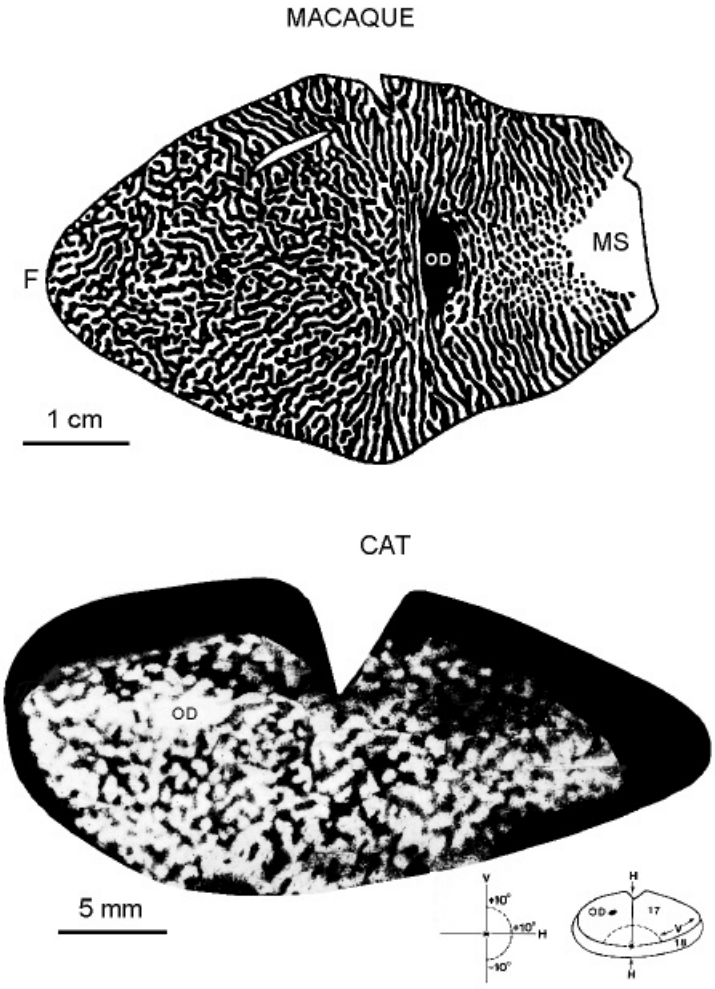

Figure 2.9 – Ocular dominance columns in monkey and cat. F stands for the fovea, OD the optic disc, MS the monocular segment, V the vertical midline and H the horizontal meridian. Figure from Swindale (1996).

Spatial Frequency Map

Spatial frequency preference is clustered on the cortical surface (Shoham et al., 1997; Everson et al., 1998; Issa et al., 2000; Tootell et al., 1981), even though the clustering is weaker than orientation selectivity or ocular dominance. Spatial frequency domains are also organized continuously on the cortical surface. Some studies suggest that spatial frequency domains are organized around pinwheel centers, even though there is no circular organization as in orientation domains (Everson et al., 1998). Some other studies claim that these findings occur when thinking spatial frequency maps combined with orientation selectivity (Issa et al., 2000). Everson et al. (1998) noted that even if the spatial frequency selective regions are

organized around pinwheels, extreme frequencies represent a smaller region on the cortex, therefore spatial frequency domains cannot be explained by a circular continuity as it is the case for orientation domains.

CO Blobs

Cells that contain high concentration of the Cytochrome oxidase (CO) enzyme are clustered in the visual cortex. These regions are shown to be mostly sensitive to color in primates, as they receive mostly parvocellular input. CO blobs also exist on other species such as owl monkey and cat, which have a weak color vision.

Relationship and dependency between visual cortical maps

Although cortical maps provide information about how the cortical sheet is organized in order to represent a single feature, how these different features communicate in order to represent more complex stimuli that involve multiple features is still not clear.

One of the firstly studied subjects concerning interdependence of maps is the correlation with retinotopy and orientation maps. Durbin and Mitchison (1990) used dimensionality reduction model to show that the receptive field shifts should be inversely correlated with orientation singularities. However, Das and Gilbert (1997) observed by combined multielectrode recordings with intrinsic imaging that the receptive fields of neurons show local shifts near pinwheels, indicating a modification of the retinotopic map around orientation inhomogeneities in cat. Following studies on cat visual cortex (Buzás et al., 2003) and ferret visual cortex (Bosking et al., 2002) showed that the local variability in receptive field positions is not significant at the population level.

Another related topic is the spread of local oriented stimulus in the cortex. Following the visiotopic organization of the visual system, and the local and patchy connections that are made by single cells, nearby cells as well as some other cells with similar receptive field properties in the near periphery are strongly connected. Therefore, each local population of neurons integrates information from populations of neurons over several millimeters wide cortical area. As an analogy to the RF property of single cells, at the population level, it is more appropriate to talk about the cortical response field i.e. the cortical surface whose spatio-temporal pattern of activation is influenced by a particular stimulus (Grinvald et al., 1994; Sharon et al., 2007). Cortical spread explains how the local information spreads in the cortex in order to provide a global interpretation. Using VSD imaging, Sharon et al. (2007) showed that a 4° oriented stimulus at eccentricity of [4°, -2°] evoked response on a

~16 mm^2 region on area 18 with a high plateau of ~9 mm^2. Orientation-selective domains to the grating peaked at the top of this plateau.

Benucci et al. (2007) showed that it is possible to predict the responses to local oriented stimulus by pointwise multiplication of the two maps, indicating the independence of the maps. More recently, Chavane et al. (2011) showed by using a smaller stimulus that the orientation selectivity of the lateral spread decreases exponentially with distance. Using a small size stimulus, they avoided evoking more cooperative spiking responses which may enhance orientation selectivity of the periphery, restricting the lateral spread only to the subthreshold activity. The size and the orientation selectivity of the lateral spread were in coherence with lateral connectivity (see Chapter 2.3.3).

Some structural properties are known about the interdependence of the maps in the visual cortex. For example, pinwheels and fractures tend to be located in the middle of the ocular dominance columns, as well as the CO blobs while only half of all pinwheels are associated with CO blob locations. CO blob locations coincide also with low frequency selective regions of the spatial frequency maps, while intermediate selectivity regions mostly avoid them. Moreover, pinwheels that are not placed at the same location as CO blobs coincide with high spatial frequency selective regions (Bonhoeffer et al., 1995; Issa et al., 2000). Another relationship between the cortical maps is that the borders of ocular dominance columns and borders of iso-orientation domains intersect at right angles (Hübener et al., 1997; Obermayer and Blasdel, 1993), as suggested earlier by Hubel and Wiesel (1974).

Despite big efforts, no systematic spatial relationship that is coherent among species has been found. Moreover, results obtained by different teams are very controversial, especially when species-specific differences are considered (for a review, see Horton and Adams (2005)). One common conclusion to retain is that the right angle intersection provides the optimum coverage (Hübener et al., 1997; Obermayer and Blasdel, 1993; Hubel and Wiesel, 1974). Another common property seems to be that the singularities of one map are found on the isotropic regions of another map. Moreover, although different maps are responsible for processing of different features of images, the maps are dependent themselves on each other. Basole et al. (2003) showed that short orientation bars that move in a direction not orthogonal to the orientation of the bar evoked responses on orientation domains that are selective to another orientation than the orientation of the bar. Their results indicate that the maps are dependent on other maps in the cortex, indicating that the local columns are functionally undetachable. Mante and Carandini (2005) suggested that this kind of complex interactions may be explained by considering RFs as filters in frequency space selective for multiple features. Their integration at the population level defines a volume visibility. Protocols that are expected to reveal

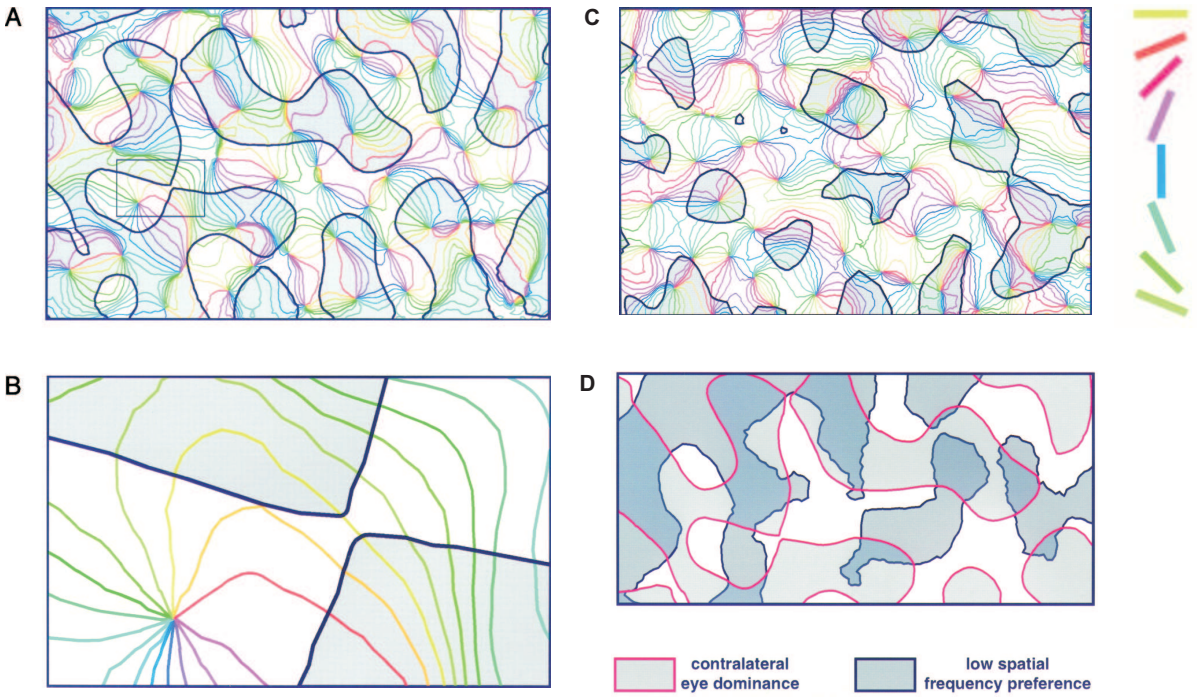

Figure 2.10 – Relationship between the cortical maps for orientation selectivity, spatial frequency selectivity and ocular dominance. **A**: Iso-orientation domains and ocular dominance regions. Gray regions represent dominance for contra-lateral eye. **B**: Close-up view of a region around pinwheel shown in **A**, showing the tendency for right angle intersections between two maps. **C**: Spatial frequency and orientation maps. Gray regions preferred low spatial frequencies. **D**: Ocular dominance and spatial frequency domains. Adapted from Hübener et al. (1997).

independent features of processing in V1 should be carefully selected in order to avoid the interdependencies of the stimulation itself.

The first explanation of how different features of visual processing are organized on the cortex was the ice-cube model. Discovery of spatial frequency selectivity maps motivated the scientists to modify the original ice-cube model by introducing an organization principle that considers the orientation and spatial frequency selectivity to be organized around a pair of pinwheels. In this direction, Bressloff and Cowan (2002a) suggested the spherical model of a cortical column. In this model, they added an additional dimension to the ring model in order to include spatial frequency preference. However, how new maps can be added to this model is not clear, as we do not have enough information about the interdependence of cortical maps.

Emergence of Cortical Maps as a Problem of Pattern Formation

The reason why the cortical maps exist and why they are dependent on each other is still an important debate. Plausible explanations include wiring length minimization (Chklovskii and Koulakov (2000)), dimensionality reduction (Durbin and Mitchison, 1990), and uniform coverage (Swindale et al., 2000). In fact, even salt and pepper organization may provide effective coding in certain cases where only a small number of neurons are involved in coding, thus neural wiring length is not a concern. However it should be noted that this is the case for less complex coding schemes, such as in rat visual cortex. Koulakov and Chklovskii (2001) compared salt-and pepper organization, linear zones and pinwheels and showed that each of these regimes can be efficient given some functional properties. Why a particular strategy is implemented in a certain animal brain can be understood by connectivity restrictions. On the other hand, self-organizing maps are capable of generating cortical maps when trained by retinal waves and natural images (Mikkulainen, 2005; Bednar, 2012), showing that natural environment and initial training plays an important role shaping the connectivity.

Ocular dominance like patterns can emerge from an homogeneous initial state, as a result of the competition between the inputs from each eye (Swindale, 1980; Miller et al., 1989). As the neurons that fire to the same stimuli tend to be closer for wiring length minimization, functional domains cluster together. The patterns created by this model is analogous to the Turing instability, a phenomenon that occurs in reaction-diffusion systems where there is a competition between excitatory and inhibitory mechanisms. Stripe-like patterns occur in reaction-diffusion systems in presence of lateral inhibition, as it is the case in the binocular input to visual cortex.

Chapter 3

Dynamics of Visual Cortical Activity

Functional classification of the individual parts of the visual cortical network is important in order to understand the role of each cell, population, or cortical area in information processing. In the recent years with the development of large scale recording tools such as functional magnetic resonance imaging (fMRI) and magnetoencephalography (MEG), neuroscience research is oriented towards this kind of system identification approach. The hard-wiring that leads to parcellation of functionally distinct brain regions is possibly defined by genetics (Rakic, 1988); even though during development several factors may alter this genetically pre-defined wiring. As we go lower in the organization, connections between the subunits become much more plastic, and system identification may not be valid anymore except for very short time scales. For example, sensory neurons adapt their response properties to the statistics of the external stimulation (Attneave, 1954; Barlow, 1961; Simoncelli and Olshausen, 2001; Schwartz and Simoncelli, 2001; Fournier et al., 2011). As a result of this adaptation, a cell that is identified to have a certain property may show a completely different behavior under different conditions.

System identification approach has often been preferred, partly because of the claim of considering the brain as a Turing machine. However, there are major differences between computers and brains. First of all, computer architectures such as the von Neumann model claim a distinction between processing, memory, and input/output streams. This is not the case in real neuronal networks (Koch and Laurent, 1999), in which neurons have the capacity to both process the information, and keep traces of each processed event in the structure of the network. Remembering the past events is done by adjustment of the synaptic weights and rewiring of the network. This process may even permit the usage of a neuron outside of its

putative role in the network, and may even cause suppression or recreation of new units.

Moreover, the notion of hardware and software becomes undetachable in the context of neural processing, and the "brain software" is highly dependent on the "brain hardware", which makes the brain architecture different than Turing machines (Petitot, 2003). This flexibility of hardware gives way to phenomena such as plasticity and learning, which lets animals adapt to their environment and survive.

In this sense, neural computations are highly time and context dependent. Neurons are often responsible of multiple tasks rather than doing an originally coded one single facet (Leventhal et al., 1995). The amount of active synaptic inputs to a neuron is estimated to be only 5-10% of all synaptic inputs (Shadlen and Newsome, 1998; Scannell and Young, 2002). Understanding the role of neurons in different contexts is crucial in order to better understand the neural code.

Dynamic aspect of neural activity is important for various tasks that are important for the survival of the animal such as decision making, perceptual binding, multimodal integration, and selective attention. How different areas of the brain, neural populations or single neurons that are responsible for distinct tasks communicate dynamically between them is a big question that has to be answered in order to understand how perception emerges. Here we will primarily focus on the problem of visual perception.

3.1 Coding strategies

3.1.1 Temporal vs. rate coding

Interpretation of the activity of a single cell in the context of the whole craves a plausible coding strategy. Two of the most popular hypothesis for neural coding are temporal coding and rate coding. Temporal coding indicates that the precise timing of action potentials codes for stimulus information. Rate coding indicates that frequency of firing of a cell rather than the precision of spike timing carries the necessary information to code a stimulus.

Relevance of the single neuron activity requires reliability as well as precision. Both of these aspects are considered to lack in temporal occurrence of action potentials of a single neuron, hence temporal coding is often presumed to be a bad strategy. Measures of discharge rate and total number of spikes are rather stable compared to temporal occurrence (Barlow, 1972). Shadlen and Newsome (1998) argued that rate coding should be considered as the main coding strategy in the cortex because of the low reliability of the temporal code. However, it should be noted that a

considerable amount of variability of discharge rates is also reported (Dean, 1981; Vogels et al., 1989). On the other hand, higher order moments of the temporal responses are as precise as a few milliseconds (reviewed in Abeles (1991)), and under naturalistic wide field stimulation neural activity is highly reliable (Baudot et al., submitted; Haider et al., 2010). Usually either of these two coding strategies is retained, but probably both are used in neuronal coding.

3.1.2 Coding by synchrony

Synchronous neural activity is found in many regions of the brain, at multiple temporal and spatial scales. According to Usrey and Reid (1999), synchrony in the brain could arise from three reasons: anatomical divergence, stimulus dependence, and emergent oscillatory activity. Synchrony by anatomical divergence results from the common input that cells receive and the strong hard-wiring between the neurons as explained in the previous chapter. This type of synchrony occurs in millisecond time scale, and mostly during the early processing. Stimulus-dependent synchrony does not necessarily result from anatomical connectivity: neurons may respond in a time-locked fashion even though they are not connected depending on the features of the stimuli. However, it should be noted that in V1, neurons that share common functionality are often connected. Emergent synchrony arises from the network activity as a whole, involving ensembles of neurons firing together.

One popular theory related to the role of synchronous activity in perception is the *binding problem* (reviewed by Gray (1999)). This hypothesis claims that the multiple brain regions, each responsible of detecting a particular independent feature, communicate between each other by synchrony and give rise to the perception of the object that arises from combination of each of these features. The idea is initially suggested theoretically (Milner, 1974; Grossberg, 1976; Von Der Malsburg, 1981) and the first experimental evidence was provided by Mioche and Singer (1989). The authors discovered that spatially segregated neurons were synchronized around 40 Hz in response to drifting gratings. Wolf Singer's team leaded the binding by synchrony hypothesis, suggesting that the Gestalt rules arise from synchronous representation of the parts (Gray et al., 1989; Gray and Singer, 1989) giving rise to the perception of the whole. It should be noted that these experiments were conducted on anesthetized preparations. Synchronous activity of functionally related neurons in anesthetized preparations may sign the "tendency" of functionally correlated neurons to synchronize (Kelso, 1995), probably arising from the first group of synchrony (anatomical divergence) suggested by Usrey and Reid (1999), rather than the second class of synchrony (stimulus dependence) which would confirm the binding hypothesis. If we think the brain as a dynamical system consisting

of neurons acting as coupled oscillators, the information coming from the sensory organs will be coupled to this oscillatory activity, resulting in a loss of the incoming information. This is indeed the case with the neurons in IT region which is a relatively high level structure in the brain, that do not show any or but a little response to sensory stimulation while the EEG is in a high voltage, slow and synchronous state (Gross et al., 1972). Some strategies for decorrelation of synchronous activity may be implemented in the brain in order to control the balance between the incoming sensory information and the internal percept that is created from the recent activity. This dilemma will be explained in more details further in this text.

3.1.3 Propagation in a cascade

A classical view to consider the perception to arise from coherent activity of a group of cells instead of a single cell goes as back as to Hebb (1949). He showed that slow processes that introduce "learning" by reinforcing the strength of connections among simultaneously active neurons are as important as short events for perception. This idea was further evolved to the *synfire chains* (Abeles, 1982). A synfire chain is a group of cells that fire in response to a particular stimulation triggering an activation of another group of neurons and so on in a chain of feed-forward and recurrent excitations, either in a synchronous or asynchronous mode. Abeles (1982) argued that the only stable mode of transmission is the synchronous mode. Later on, Izhikevich (2006) showed that time-locked but not synchronous firing may also reproduce interesting regimes such as gamma rhythms and conversion of firing rates to spike-timings. He called this principle as *polychronization*. Correlated activity in synfire chains depends on the distance between neurons, and may emerge independent of firing rate modulation (Vaadia et al., 1995), implying temporal coding strategy.

Dynamics of feed-forward activation of groups of cells in chain depend on the balance between excitation and inhibition. If the inhibition is dominant over excitation, the depolarization will spread a little or will not spread at all. If the excitation is dominant over inhibition, the activity will spread along all over the network. In between these two regimes, there is a critical point which is achieved by a particular balance between inhibition and excitation. In this critical regime, the depolarization can spread in cascades of bursts, activating a part of the network at once. This theory, introduced by Beggs and Plenz (2003) is referred to as *neuronal avalanches*, because of the similarities of the avalanches observed in critical sandpile models (Bak et al., 1987). Beggs and Plenz (2003) showed that the size of the bursts activated by a local discharge on slice preparations follow a $1/f$ distribution, which is often observed in complex systems that operate in a self-organized critical state.

3.1.4 Sparse coding

Since birth, animals observe the natural environment which is often locally continuous, exhibiting 1/f distribution in space and time (Ruderman and Bialek, 1994). The neural circuitry that is predefined by genetics is shaped by these particular statistics after exposure to external input. Photoreceptors in the retina provide very precise high-pass filtered extraction of a "pixel by pixel" information with highly overlapping, less than 1° receptive fields. In order to extract relevant information from this highly complex detection, it is possible that the brain performs some "compression", maximizing the information content of the incoming visual signal by using strategies such as redundancy reduction (Attneave, 1954; Barlow, 1961), noise filtering and generalization (Atick, 1992).

We, humans, are able to distinguish differences between very similar objects and notions. We can consider the language to reflect the notions that we are able to distinguish. In this case, the English language containing a quarter of millions of words may give an idea about the number of notions available for an English-speaking person. The words in a dictionary of course include synonyms, and an individual may not know all the words in a language. Even so, dictionaries lack the proper names that correspond to an individual object that a person can recognize ("my grandmother", "your pencil", "my neighbor's yellow Volkswagen car" etc.) which compensates for the lack of knowledge of certain notions, and may even surpass the number of distinct notions in a dictionary. Taking into account the number of each individual object, the number of distinct notions for an individual increases drastically.

If the number of notions that we are able to distinguish is so vast, how does the brain code for each object? Hierarchical organization of the visual system favors interpretation of more specific objects as we go further in the hierarchy. If we go on the top on the hierarchy, are there neurons that respond to only a specific object? This problem is referred to as the *grandmother cell* paradigm. The idea was used first by Jerry Lettvin around 1969 to question whether there are neurons in the cortex that are active only when a grandmother, or any specific subject is present in the sensory scene (Barlow, 1995; Gross, 2002). If this is true, removal of these cells from the cortical network would remove this notion from the brain, as pointed out in Lettwin's original short story (available as appendix in Barlow (1995)). Considering that the number of neurons in the brain would be too small compared to the number of "percepts" invalidates this possibility, as pointed out by the *yellow Volkswagen cells* hypothesis by Harris (1980).

Despite all these persuading counter-theories, a remarkable degree of sparsity is shown to exist in the human brain. Barlow (1972) first pointed out that the neu-

rons that are placed in higher areas in the hierarchy are much less active than the neurons in early stages. He argued that neural networks of a higher order structures attempt to form more specific representations. A recent study has shown the existence of cells that respond to the images or notions related to a particular person (for instance, the actress Jennifer Aniston) in the human medial temporal lobe (Quiroga et al., 2005), stating out that neuronal representations may be extremely sparse.

Sparse coding is shown to be an efficient strategy for pattern learning and memory storage, making the structure of the natural sensory input explicit, producing a low-dimensional manifold in the high-dimensional data space, and for energy efficiency (reviewed by Olshausen and Field (2004)). Sparseness is maintained by decorrelation of neuron pairs by an interplay between feed-forward excitation and surround suppression (Vinje and Gallant, 2000).

Field (1994) suggested that visual coding is optimal if natural scenes are represented by sparse coding in the brain. He explained the natural scenes to lie on a *state space*: Every statistical regularity would define the location and the shape of the particular image in that state space. He was the first one to notice that statistical measures such as principal components analysis (PCA) gives Fourier-like components of the data, similar to the receptive fields of the simple cells in primary visual cortex. He also pointed out that PCA is not enough itself for encoding. He argued that the features of natural images should be coded by kurtosis, which is a measure of sparseness.

Later on, independent components analysis (ICA) came on the scene (Comon, 1994). This method is indeed based on separation of components based on their kurtosis. Bell and Sejnowski (1997) showed that ICA on natural images can calculate the edge filters of the natural scenes. van Hateren and van der Schaaf (1998) compared the RF properties of simple cells in macaque visual cortex to independent component filters of natural images. They compared spatial frequency bandwidth, orientation tuning bandwidth, aspect ratio and length of the RFs to those of independent components, and observed that those properties match well. ICA on natural movies revealed similar results (van Hateren and Ruderman, 1998). An example of independent component activation in time is shown in Figure 3.1. The major difference between static images and natural movies was that natural images had a higher proportion of low spatial frequency filters. This result comes from the difficulty to track fast moving high spatial frequencies. These results are in coherence with optical imaging recordings that show that only low spatial frequency domains being activated by quickly moving stimuli, while both high and low spatial frequency domains get activated in response to slowly moving stimuli (Zhang et al., 2007).

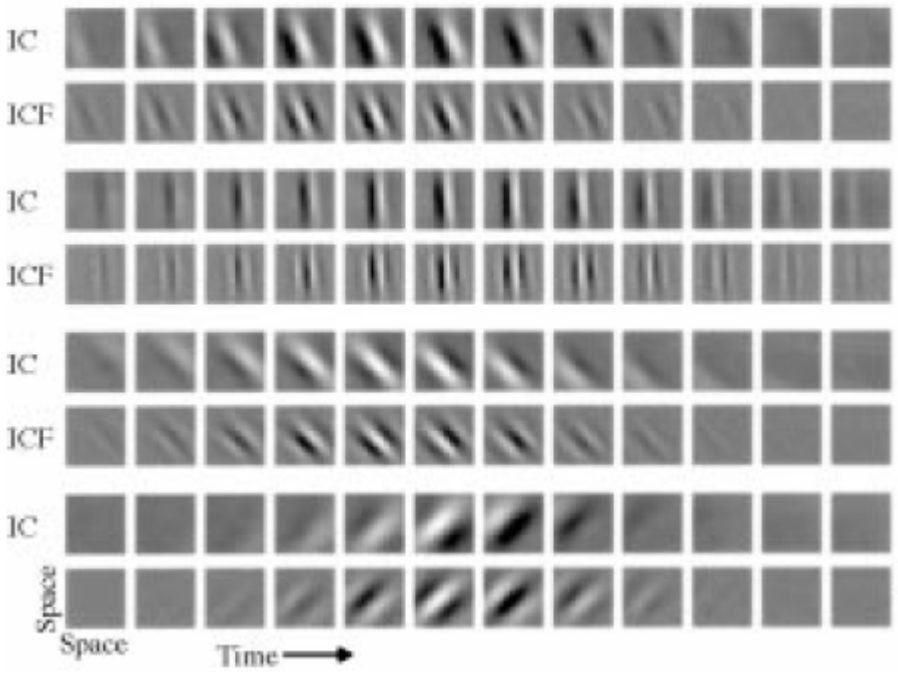

Figure 3.1 – Independent components (IC) of natural movies and corresponding filters (ICF) in time (from van Hateren and Ruderman, 1998).

3.1.5 Dynamics of inhibition and excitation in shaping neuronal responses

Neuronal dynamics are born out of a rich interplay between the activation of the ion channels. We can simplify this complex picture by considering two groups that summarize these interactions: inhibition and excitation. Control of the balance between inhibition and excitation maintains the dynamics of connectivity creating sub-networks and provides a fine tuning of this balance by timing of the inhibition and excitation, which provides sparse coding.

Main computations in the visual cortex are classically explained by the anatomical convergence of the feed-forward excitatory inputs (Hubel and Wiesel, 1962). However, cortical inhibition plays an important role in various tasks, including shaping of the orientation and direction selective tuning (Sillito, 1979; Monier et al., 2003) and spike timing (Harsch and Robinson, 2000; Bacci and Huguenard, 2006). Fast feed-forward excitation followed by cortical inhibition can also explain a number of observed phenomena such as reduction of trial-to-trial variability (Monier et al., 2003), sparse and precise coding and propagation of synchronous cortical activity (Litvak et al., 2003; Kremkow et al., 2010), and thalamic bursting that occurs during naturalistic stimulation (Wang et al., 2007). Diversity of interneuron types on the cortex is possibly pointing importance of inhibition and the variety of different task in which they are involved (Gupta et al., 2000; Monyer and Markram, 2004).

3.1.6 Dynamics of orientation tuning

On a theoretical point of view, feed-forward models predict that the orientation selectivity remains constant during visual response (Hubel and Wiesel, 1962; Troyer et al., 1998) while models with dominant intracortical activity predicts sharpening of orientation tuning (McLaughlin et al., 2000). Imaging studies showed that orientation tuning of small populations of neurons does not change with the duration of stimulation (Sharon and Grinvald, 2002; Benucci et al., 2007).

Sharon and Grinvald (2002) used VSD imaging to investigate the dynamics of orientation tuning at the population level. They showed that the tuning width remains constant during 300 ms of visual response to square-wave oriented gratings. The first response they observed was brightening of the signal across all the recorded area at 36 ms after stimulus onset. Right after this first response, orientation-selective response started and reached its maximum reproducibility at 46ms. Orientation selectivity peaked at 55 ms, and started to decrease for about 20 ms, and started to increase again. They called this temporary suppression "deceleration-acceleration" (DA) notch. The authors also showed that the selectivity reaches its peak at the same time as the first peak of orientation selectivity around the notch, and decreases to one third of its value around 100 ms. DA notch is possibly is a landmark of dynamics of inhibition and excitation (Borg-Graham et al., 1998). Chemla and Chavane (2010a) suggested that the DA notch is the residual of a phasic response to stimulus onset hidden under horizontal convergence of input coming from neighboring columns. It should be noted that the notch is not observed all the time, and it is often absent in awake animals. In response to natural movies, only deceleration is observed (Onat et al., 2011a).

3.2 Operating Regimes of the Visual Cortex

3.2.1 Variability of Neuronal Responses

As pointed out in Section 3.1, noise is encountered in every level of organization of the brain, revealed by any method, explained by any strategy. The spiking activity of a neuron in response to a visual stimulation is reported to exhibit high temporal trial-to-trial variability (Attneave, 1954; Barlow, 1961) *in-vivo*, corresponding to a Poisson or supra-Poisson behavior (Schiller et al., 1976; Heggelund and Albus, 1978; Vogels et al., 1989; Dean, 1981). Membrane potential fluctuations are also highly variable, following a Gaussian distribution (or bimodal distribution in case of up-and-down states). There are several reasons behind the variable activity observed in neural recordings. First of all, any system operating at more

than absolute zero temperature has noisy behavior. Thermal noise will be more effective on nanoscale activity at single ion channel level, resulting in random trial-to-trial fluctuations of ion channel functioning. Second important reason occurs at the microscopic scale: As a neuron integrates relevant information from hundreds or thousands of synapses, stochasticity among different synapses will be reflected in the neuron's output. Since the spiking activity is considerably reliable *in-vitro* (Mainen and Sejnowski, 1995), the high variability observed in *in-vivo* recordings is considered to be a result of the network activity. Third reason for observation of high variability is the technical methods used for recording neurons. Any invasive method that is used for recording neuronal activity, especially electrophysiological techniques, involves alteration of the physical structure of the neuron. This would lead the decrease in quality of the preparation over time, modifying the activity of the neuron. Fourth reason is the choice of measure used in assessing variability. Simple statistical measures such as standard deviation may not reveal the real structure of the variability. For example, a drift in the recording would lead to a high standard deviation while the important structure may be encoded in a different frequency range.

The possibility of a putative role of the noise led to different hypothesis about the neural code. At first, high variability was considered to be a limiting factor for sensitivity and information transfer efficiency of sensory neurons (Tolhurst et al., 1983; Heggelund and Albus, 1978). Later on, theoretical models showed that this is not the case and new theories were more focused on the advantages of noise for information transfer (Shadlen and Newsome, 1998; Abbott and Dayan, 1999; Litvak et al., 2003). Various explanations include predictive feedback from higher areas (Ringach, 2009), maximization of information transfer via stochastic resonance either by the strength (Wiesenfeld and Moss, 1995) or statistics of the noise component (Rudolph and Destexhe, 2001), and exploration of the phase space in decision making. Moreover, Marre et al. (2009) used the *frozen paradigm* to show that the ongoing activity should be considered as a result of information propagation in the network.

Considering the hierarchical structure of the cortex, uncontrolled noise may be amplified at each step of processing, resulting in a completely stochastic behavior of the global activity at the end. Hopefully, this is not the case in the cortical hierarchy. Shadlen and Newsome (1998) showed that the balance between excitation and inhibition in an integrate-and-fire neuron network model maintains the level of noise to stay at the same level in different layers of a feed-forward architecture. In contrast, Kara et al. (2000) showed that in anesthetized cats, level of noise increases from retina to LGN to cortex, nevertheless the maximum level is much less than what is thought before. What is to retain from these studies is that noise may

either stay at the same level at all layers of hierarchy, or may increase slightly from one layer to the other. But in any case, noise level never exceeds a certain value (certainly accepted as the level of the noise in a Poisson process).

Kara et al. (2000) explained the increase of response variability in the hierarchy by decreasing fire rates and decreasing absolute and relative refractory periods. Few other studies along with Kara et al. (2000) argue that the visual neurons are more reliable than previously thought. Gur et al. (1997) reported that variability of visual cortical neurons are much lower in alert monkeys during fixation. They argued that the high response variability observed in in-vivo awake recordings are dramatically reduced when influence of the eye movements are minimized. In a more recent study, the same team showed that the responses are as reliable as inputs from the retina and the thalamus when only responses during fixational eye movements are considered (Gur and Snodderly, 2006).

Previous results in our laboratory, with intracellular recordings and stimulus-locked frequency- time wavelet analysis, showed that noise and temporal reliability in neural activity depend on the visual input statistics context (Baudot et al., submitted; Frégnac et al., 2005; El Boustani et al., 2009). Natural scene animation was shown to evoke temporally precise sparse spike response and large and highly reproducible irregular fluctuations in the sub-threshold membrane potential, while drifting grating responses were highly unreliable for frequency bands other than the frequency of the stimulus. Spatial structure of natural scenes and the temporal dynamics of natural eye-movements increase the signal-to-noise ratio by a nonlinear amplification of the signal combined with a reduction of the sub-threshold noise. It is expected that large and reproducible fluctuations in the membrane potential of a single cell for a large frequency range during natural stimulation will be the reflect of distributed and precise stimulus-driven correlations in the cortical network activity. Any unrealistic stimulation would create a stochasticity at the network level, resulting in a highly variable response.

An interesting approach about the noise in the brain is the *free energy* principle (Friston et al., 2006). The idea comes from the tendency to disorder of the parts of a complex system in order to minimize the entropy of the states. Free energy is the unexpected happening of the joint occurrence of sensory input and its causes. Brain constantly tries to predict the incoming input and needs to minimize the prediction error. The information content that is received from the external world is therefore complemented with internal fluctuations in order to maintain a thermodynamic equilibrium in the brain. As a result, natural image responses, which is rich in information content pushes the neuron to completely focus on the incoming sensory input. When the incoming signal carries poor information (as in case of drifting grating stimuli), brain creates internal dynamics in order to provide more

information to neurons. This theory also explains why rich dynamics are observed during spontaneous activity. A recent work showed that stimulus and error coding coexist in the brain, providing evidence for the free-energy model (Eriksson et al., 2012).

Variability of neuronal responses may also be an important factor for evolution (Mainzer, 2007; Fontanini and Katz, 2008). Evolvability of a system requires exploration of different possibilities to solve a problem. Trials and failures, or success, would lead the system to keep or change a certain strategy that is previously implemented. If the neurons always do the same task, other possibilities could not be observed and the system cannot evolve.

3.2.2 Structure and Role of the "Cortical Noise"

A number of studies report that the "neuronal noise" may have a common structure among different neurons in the same network (Lee et al., 1998; Shadlen et al., 1996; Zohary et al., 1994). Correlation of the noise between two neurons depends on similarity of the receptive field properties (for instance, direction selectivity (Zohary et al., 1994)) and distance between neurons (Lampl et al., 1999). On the other hand, even though synaptic noise is often bad for reliability, noise correlations between excitatory and inhibitory conductances may sharpen the stimulus-specific tuning, hence increase response fidelity (Cafaro and Rieke, 2010; Salinas and Sejnowski, 2000).

Shared noise that decreases as a function of spatial distance or receptive field similarities was the first evidence that the noise in the brain might have a spatial structure (Zohary et al. (1994); Shadlen et al. (1996); Lee et al. (1998); Lampl et al. (1999)). Spatio-temporal profile of the ongoing activity was examined by Arieli and colleagues (Arieli et al., 1995, 1996)) by performing VSD imaging and microelectrode array recordings on cat visual cortex. They claimed that the neuronal response is a sum of a reproducible spatio-temporal component that adds up to another spatio-temporal pattern of activity that presumably reflects the initial state of the cortex. These results that were discovered using population recordings were further confirmed by intracellular recordings of membrane potential and spiking activities of adjacent cells (Azouz and Gray, 1999).

It should be noted that, as for the variability of single cells explained above, most of the work that found high noise correlation between nearby neurons are performed on anesthetized preparations. Studies on awake animals showed that these correlations seem to be strongly state dependent (Poulet and Petersen, 2008; Ecker et al., 2010; Civillico and Contreras, 2012). Moreover, spontaneous and evoked activities

may have different spatio-temporal structures during different brain states (Brunel, 2000; Vogels et al., 2005; Fontanini and Katz, 2008).

How the correlation between neurons is measured is of extreme importance. Estimation of the correlation coefficient from finite data may result in erroneously high values (Ecker et al., 2010). Moreover, indirect measures of the neuronal activity (such as calcium or VSD Imaging), or of metabolic measures (such as fMRI) include other signal sources that may not be related to neuronal activity at all. Presence of such artefacts may increase the level of observed correlation.

Spontaneous activity: is it simply the "ongoing noise"? Brain generates spontaneous electrical activity even in absence of any external stimulation. This activity is referred to as the "spontaneous activity", and whether this phenomenon is related to the ongoing noise that is present in evoked recordings or not is still ambiguous. In this text, we will use the term "spontaneous activity" to define brain activity in absence of external stimulation, and "ongoing activity" to refer to the stochastic component in the evoked signals.

Neural circuits are active even before the exposure to external stimuli. During development, retina, LGN and cortex are highly active, producing waves, spindles and slow wave oscillations respectively. This spontaneous activity during development plays a crucial role for the refinement of the neuronal connections before sensory experience (reviewed by McCormick (1999) and Sur and Leamey (2001)). For example, retinal activity during development is necessary for the development of layers and ocular dominance in the primary visual cortex (Shatz and Stryker, 1988; Stryker and Harris, 1986). These studies show the importance of internal fluctuations in shaping the network. While neuronal activity is shaped by internal sources during development, incoming stimulation from the external world becomes more important in shaping the structure and therefore the neuronal activity after development.

Spatio-temporal activity patterns observed in the spontaneous activity are reported to show signs of the evoked activity. The most striking example of spatially organized spontaneous activity is the appearance of orientation selective patterns during blank response in VSD imaging of the primary visual cortex (Kenet et al., 2003). This was also observed in multielectrode recordings by the same lab (Arieli et al., 1995). Han et al. (2008) showed that freshly experienced evoked states are replayed by the following spontaneous activity. The authors showed that the repetitive presentation of the stimulus response patterns persisted for several minutes of spontaneous activity. They argued that this effect may contribute to the short-term memory and learning. Berkes et al. (2011) showed that correlations between

spontaneous and evoked states increase with age and that they become more correlated with natural scene responses than synthetic stimuli. This evidence shows that not only in short-term activity, but also in large time scales, spontaneous activity is shaped by the percepts of the natural environment. This is probably due to the rewiring of the cortical networks by adaptation of the neuronal activity to the statistics of the natural environment. Indeed, Marre et al. (2009) showed in a modeling study that reliable spiking and subthreshold activities are obtained if the statistics of the external drive matches to those seen in the spontaneous activity. Moreover, in rat auditory and somatosensory cortex, patterns observed during spontaneous activity was shown to include an ensemble of possible evoked patterns both in anesthetized and awake animals, probably reflecting a vocabulary of events (Luczak et al., 2009). The authors emphasized that the stimuli they used are never experienced by the animal before; therefore the similarities between the evoked and spontaneous activities may result from cortical circuitry constraints, and not the replay of the previously learned patterns. Even so, this does not change the fact that the animals were previously exposed to other stimuli that are not 'completely' different than those used in the experiment. The stimuli used in the experiments were pure tones and natural sounds, and the recordings were performed on single cells. We can think this problem in the sparse coding context, indicating that the neurons in the brain provide optimal coding when they code sparse representations of the natural stimuli (Field, 1994). Therefore, even if a particular stimulus is never heard, the cortical vocabulary that is learned by exposure to other natural stimuli provides means to encode other stimuli.

We previously recalled the notion of Turing instability to explain cortical map formation. Turing instability can also reveal the appearance of orientation selective patterns during the spontaneous activity (Bressloff and Cowan, 2002b). Turing instabilities occur in media with competing activation and inhibition processes. Lengyel and Epstein (1991) showed that the inhibitory medium plays an important role in shaping the pattern formation for Turing structures in reaction-diffusion systems. Certain anesthetizers, including pentothal which is used by Kenet et al. (2003) and pentobarbital which is used in Han et al. (2008) act directly on inhibitory sites and enhance inhibition. Moreover, Mennerick et al. (2010) argued that voltage sensitive dyes modulate $GABA_A$ receptor function. Particularly, The blue voltage sensitive dye RH 1691 acts similarly like benzodiapezine, enhancing $GABA_A$ activation. It should also be noted that, recordings presented by Kenet et al. (2003) are performed with long exposure times (30s), which may aggravate this effect, and may damage the cortex by phototoxicity. Therefore, these studies may not reflect the operating regime of the cortex, but may explain how the network would behave in case of an extreme regime dominated by inhibition. Enhanced inhibition may re-

strict the spontaneous activity to the strongest connections rather than the others, which correspond to the orientation-selective connections in V1. Another critic to the approach of Kenet and colleagues is made by Goldberg et al. (2004). The authors showed that the self-organized feature map approach detects the dimensions in the data with maximum variance even when this variance is small compared to the overall variance.

3.3 Attractor States and Transient States

Efficiency in neural coding requires two competitive tasks: First, changes in the external world should be successfully detected and transmitted. This would force the brain to favor the external stimulation. Second, brain should construe this information in a more global context which is shaped by the present and recent past of the global network activity. This second requires the incoming information to be shaped by the internal activity in the brain. These two principles are accepted to underlie the brain functioning, which involves conservation of global coherence (functional integration) while maintaining regionally specific dynamics (functional segregation). Interplay between those two principles is reflected in the complexity measures, which evaluate the statistical independence between neuronal subgroups (Tononi et al., 1994; Friston et al., 1995). Results on brain networks and nonlinear systems with same connectivity profiles as the brain shows that high complexity measures are achieved when the interplay between local computation (segregation) and global activity (integration) are maximized.

In order to achieve this optimal interplay, it is possible that the brain circuits are continuously modified by favoring or penalizing connections with respect to the computational needs. Fine tuning of the connections would yield to emergence of patterns of connectivity, or *motifs* that reflect an instantaneous organization in the brain. Sporns and Kötter (2004) showed that the functional motif number and diversity in the real brain networks is very high compared to random networks, while the structural motif number stays comparably low. They interpreted the high number of functional motifs as maximizing the repertoire of functional circuits, and the low number of structural motifs as efficient assembly and encoding. Their results show that anatomical organization provide very limited information about how the brain networks organize in response to a naturalistic stimulation.

It is useful to borrow notions from dynamical systems theory in order to study how the brain activity is organized in temporal domain. A dynamical system is in an *attractor state* when the pattern of activity does not change in time under same conditions. When the patterns of activity change from one attractor to the other,

the system is in a *transient state*. When the attractor is continuous and is not only a simple point, movement of the system from one part of the attractor to another part may create an illusion that the attractor is changing. In this case, the system is in a *metastable state*. Metastable regimes in the brain are defined as a collection of simple attractors that are connected via an embedding on a more complex manifold. When the system is in an attractor state on this complex manifold, it will stay at a certain attractor point until the connection to another state is found by the trajectory. In these systems, noise is enough to switch the system from one state to the other (Kelso, 2012). Hence, stable states of a metastable system are also its transient states. Friston (1997) defined this kind of attractors as *complex attractors* and showed that this type of dynamics occur when the connectivity among simulated neural populations is sparse. Rabinovich et al. (2008) stated that the transient cognition would require metastable states, in which the reproducible transients are represented by a stable heteroclinic channel that consists of saddle points and unstable separatrices. This would result in a winnerless competition and robustness, and reproducibility may be achieved with this kind of metastability.

Models of neural systems such as Hopfield nets, integrate and fire models etc. study how the interactions between spiking neurons lead the system to an attractor state, which codes for a particular feature. This type of models may be more useful in order to study tasks that involve global dynamics such as short-term memory and decision making. Brody et al. (2003) argued that persistent activity can be a substrate for working memory. The authors reasoned that the persistent activity is coded as attractor states, and for this purpose the states should be persistent against distractors and noise at least over a period. This helps the short term memory to be encoded in the network state. However, recognition of new patterns is done in much more fast time scales and hence metastability may be difficult to be studied by these conventional methods. Maass et al. (2002) argued that *liquid state machines* are more appropriate for coding transient dynamics. They suggested that a readout neuron can extract salient features from the hundreds or thousands of inputs that it receives without needing to converge to an attractor state.

This paradigm also puts into question the experimental procedures that are used for system identification. Classically used stimulation profiles (such as drifting gratings for the primary visual cortex) are useful to identify single cell response profiles under a very restricted global context. This kind of stimulation profiles drive the cortical populations to converge to an attractor state. However, this kind of visual scenes are not common, and even impossible if we take into account eye movements. Taken into account that the time constants of neurons are about tens of milliseconds, rapidly changing visual scenes may not have enough time to drive the network to an attractor state. In contrast, natural stimulation is shown to drive

the network dynamics to rapidly changing spatio-temporal activity patterns in various systems. Theoretical explanations start as early as the notion of synfire chains (Abeles, 1982), which is also confirmed experimentally (Vaadia et al., 1995). These studies showed that neurons can rapidly form functional groups in order to perform a common task, and that these patterns change systematically following behavioral events. Sequences of patterns that are activated following of a stimulus is found to be reliable even though exact timing of the temporal activity is not precise in the olfactory antennal lobe of locust (Wehr and Laurent, 1996) and in the gustatory system of the rat (Jones et al., 2007). These results indicate that population coding by rapidly changing spatio-temporal activity patterns which would correspond to a succession of states (or the transient) provide more efficient coding than single unit coding.

Multichannel recording tools provide means to record temporal activity over multiple recording channels in which spatio-temporal neuronal activity can be studied. Dimensionality reduction methods such as PCA provide not only the spatial activity patterns, but also would show how these patterns are activated in time. This approach is used in various studies in order to investigate how neuronal activities are coded by different patterns in time (Stopfer et al., 2003; Mazor and Laurent, 2005; Briggman et al., 2005; Broome et al., 2006; Yu et al., 2009, review of techniques and results in Briggman and Abarbanel, 2006; Churchland et al., 2007). Using these methods it was shown that population responses discriminate distinct stimuli (Mazor and Laurent (2005)) or decisions (Briggman et al. (2005)) earlier than single neurons, during the transient response. These evidences show that neuronal populations are very efficient for discrimination during even very early responses.

Another related concept is how the patterns of activity or motifs that are evoked by external stimulation in the brain are related to the patterns that are observed during spontaneous activity. Goldberg et al. (2004) studied this question in a theoretical aspect and showed on a model that according to the relationship between the gain of cortical interactions (λ) and the ratio of the mean of the LGN input to its standard deviation (T/σ), three regimes of spontaneous activity are possible: Homogeneous, marginal and instable. In the homogeneous state, spontaneous activity can be explained by a single state, in which the fluctuations of distant pixels will be uncorrelated. This would be the case if both λ and T/σ are low, or when T/σ is dominant over λ. Instable state is obtained when λ is larger than 2. In this regime, the network is dominated by an uncontrolled excitation and diverges. In the marginal regime, spontaneous activity wanders on a continuous multidimensional attractor manifold. They reported that considering a high dimensional encoder that takes into account multiple visual features, same regimes are obtained given that preferred orientations are represented uniformly on the cortex. Nonuniform dis-

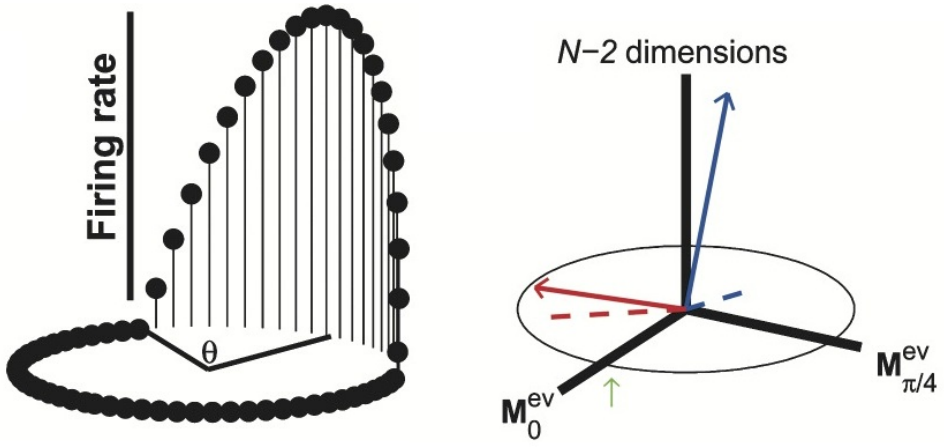

Figure 3.2 – Evoked and spontaneous maps on the continuous ring attractor of orientation selectivity. In the evoked state, firing rate of each column on a ring has a hill-shape, centered on the preferred orientation. Spontaneous maps reside in a N-dimensional space, two of which represent the evoked state dimensions that include the orientation-selective circle. In the multiple state scenario, spontaneous activity (red line) projects mostly onto the evoked maps (red dashed line). In the single state scenario, spontaneous activity (blue) will have a small projection onto the evoked state dimensions (blue dashed line). Adapted from Goldberg et al. (2004)

tribution of preferred orientations resulted in a collapse of the ring attractor to a small number of possible states. They concluded that only possible scenarios that are consistent with the empirical time scales of the fluctuations and the normal distribution of the similarity index between spontaneous and evoked states are the single state scenario, and the multiple feature scenario encoding at least ten different features, given that the preferred orientation is uniform on the cortex.

In conclusion, not only structure and connectivity of single units, but also the dynamic interplay between them is important for neuronal coding. Study of the visual cortical network as a complex dynamical system would help us better understand how single neurons get involved in coding by populations. In this sense, an important point to understand is the state space of visual dynamics, and the trajectories that are followed in this space under different stimulus conditions.

Chapter 4

Analysis Approach: Composition of VSD Imaging Recordings and the Source Separation Problem

As we pointed out in Chapter 1, the main drawback of VSD imaging is the weak signal-to-noise ratio. The neural re-emitted fluorescence signal related to the evoked neural activity constitutes indeed only about 0.1% of the total signal recorded by the camera. This signal reflects a mixture of instrumental and physiological artefacts, neural signal and background noise. Moreover, stimulus-induced neural-related activity contains evoked deterministic response and neuronal noise. In order to perform a single-trial analysis on the data, it is necessary to extract the neural-related signal by using a proper method. In this Chapter, we will explain various sources in VSD Imaging recordings, and we will present the strategies to extract the neural-related components in this rich mixture.

4.1 Composition of VSD Imaging Recordings

Baseline fluorescence and bleaching Bleaching and baseline fluorescence are the strongest artefacts that are observed in VSD Imaging. Light exposure diminishes the fluorescence of dye molecules by damaging their chemical structure, resulting in a decrease in light intensity following light exposure. This phenomenon is observed as a decay in the amplitude of the fluorescence, which is referred to as the *bleaching* effect. Although most of the studies retained single-exponential model for bleaching, we observed a double-exponential phenomenon. Double-exponential nature of bleaching is common in fluorescence recordings (Eggeling et al., 1998;

Gavrilyuk et al., 2007). This decay adds up to the baseline fluorescence that reflects the initial state of the cortex as well as a DC value for staining. Baseline fluorescence is highly variable among trials.

Blood supply The strongest biological noise source is the blood supply. Blood pulsation not only introduces a physical warping to the cortical tissue, but also supports the metabolic changes related to the neural activity. Biological artefacts that are related to the blood supply can be categorized as direct and indirect artefacts. Direct artefacts consist of the image of the vasculature and the physical warping. Using conventional methods, image of this kind of vasculature can be efficiently removed by first frame analysis. However, image of the vasculature may change after almost one second of stimulation as a result of metabolic blood volume change. Indirect vasculature artefacts are related to the neural activity. These include all the metabolic changes resulting from blood flow in response to neuronal activity. Vasculature patterns are closely correlated in space with the functional organization of the cortex (Zheng et al., 1991; Wang and Roe, 2011). In this case, nonlinearities may occur and spatial profile may change as a result of blood volume alteration. Moreover, frequency of the heart beat cannot be controlled externally; therefore the rate may vary over time. For the same reason, irregularities from one beat to the other may occur.

Intrinsic signal Although intrinsic signal can be investigated under indirect blood-flow related artefacts, it is more convenient to consider this signal separately as it is well studied by the intrinsic optical imaging community in order to understand the nature of the intrinsic signal. Additionally, oxygenation-related intrinsic change occurs at the neuronal sites rather than blood vessels, which distinguishes this signal from other blood flow-related artefacts.

Neural stimulation induces activity-dependent changes related to the oxygenation and blood volume change in the brain, as explained in details in Chapter 1.3. This intrinsic change is also observed within the illumination range of VSD Imaging, therefore it contaminates the fluorescent signal. Oxygenation change of the tissue is reported to be a linear combination of oxyhemoglobin and deoxyhemoglobin concentrations, which can be modeled as $\Delta[O_2] \propto \Delta[Oxy] - \Delta[Deoxy][Oxy]_0/[Deoxy]_0$ (Vanzetta and Grinvald, 1999).

It should be noted that the intrinsic signal recorded by VSD imaging is not the same as the one of intrinsic optical imaging, because of the different wavelengths of the light that is used in two techniques.

Respiration Air pumping from the lungs to the rest of the body results in a very slow (~0.4 Hz) physical warping. In our case, this mechanism is controlled externally by a pump, therefore this artefact is synchronized among trials and it is not difficult to remove it by conventional methods. This signal is often discarded from the analysis because it is slow enough to be discarded in short timescales of acquisition (~1 sec); but in any case it is present as well for short recordings.

Neural-related activity VSD Imaging records the fluorescent signal emitted as a reflection of the instantaneous membrane potential by the activation of dye molecules that bind to the external surface of cell membranes. The amplitude of the fluorescent signal is considered to be linearly correlated with the membrane potential and the total stained membrane area under a pixel (Grinvald and Hildesheim, 2004). Visual full-field drifting grating stimulation evokes an increase in fluorescent signal on the cortical surface and has proportional amplitude with respect to the orientation (and direction) selectivity of the imaged column (Shoham et al., 1999). Although the deterministic sensory-evoked response can be easily observed this way, there is a high trial-to-trial variability of the membrane potential response that should also be taken into account.

Other sources We also observed a lateral warping of variable frequency and amplitude among periods of oscillation at higher harmonics of the heartbeat rate. The warping was strongly synchronized with the acquisition. This component was very strong in amplitude, and was also present in BS-cleaned responses. This signal is possibly related to the arterial pulse wave that results from the opening/closing of the arterial valves, revealed in higher harmonics of the heartbeat frequency. It often had slightly variable amplitude and frequency per each peak, which makes it very difficult to be removed by any method cited in this study.

Illumination noise at 10Hz with 5 harmonics reported by Reynaud et al. (2010) was not very strong (almost and often absent) in our recordings. One important instrumental noise source was 50Hz line noise, which cannot be controlled and synchronized among trials.

Some recordings were contaminated by a patterned camera noise, organized as 3 square groups of 16 pixels each with altered fluorescence (one very high, one very low, one flat). These patterns occurred randomly on different places for different frames, and were not predictable. This artefact is related to the design of the acquisition system that sends the packets by groups of adjacent pixels. Square patterns were observed previously by the imaging community (Reidl et al. (2007), Isabelle Ferezou, personal communication).

Shot noise related to the stochastic fluctuations of light also contaminates the recordings. It is impossible to remove shot noise with any statistical method, as it is of non-deterministic nature. Furthermore, this noise source is indistinguishable from the neuronal noise; therefore it is more convenient to leave it in the signal than removing.

4.2 Denoising strategies

VSD imaging measures the neural activity by means of fluorescent light, and most of the time desired signal is highly contaminated by artefacts. A common way to isolate the signal from the artefacts is to perform repeated recordings of the same protocol in order to calculate average signal in response to stimulus. A 'blank' response to uniform luminance screen is recorded as a control, and this signal is subtracted or divided from the stimulus-induced evoked response. More sophisticated approaches have been also developed for denoising VSD imaging recordings. In the following of the text, we will explain the classical methods and statistics-based alternatives for denoising.

4.2.1 Conventional Methods for Denoising VSD Imaging Data

Conventional methods for denoising of VSD recordings involve utilization of the average of blank response trials as a control. This signal is subtracted from the trials of the evoked response in order to remove repetitive artefacts. This method is referred to as *blank subtraction*.

Blank subtraction is often done after *first frame analysis*, which consists of dividing each frame of a trial by the mean of the first frames. This procedure permits removal of supposedly-constant spatial structures such as baseline fluorescence and vasculature image. This method assumes that the first frames reflect mostly the baseline fluorescence, and neural-related fluctuations are either negligible or that evoked activity sums up to the spontaneous activity (Arieli et al., 1996) which permits extraction of evoked reproducible signal independent of spontaneous fluctuations in the neuronal network.

Other well-known methods include blank subtraction with linear detrending that permits removal of low-frequency trends in blank-subtracted signal (Chakraborty et al., 2007; Chen et al., 2008) and removal of bleaching by exponential fit followed by removal of heart-triggered average (Lippert et al., 2007).

For all these methods, recording multiple trials of the responses to same stimulus in order to calculate the ensemble average is necessary. Although the methods based

on using average blank as a control are useful to determine the evoked reproducible part of the signal, an important non-deterministic part of the dynamics is neglected by this approach. First of all, blank response includes not only artefacts but also the spontaneous activity which may have a spatio-temporal structure (Kenet et al., 2003). Even after averaging of multiple trials of blank recording and filtering high frequency components, some patterns may still be present in the resulting blank condition. Second, during the control condition, artefacts are supposed to be synchronized among trials of evoked and blank responses. Even though this holds for some artificially-controlled components (such as respiration, illumination), it is not always possible to control non-reproducible components such as 50Hz line noise. Heartbeat rate may also vary in time, resulting in a phase shift in heart beat artefact towards the end of the trials. Moreover, this approach discards the event-related modulation of single-trial activity which may result in trial-specific evoked activity, possibly involving nonlinear interactions between ongoing and evoked states (Truccolo et al., 2002). Development of methods that permit single-trial analysis is necessary in order to investigate real-time dynamics of VSD signal. In order to develop adequate methods for denoising, one possibility is to consider the nature of each source contributing to the final mixture, and the relationship between these sources. Now we will explain the statistical measures that take into account these points.

4.2.2 Statistical Methods for Source Separation

A better approach for denoising would be to investigate the nature of each signal source and the correlations among sources, then to use an adaptive strategy for each trial to remove unwanted contributions to the signal. Estimating the nature of these sources in the imaging signal is crucial in order to better understand the observed VSD imaging data, and to extract the signal of interest.

Separating multiple signal sources from a mixture is a common problem in digital signal processing. A good illustration of the source separation problem is the *cocktail party problem* (Figure 4.1): The problem consists of extracting voices of n people talking in a cocktail party, recorded by a number of microphones. Sources are supposed to be mixed by a procedure that will be recovered by using the assumption about the mixing procedure and resulting mixtures, with or without any knowledge about the nature of the sources.

Linear source separation methods assume that the observed signal is a linear mixture of a number of sources, and that these sources are mixed in a way to permit separation by using a linear technique. In case of neuroimaging, mixture of the sources can be formulated as

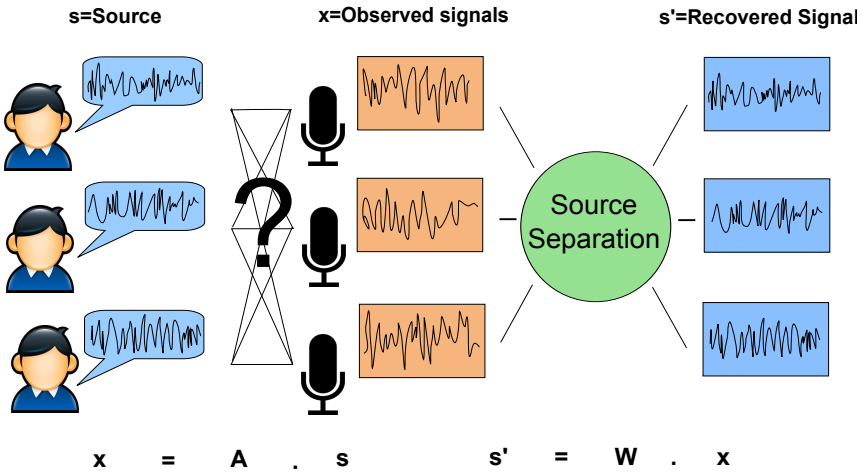

Figure 4.1 – Cocktail Party illustration

$$S(x, y, t) = \sum_n \lambda_n a_n(t) M_n(x, y)$$

where $a_n(t)$ stands for the temporal activation of the spatial map denoted by $M_n(x, y)$, and λ_n is the total energy of this combination. The aim of source separation is to find each of these components, or to provide a separation of meaningful components. In the cocktail party analogy, $a_n(t)$ would be the speech of a person, and $M_n(x, y)$ would be the location of each microphone.

The way how this source separation can be done raised a big debate in the neuroimaging community (Friston, 1998; Stone, 2002). The most common methods can be investigated under two groups: *model-based* and *data-driven* methods. Model-based methods are based on fitting the observed data to a set of source vectors that are defined a priori. Data-driven methods take into account the correlation or dependence of signal sources on each other, without any prior knowledge concerning the nature of the signal sources. Both methodologies have advantages and disadvantages, and the choice of appropriate method depends on the nature of the data to be analyzed.

Advantages and disadvantages of these two strategies are shown in Table 4.2.1. We can see in this table that the advantages of one approach are often disadvantages of the other. The most important factor for choosing an appropriate method is the availability of prior knowledge about the nature of sources. If the nature of the signal sources is well known, model-based methods do good job. If no prior knowledge is available, data-driven methods should be used instead. Data-driven methods are based on weak models of the data, implying only constraints about the nature of dependence between sources rather than their exact form, as it is the

case for model-based methods.

Model-based methods are appropriate as long as the contributing signal sources are well known from the beginning and the dependence between sources is rather ambiguous. On the other hand, unpredicted sources may be extracted more efficiently by data-driven methods. One consequence of the data-driven approach is the difficulty to interpret meaning of the extracted signal sources: It may be difficult to evaluate the underlying mechanism of a resulting component from ICA or PCA if we cannot make any interpretation about the nature of the component. On the other hand, model-based methods restrict the signal strongly to the predefined source set, while the same problem arises for data-driven methods about the hypothesis underlying the relationship between sources.

	Model-Based Methods	**Data-Driven Methods**
Pros	-Good if the nature of the signals sources are known	-No prior knowledge is needed regarding the nature of the sources -Takes into account spatial correlations
Cons	-Restricted to user-defined model signals -Signals are difficult to be specified a priori explicitly -Same model may not hold for all pixels for the basic models	-Strong dependence on method requirements -Difficult to evaluate meaningfulness and statistical significance of resulting sources -Results may not be repeatable among trials, subjects, and tasks -No assumption is made about the nature of extracted components
Examples	General Linear Model (GLM)	Principal Component Analysis (PCA) Independent Component Analysis (ICA)

Table 4.2.1 – Comparison of model-based vs. data-driven source separation strategies.

Another important issue concerning the model-based techniques is the domain of interest for signal separation. Spatio-temporal nature of the signal gives the opportunity to think of the separation problem either in temporal or spatial domains. Model-based techniques generally investigate the problem in temporal domain, as it may be difficult to make assumptions about the spatial structure of the recordings that differ among individuals. Data-driven methodologies provide the opportunity to search either spatial or temporal sources of the signal. Another difficulty while using model-based techniques is to predict the activity that may have different latency for different pixels.

Most of this source separation discussion is conducted by the fMRI community. As it is for fMRI, denoising and neural population discrimination can be both considered as source separation problems for VSD imaging. Now we will explain in

details the most well-known techniques for both approaches, and their application to multichannel data.

Data-Driven Source Separation

Data-driven methods assume that artefacts and evoked signal are statistically uncorrelated or independent. Data-driven methods aim to separate different sources of signal with respect to their statistical distributions. This approach is also referred to as *blind source separation* as the separation is done only by observing the output without any knowledge about the nature of the sources. Consequently, data-driven methods do not explicitly define the nature of signal sources. An additional method is often needed in order to detect whether a resulting source is related to the neural activity or not.

The most well-known methods that use a data-driven strategy are PCA and ICA.

Principal Component Analysis PCA is the most primitive approach among data-driven methods. It provides an orthogonal transformation of the data in which the basis vectors are separated with respect to their variance, and ordered with respect to their energy. Eigenvalue decomposition of the covariance matrix and singular value decomposition (SVD) algorithms are the most common strategies to perform PCA. These two methods are very similar. We will explain the covariance method as the relationship with statistics is clearer.

PCA by covariance method involves finding eigenvectors of the covariance matrix. In other words, decomposition is based on finding orthogonal axes that maximize the covariance among signal sources. Principal components are the projections of the raw data on the eigenvectors of the covariance matrix.

PCA is based on the second order moment about the mean, which is proportionate to the variance. This fact implies that the method relies on the hypothesis that the signal sources are linearly uncorrelated.

Although it is tempting to do PCA on the domain that consist of smaller dimensionality, orthogonality assumptions may not hold for both domains. One common approach is the *snapshot method* (Sirovich, 1987). This method suggests that the eigenvector decomposition of the covariance matrix of the large dimension (in our case, pixels) is the same as those for the smaller dimension (in our case, frames). This method provides a proof for the interdependence between the eigenvectors of the two dimensions, but discards the fact that the data has to be centered before this application. In other words, when PCA is done on the temporal domain, temporal activation of each pixel has zero mean. When PCA is done on space, each frame

would have zero mean. Zero mean for one dimension does not apply for zero mean for the other. Although temporal and spatial PCA give similar results, they may not give exactly the same values. It is more convenient to consider the signal sources to have temporal profile in VSD imaging data. In this case, mixing procedure is done by each pixel (like the microphones in Figure 4.1). Therefore, it is more convenient to consider PCA in temporal domain.

PCA-based methods are reported to be successful for extracting the signal of interest for intrinsic imaging (Everson et al., 1997; Gabbay et al., 2000; Stetter et al., 2000; Sirovich and Kaplan, 2002; Sornborger et al., 2003), fMRI (Mitra and Pesaran, 1999), and VSD imaging (Prechtl et al., 1997). The latter was done by applying PCA in the frequency domain, in order to extract waves of activity in turtle visual cortex rather than removal of artefacts.

PCA-based methods often use a supplementary method in order to discriminate the desired signal from the unwanted components. The methods previously used in the literature include indicator function (Everson et al., 1997), truncated difference (Gabbay et al., 2000) and periodic stacking (Mitra and Pesaran, 1999; Sornborger et al., 2003). Fekete et al. (2009) used spatial PCA on VSD imaging data and used the first components as vascular pattern templates. They removed the vascular-related patterns from the recordings by performing a local similarity minimization on each frame. Another variant of PCA is the generalized indicator functions, which is developed by Yokoo et al. (2001) in order to analyze intrinsic imaging signals.

PCA-based analysis methods cited above are mostly aimed for searching spatial activity patterns rather than the temporal dynamics of the cortical activity. This is partially a result of the temporal frequency limitation of intrinsic imaging and fMRI recordings. One exception is Prechtl et al. (1997) where the authors searched spatial patterns that are activated by different frequency bands and reconstructed waves of activity in VSD imaging recordings on turtle visual cortex. On the other hand, when used for separation of independent or uncorrelated neuronal populations rather than the denoising aspect, PCA and other blind source separation methods provided good separation of neural populations that have different temporal dynamics in electrophysiological recordings (Stopfer et al., 2003; Mazor and Laurent, 2005; Briggman et al., 2005; Yu et al., 2009). These studies are often performed on multielectrode recording data which provide good temporal resolution but lack spatial resolution (except Briggman and Abarbanel (2006), where the authors used VSD imaging to evaluate both temporal and spatial profiles of neuronal activity). Moreover, in most of the studies in the literature, recordings are done on cortical areas which lack spatial organization of receptive field properties. VSD imaging provides a compromise between high temporal and spatial resolutions in which we can investigate both spatial and temporal aspects of the neuronal re-

sponse in the visual cortex of cat. Recently, Onat et al. (2011b) used PCA on the stable region of the average response to a single drifting grating (400 ms following stimulus onset). The authors showed that the direction of motion of the grating is separable with PCA. Their results show that other interesting features of VSD data rather than the common activation of the orientation-selective regions in response to drifting gratings may be extracted using PCA.

PCA provides an orthogonal basis in which the variance among signal sources are maximized. This implies that PCA finds signals that are uncorrelated. Uncorrelatedness states that the covariance between observations of two variables is zero. In case of zero-mean vectors, this implies orthogonality. However, uncorrelatedness does not imply independence. For example, consider X to be a continuous random variable uniformly distributed on $[-1, 1]$, and $Y = X^2$. Observations of X and Y will be uncorrelated even though we can determine the values of one with only the knowledge of the other. Therefore, uncorrelatedness criterion is not enough in order to determine signal sources that do not depend on each other.

Independent Component Analysis Two random variables are statistically independent if the knowledge of one does not imply any information about the other. A number of different algorithms have been developed in order to provide separation of signal sources depending on independence (see Comon (1994) for a review). The most well-known algorithms applied to neuroscience are *Infomax* (Bell and Sejnowski, 1995), and *FastICA* (Hyvarinen, 1999). Infomax is based on maximization of the information flow in a network of nonlinear units. FastICA is based on maximization of negentropy of sources estimated by kurtosis, which is proportionate to the 4th order moment around the mean. Although two algorithms are different, they are both based on higher order moments. One advantage of the FastICA is that it can very rapidly converge to a solution.

Usually, FastICA is applied to data already whitened by PCA. On the orthogonal low-dimensional space defined by PCA, the algorithm searches the axes that maximize kurtosis. This leads to finding sparse representations of the data. The main idea comes from the central limit theorem which indicates that the distribution of sum of independent random variables tends toward a Gaussian distribution. Therefore, maximizing the non-Gaussianity of the source vectors at each step by using kurtosis or any other method permits detection of independent sources that contribute to the signal. Main hypothesis of ICA is that sources are statistically independent and non-Gaussian.

ICA is widely used in EEG, fMRI and other neuroimaging tools in order to remove the artefacts and for finding the patterns of neural activity (McKeown et al., 1998; Jung

et al., 2001; Makeig et al., 2004). Some attempts have been done also for using ICA on optical imaging data. Reidl et al. (2007) showed that spatial PCA of VSD imaging recordings on olfactory bulb and somatosensory cortex of mice as well as on the visual cortex of monkey could not successfully remove artefacts from the neural activity, while spatial ICA following PCA could achieve this goal. It should be noted that the results of ICA on monkey cortex reported in this paper seem to contain a mixture of artefacts and noise, hence it is useful to exploit this method to have a rough idea about the sources, but the separation by ICA is not ideal for removing all the noise from the signal. Brown et al. (2001) used temporal ICA to separate independently active neural populations in sea slug revealed by optical imaging. Maeda et al. (2001) used temporal ICA to separate noise from signal obtained by VSD imaging of the auditory cortex of Guinea pig. These two works seem to provide good separation, however it should be noted that the biological artefacts such as heartbeat are much less strong in smaller animals.

Another method for blind source separation is extended spatial decorrelation, which relies on only second order statistics (Schießl et al., 2000). The authors showed that this method outperforms PCA and ICA on intrinsic imaging data.

Model-Based Source Separation

Model-based methods require all the possible signal sources to be determined a priori. Then, these signals form a regressor base in which the raw data will be projected. Most well-known example is the GLM.

General Linear Model The main assumption of GLM is that the observed signal is a linear mixture of all the source signals. In the most basic form of the model, all pixels are considered individually. Raw signal *S(t)* is considered to be a linear combination of different signal sources, and the noise:

$$S(t) = \sum_n \lambda_n a_n(t) + r(t)$$

For the denoising aspect, it is convenient to divide these signal sources into two groups as signals and artefacts. To solve the linear decomposition problem, all possible signal sources are included in an appropriate base of regressors, and their energies are estimated by finding the Moore-Penrose pseudo-inverse by least-squares fitting of the regressor basis on the original data. The only constraint on the regressor basis is to have full rank. Orthogonality as in PCA, or independence as in ICA among the vectors of the regressor basis are not necessary.

Model-based methods are based on fitting the data onto a regressor basis in order to find the contribution of each possible signal source to the observed signal. GLM is a model-based method and is the conventional technique for fMRI analysis (Friston, 1998; Woolrich et al., 2004). The original model which had been developed for fMRI was used for denoising of synoptopHfluorin imaging (Bathellier et al., 2007) and VSD imaging (Reynaud et al., 2010).

Reynaud et al. (2010) were the first to develop a model-based denoising approach for VSD imaging data. In order to perform the GLM, the authors inquired nature of all the sources that contribute to the VSD imaging recordings on awake monkeys. First, they performed synthetic experiments on a piece of paper. This permitted them to characterize the noise related to camera and dye bleaching. They observed an illumination noise at five harmonics of 10Hz and they declared the dye bleaching to follow a single-exponential decay. Second, they determined the physiological sources by calculating the power spectrum density (PSD) of blank recordings. They observed an additional peak that corresponded to the heartbeat frequency in the PSD of the blank compared to the synthetic experiments. Third, they modeled the evoked response to rise after stimulus onset with a variable delay and slope, stay on a plateau during stimulus, and decay with a variable delay and slope after stimulus offset. They performed PCA on a set of possible evoked responses with variable slopes and delays, and retained less than 10 of the first principal components to include in the regressor basis. The set of regressors they used, and resulting GLM fitting is shown in Figure 4.2.

The GLM approach developed by Reynaud et al. (2010) provides a good denoising of VSD imaging data, with a clear view of the nature of sources contributing to the signal. In the work presented in this thesis, we first developed a modified version of their GLM regressor basis. The reason behind this choice is simply because regressor basis for GLM would not be the same for different experimental preparations. We work on recordings performed on anesthetized cats, which makes synchronization of physiological artefacts easier compared to awake monkey preparations. This provided us the possibility to check the performance of GLM by evaluating the synchrony of artefactual components. We divided the resulting sources into two groups as neural-related and artefact-related components. We applied PCA on these two groups in order to evaluate the success of GLM denoising. This step permitted us to detect the amount of contamination in these two groups by evaluating the amount of synchrony between the average blank and evoked activities for each component. Combining the GLM method with PCA also overcomes the problems of working with only one approach alone. Once we denoised the data, we applied PCA and ICA in order to separate uncorrelated or independent neural populations. In the following chapters, we will present the results of this approach.

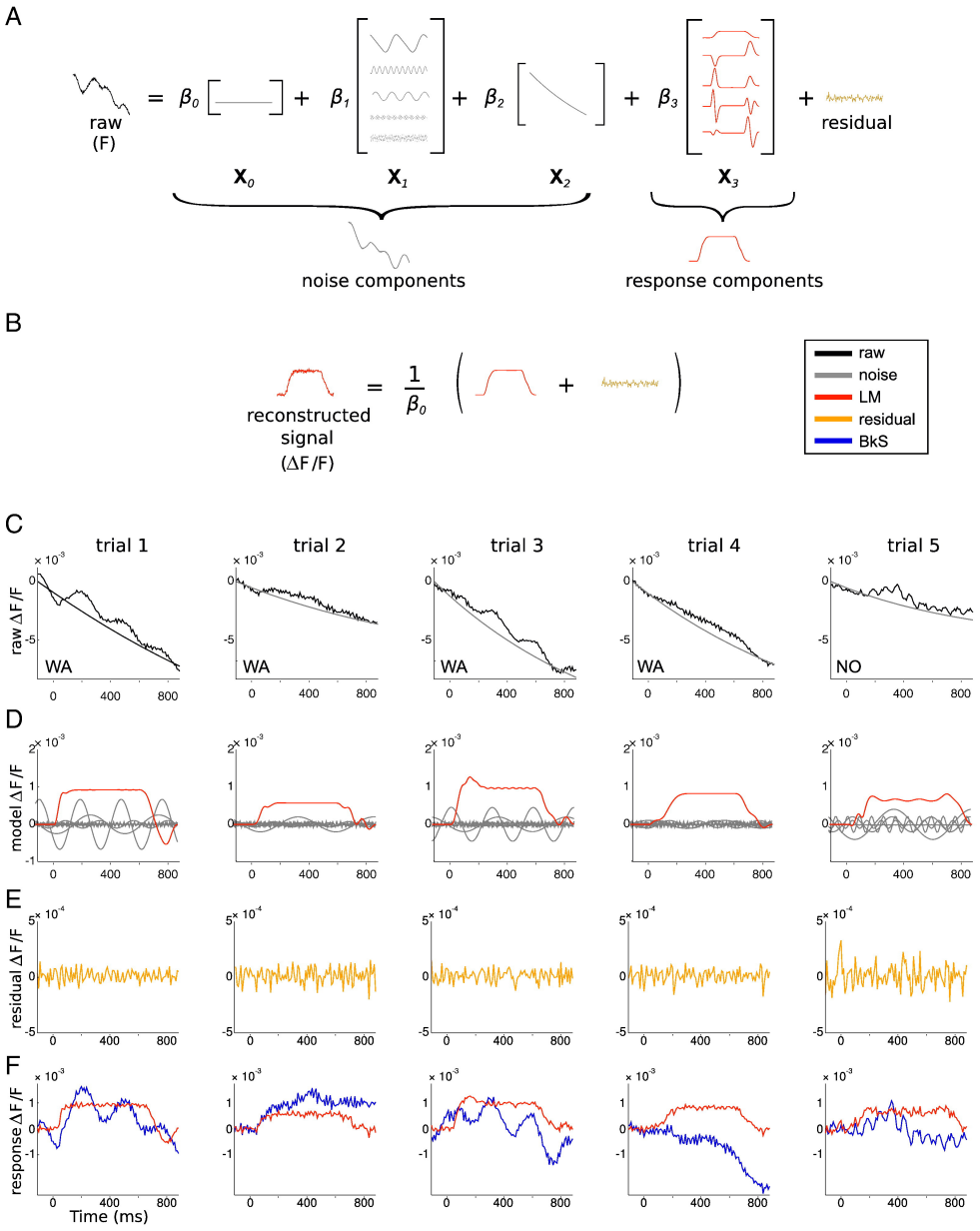

Figure 4.2 – GLM regressor base (A) and resulting reconstruction on monkey VSD imaging data (C). B depicts the retained signal sources. Reproduced from Reynaud et al. (2010).

Part II

Methodology

Chapter 5

Experimental Setup and Data Analysis

In order to study mesoscopic dynamics in primary visual cortex of the cat, we performed VSD imaging on cortical areas 17 and 18.

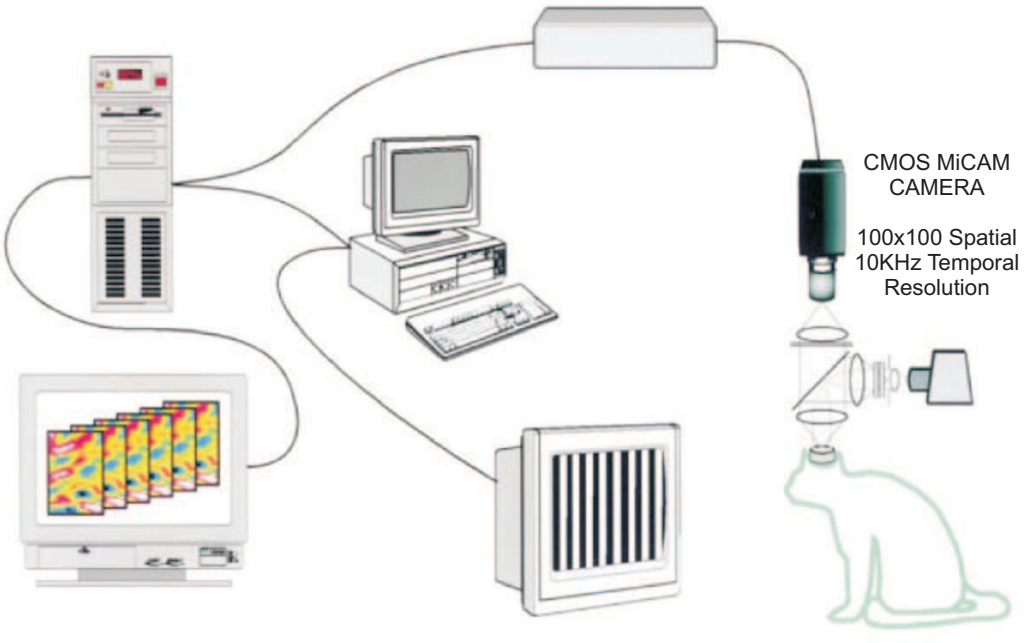

Figure 5.1 – Experimental setup (modified from Shoham et al. (1999)).

The main components of the experimental setup are shown in Figure 5.1. More details about the setup can be found in Shoham et al. (1999). Acquisition, visual stimulation and preliminary online analysis is controlled by the Elphy software (on the central computer) by communicating with the acquisition program provided by

the Imager system (Figure 5.1, on the left).

We used a CMOS MiCAM camera which provides 100x100 pixel resolution and up to 10 KHz temporal resolution. We recorded at 200 Hz temporal resolution in order to obtain a better sampling of the emitted photons. One pixel in our recordings corresponded to ~60x60 μm of cortical sheet.

5.1 Animal Preparation

We performed VSD imaging on 6 adult cats. For each animal, data was recorded on only one hemisphere. On one animal, two different recordings from the same hemisphere is analyzed. Three of the recordings included both areas 17 and 18. If this was the case, regions of interest that contain only one of areas 17 and 18 are analyzed separately. All the other recordings included only area 18. With the separation of the two visual areas, we analyzed 10 cortices in total.

Animals were initially anesthetized with intravenous alfaxolone (10mg/Kg). Following tracheotomy, animals were artificially respirated and anesthetized with 1-1.5% (0.6-1% during recording) isofluorane gas added to the 1:1 N_2O and O_2 mixture. Minimum alveolar concentration (MAC) is kept above 1%. Animals were head fixed on the anti-vibration table. The skull was opened above areas 17 and 18 (size of the craniotomy was ~1.5 cm in diameter), and the dura was resected. Paralysis was maintained by pancuronium bromide (0.4 mg/kg per hour, intravenous) administered starting <3 h before imaging in order to abolish eye movements. Accommodation and pupil contraction were blocked by atropine and neosynephrine. Three-millimeter artificial pupils were used and appropriate corrective optical lenses were added if it was necessary. The position of the area centralis of each eye was projected on the screen with light source before and after imaging. Respiration was controlled by an external pump. Electrocardiogram, expired CO_2, and body temperature were continuously monitored during the experiment. Image acquisition was synchronized with electrocardiogram (ECG) and respiration signals in order to provide synchronization of these oscillatory artefacts.

In order to apply the dye on the cortex, a stainless-steel chamber was mounted on the skull over an area which included areas 17 and 18 of both hemispheres. The cortex was stained for 2.5-3 h with the oxonol dye RH- 1691, and unbound dye was washed out after staining. Afterwards, the chamber was filled with CSF-saline or silicone oil and closed.

5.2 Visual Stimulation

In order to map orientation response on the cortex, we used full-field drifting grating stimulation. The protocol included 8 or 12 directions of gratings, spanning all the orientation domain. Each grating moved in two opposite directions orthogonal to the orientation of the grating. Stimuli consisted of 100% contrast gratings of 0.2-0.6 cycles/degree drifting at 2-6 Hz temporal frequency. Stimuli were pseudo-randomly interleaved with recording epochs in which the screen was blank. Stimulus was presented for 300-500 ms, and the recording duration for one trial was 1280 ms long. Stimulus is presented full-field on a 22' CRT monitor at a 150 Hz refresh rate. The monitor is placed 57cm away from the eyes of the animal.

We also used a second protocol which included non-classical visual stimuli. This protocol was previously developed and used in our lab in order to evaluate stimulus dependency of trial-to-trial variability in intracellular recordings from area 17 (Baudot et al., submitted). Stimuli used in the protocol are shown in Figure 5.2. The protocol consists of a set of stimuli with increasing complexity: drifting grating, grating animated by a trajectory simulating the dynamics of eye movements, natural image animated with the same trajectory, and binary dense noise. In order to adapt this protocol to VSD imaging, longer recording times are required to obtain an adequate temporal frequency resolution. In this protocol, we recorded the VSD response in 5120 ms long trials, in which the stimulus was presented for 4 sec. Long stimulus times (>800ms) evoke also the intrinsic response on the cortex which contaminates the fluorescent signal. This required modification of the GLM basis, which will be explained in Chapter 8.1.

5.3 Data Analysis

Offline analysis is performed on a Intel quad-core computer (2 GHz each core) with 8 GB of memory.

GLM is performed on raw signals without first frame normalization by using Elphy software. PCA and ICA were performed by Matlab software (Mathworks, Natick, MA, USA) by using Parallel Computing Toolbox and a modified version of the FastICA toolbox for Matlab developed at the Helsinki University of Technology[1]. PCA for separation of neuronal response patterns is performed prior to normalization of trials with respect to the mean of the first frames of all trials. This approach will be explained later in details.

[1] available at http://research.ics.aalto.fi/ica/fastica/index.shtml

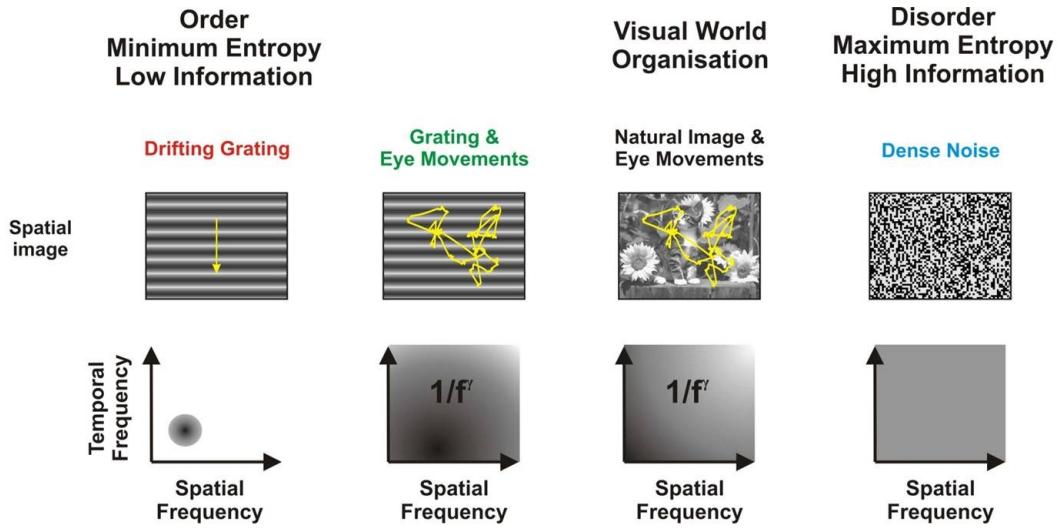

Figure 5.2 – Stimulus set used for long recordings. Spatio-temporal frequency spectrum of each stimulus is shown in the lower row. Modified from Baudot et al. (submitted).

5.4 Stimulus locked time-frequency analysis

Stimulus locked time-frequency analysis is adapted from a previous intracellular study from our lab (Baudot et al., submitted).

VSD imaging signals at each pixel were convolved for each trial with an array of complex-valued normalized Gabor functions ranging from 1 to 75 Hz (1 Hz steps):

$$\psi_f(\tau) = (a/\sqrt{f}) * \exp(-2\pi i f \tau) * \exp(-\frac{\tau^2}{\sigma^2})$$

where a is a constant such that the energy of the wavelet is equal to 1.

To improve the readability of the time-frequency representation, the Gabor decomposition presented here is largely oversampled: the Gabor filter bank is non-orthogonal, with wavelet frequencies ranging from 1 to 75 Hz (with 1 Hz incremental steps), and a temporal sampling period of 1 ms. To achieve a fine temporal resolution, the normalized Gabor function had a Gaussian window variance equal to two Gabor periods ($\sigma * \phi = 2$). The convolution of a signal X(t) with this wavelet function is of the formă:

$$S(t,f) = \int X(t-\tau) * \psi_f(\tau) d\tau$$

This decomposition allows the extraction of several time-frequency dependent measures: signal power, noise power, signal-to-noise ratio power (SNR). It can be viewed

as an extension of the signal and noise estimation proposed by Croner et al. (1993) to the time-frequency domain. We define $S_i(t, f)$ as the complex result, at time t and frequency f of the convolution between the wavelet and the response for trial i. The signal power S_{est} of the stimulus-locked waveforms is then measured as the squared modulus of the (across-trial) average vector of the wavelet transform in the complex domain:

$$S_{est}(t, f) = |\langle S_i(t, f)\rangle_i|$$

where angular brackets indicate the average across all trials and straight brackets indicate the modulus. The noise power $N(t, f)$ is measured as the average distance between the individual trial vectors and the average vector of the wavelet transform in the complex domain:

$$N(t, f) = \langle |S_i(t, f) - \langle S_i(t, f)\rangle_i|\rangle_i$$

The signal to noise ratio is measured as:

$$SNR(t, f) = \frac{|\langle S_i(t, f)\rangle_i|}{\langle |S_i(t, f) - \langle S_i(t, f)\rangle_i|\rangle_i} = S_{est}(t, f)/N(t, f)$$

Signal, noise, and SNR power spectra are obtained by averaging the squared functions over time:

$$F_{SNR}(f) = \int_{t_{start}}^{t_{end}} (SNR(t, f))^2/(t_{end} - t_{start})dt$$

$$F_{Signal}(f) = \int_{t_{start}}^{t_{end}} (S_{est}(t, f))^2/(t_{end} - t_{start})dt$$

$$F_{Noise}(f) = \int_{t_{start}}^{t_{end}} (N(t, f))^2/(t_{end} - t_{start})dt$$

Part III

Results

Chapter 6

Source Separation for Denoising of VSD Imaging Data

6.1 Introduction

In Chapter 4, we explained sources that contribute to VSD imaging recordings, and we introduced the application of statistical linear source separation methods to analysis of multichannel neuronal recordings, including VSD imaging. Now we will explain a new strategy for denoising VSD imaging data, applied to our particular case of imaging of areas 17 and 18 of anesthetized and paralyzed cat cortex in response to full-field drifting grating stimulation. Our method involves a two-step hybrid denoising, which benefits the advantages of both data-driven and model-based approaches.

Application of statistical source separation methods is rather new for the VSD imaging community. Few methods that are available use either only model-based or only data-driven approaches. Development of hybrid methods that combine both model-based and data-driven approaches would be useful in order to profit the advantages of both methodologies. Some methods that combine those two approaches are indeed reported to be more efficient on other types of neuroimaging data (McKeown, 2000; Calhoun et al., 2005; Hu et al., 2005 for fMRI, Zheng et al., 2001 for intrinsic imaging). However, these methods generally favor one approach more than the other, and the assumptions are optimized for the recording technique of interest. VSD imaging provides recording of much faster events than intrinsic imaging and fMRI, therefore noise sources as well as neural-related signal sources occur at a different time scale. This requires development of methods which are more adapted to VSD imaging.

In order to clean VSD imaging data from the artefacts, we developed a two-step

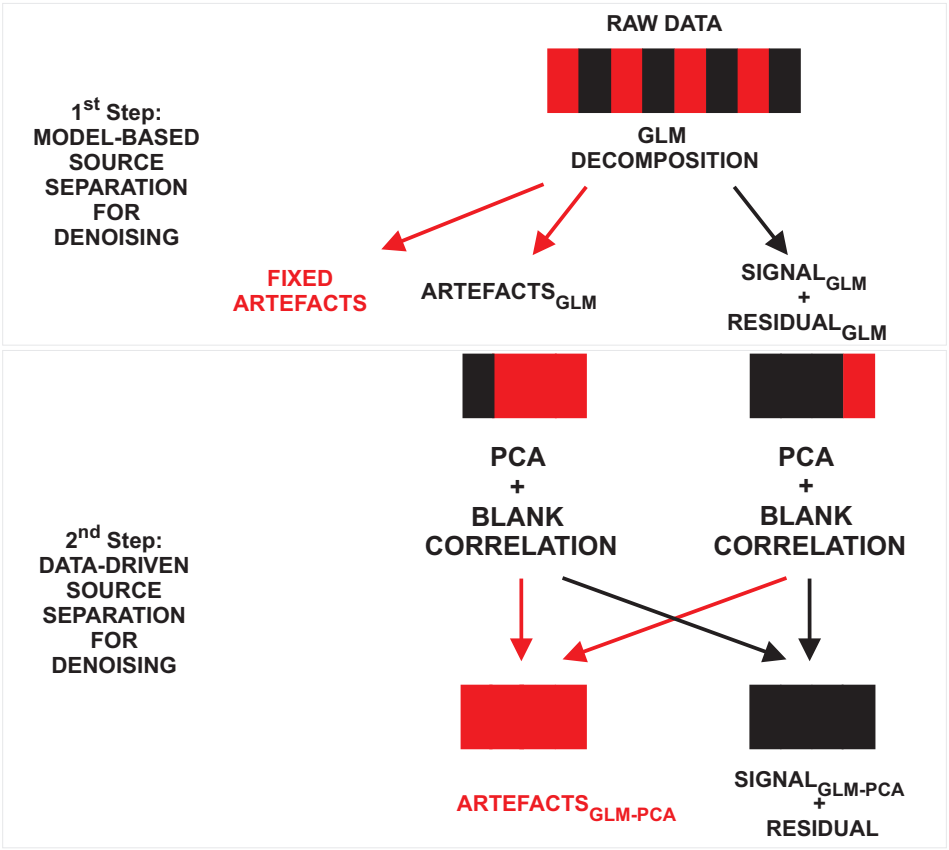

Figure 6.1 – Hybrid multi-step source separation. Black blocks represent the ideal neural response, and red blocks represent the ideal artefacts.

hybrid method which involves a preliminary analysis by GLM that provides a separation of the sources into two groups with respect to their relationship with neural fluorescence response, and then profits PCA on these two groups in order to check if there were any signals that GLM hypothesis was not able to detect. Our strategy is summarized in Figure 6.1. We consider the raw data to be a mixture of neural-related signal (black boxes), and artefacts (red). In the first step, we analyzed each trial of the raw data by GLM individually. Regressor base and corresponding regression on the data are separated into two groups, in accordance with the dependence of the regressors on the evoked response. Residual is added to the neural response-related group, in order to preserve intrinsic neuronal noise. At the end of the first step analysis by GLM, most of the artefacts can be detected, but there may be still some contamination in both signal-related and artefact-related groups. The main problem for the contamination of the artefacts group by the neuronal-related signal is the oscillatory artefacts that cannot be phase-fixed to the source of the artefact. Considering the rich nature of the neuronal activity spectrum, some neuronal-related signals of an artefact-related signal frequency may converge to the artefact group. On the other hand, as explained in Chapter 4, it is not possible to

explicitly model all the signal sources. Therefore, residual of the model which is added to the neural-related signals may also include some artefact-related sources. Adding a second step of analysis that uses a different approach would provide a better separation. After the separation of neural-related and artefact-related components, both groups are analyzed by PCA separately. Artefacts that are fixed with respect to the main artefact source (baseline fluorescence, bleaching, 50 Hz noise) are excluded from the rest of the analysis right after the first step. In the second step, all trials of all stimulation conditions and mean responses for each stimulus are concatenated. Applying PCA on this concatenation favors the extraction of the components that are common in all evoked and blank conditions, which would stand for the artefacts. In order to distinguish signal from the artefacts, we de-concatenated the principal components and calculated the correlation between blank and evoked signals for a given principal component. This two-step denoising provided better source separation than GLM and PCA methods alone.

At the first step that involves GLM, we used a modified version of the approach developed by Reynaud et al. (2010). This approach was developed in order to clean VSD imaging data recorded on primary visual cortex of awake monkey, where blank subtraction fails because of the difficulties to synchronize physiological artefacts and other trial-to-trial dependent factors that are related to awake animal preparations. In our anesthetized and paralyzed cat preparation, blank subtraction provided fairly good information about the strong artefacts. Our advantage is the artificial control of respiration, and synchronization of the acquisition and respiration with respect to the first cycle of the heartbeat. It should be noted this advantage of blank subtraction is only valid for averaged data. Blank subtraction is not enough for single trial analysis even in our case in which artefacts are much more predictable than in awake monkey recordings. We utilized average blank recordings as a control in order to check if the artefacts detected by GLM are well synchronized with blank recordings or not.

Moreover, Reynaud et al. (2010) used a regressor basis that would be suitable to analyze both full-field and local stimulation responses. Small stimuli like in their case are expected to evoke a response that peaks on the retinotopic center, which will spread on the rest of V1 (Grinvald et al., 1994; Sharon et al., 2007; Chavane et al., 2011). This would cause the pixels outside the retinotopic center to respond with a latency. In our case, full-field drifting grating stimulation evoked an activation that has almost the same latency and shape for each pixel. This permits us to use a more restricted regressor basis for signal responses. We also included components that correspond to the DA notch, which is a signal component that is not observed in awake animal recordings. This version of GLM provided an acceptable denoising of VSD recordings on anesthetized and paralyzed cat.

Nevertheless, even if the regressor base is chosen very carefully, there may be some neural-related signal that converges to artefact regressors, and vice versa. In order to check for this contamination, we applied PCA on two groups of regressors used for GLM, which standed for the neural-related signals and artefacts. We used a similar approach to periodic stacking (Mitra and Pesaran, 1999), with a difference that we conducted the analysis in the temporal domain and not in the frequency domain as suggested in the original version of the periodic stacking method. Stacking is done by concatenating different trials of different response conditions periodically as if it was a continuous recording of a periodic response. As we did not perform frequency-based analysis, the order of stacking was not important.

Once principal components of the two groups were obtained, for each component we calculated the uncentered Pearson correlation coefficient between the average principal component segment for each direction of evoked response and the average principal component segment corresponding to the blank response. This provided detection of artefacts, which are supposed to be synchronized between blank and evoked conditions. If the correlation for a principal component was above a certain threshold, this component was considered to be an artefact.

Our method is based on several assumptions. First, we assume that artefacts and neural-related fluorescent signal result from uncorrelated physical processes, which is true up to a certain point, which indicates that the relationship between signals and artefacts is linear. Second, we consider the signal sources in the temporal domain. Mixing procedure is performed by each pixel. Third, we assume that artefacts have same spatial profile on the cortex for evoked and blank recordings. This provides the detection of an artefact by the second step of denoising.

First, we will present the denoising achieved by blank subtraction and division, then we will present the results of our method in details.

6.2 Results

6.2.1 Blank Subtraction and Division on VSD Imaging Data

VSD Imaging data is usually analyzed prior to normalization with respect to baseline fluorescence and blank response. This is done first by dividing or subtracting each trial by the baseline fluorescence obtained by taking the mean of several points before stimulation. This method is referred to as the *first frame analysis*. Then, the 'blank' control sequence which consists of the response to uniform screen is subtracted from (blank subtraction, BS) or divided by (blank division, BD) each trial

of evoked activity in order to separate the evoked signal from the rest of the artefacts. This signal is often studied by taking the average response of a number of blank trials. Fluorescent signal is proportional to the stained membrane area under a pixel (Grinvald and Hildesheim, 2004); therefore normalization by division is mostly preferred to subtraction.

An example of blank subtraction and division in one of our recordings is presented in Figure 6.2. A raw data frame is shown in A. DC fluorescence is the dominant component. We restricted the analysis to the area surrounded by black. Temporal responses are shown in B. Black traces represent the responses on the pixel shown as a dot in A, which is placed in the middle of an iso-orientation domain that prefers horizontal stimulation. Red traces on raw recordings are the temporally smoothed average responses over 10 trials of blank response that are used for blank subtraction/division on the same pixel. Dashed lines represent onset and offset of visual stimulation, and the gray shade show the region in which we calculated the mean of all frames for spatial maps.

Although there is no difference at the temporal scale between BS and BD (Figure 6.2B), relative fluorescence between pixels was different as a result of the difference in baseline fluorescence resulted from uneven staining. The choice of subtraction or division is not important in the temporal domain, as the signals obtained by these two methods are proportional. In space, BD permits to amplify the fluorescence of pixels in the periphery by dividing the response with a several times lower value compared to the pixels on the center. However, fluorescence-independent noise and artefacts are also amplified (Figure 6.2C). For these reasons, we consider baseline fluorescence and the other artefacts to be additive with the signal. This assumption justifies the relevance of linear source separation methods used in our work. It should be noted that fluorescent signal may not be additive with baseline fluorescence, but our concern is to extract the rest from the neural-related signal. Hence, this problem is not important at this step.

The conventional *first frame analysis* suggests estimating the baseline fluorescence by calculating the mean over several frames before stimulation. However, imposing a strong hypothesis on the first frames may result in erroneous normalization, especially in case of blank division which radicalizes the contribution of baseline fluorescence. One of the future aims of our work was to evaluate temporal evolution of the variability, which would be affected by an erroneous normalization. Instead of normalizing each trial individually, we normalized the temporal response at each pixel with respect to the mean of all trials of all time points before stimulus onset. Removing a common mean from every trial permits keeping the neural-related variability of the single-trial activity of responses recorded in the first frames.

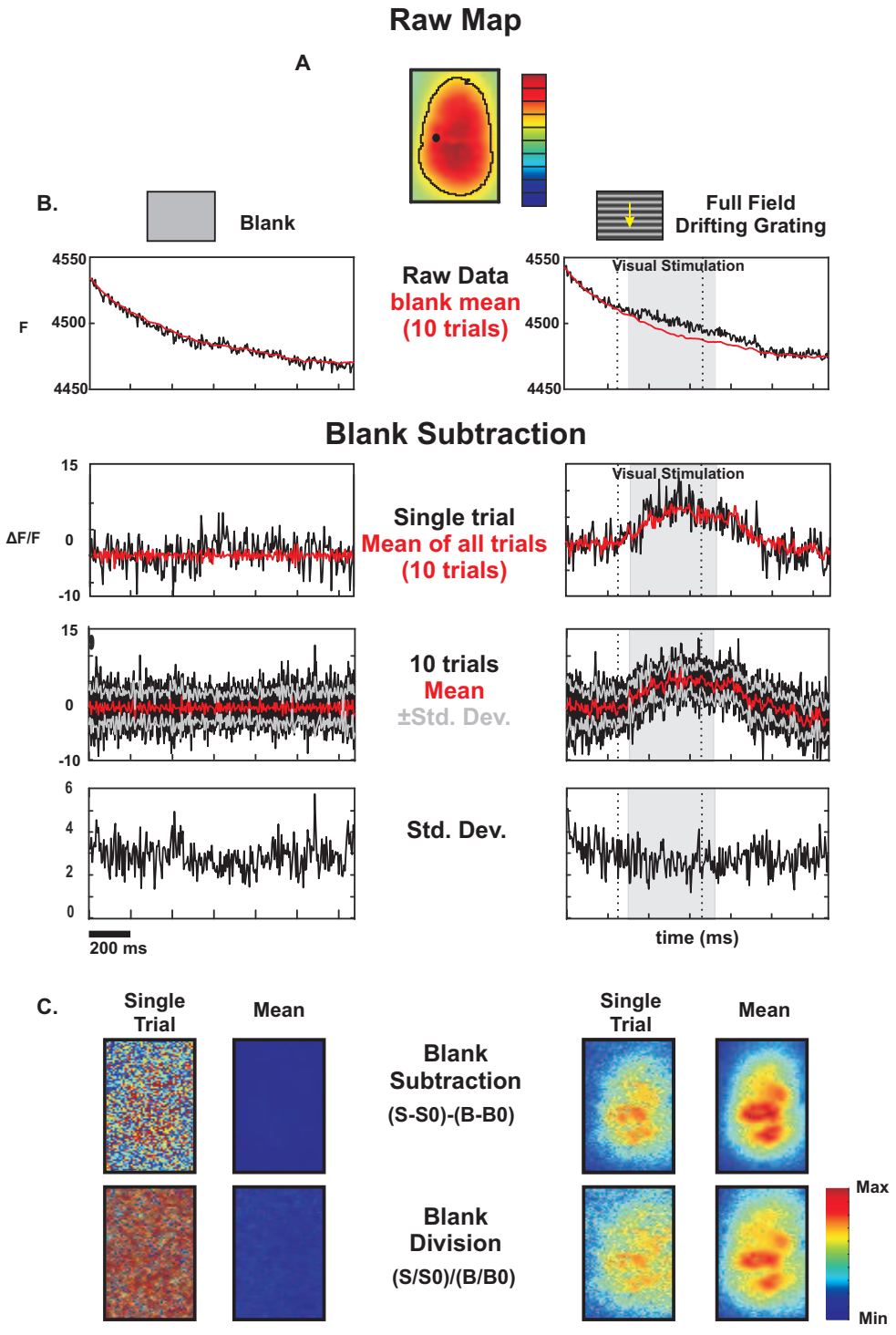

Figure 6.2 – Conventional denoising strategies for VSD Imaging. A: An example raw data frame. B: Temporal responses to horizontal drifting grating and to blank screen; before and after blank subtraction and first frame analysis. On the bottom, single trial response after blank subtraction on one pixel indicated in A (black) and on average of all trials on the same pixel (red). Superposition of all trials (black), their mean (red) ± their standard deviation (gray) is shown below. C: Mean spatial response on the evoked plateau from 150 ms after stimulus onset to 50 ms after stimulus offset, indicated with cursors in B.

Although BS and BD methods successfully remove most of the artefacts, this approach has restricted application. Synchronization of physiological parameters such as heart beat and respiration is useful up to a point, but problems may occur after a few cycles. Heartbeat frequency cannot be controlled externally and consequently heartbeat intervals may slightly vary if the recording time corresponds to more than several heartbeat periods. Moreover, artefacts that are not repetitive cannot be removed with these methods. Another problem is that these methods do not take into account the inter-trial variability of the ongoing and evoked activities.

6.2.2 Source Separation on Raw Data for Denoising

Statistical methods for source separation are shown to denoise successfully the multichannel neuronal data (see Chapter 4). Using a statistical approach for denoising VSD imaging data would provide avoiding the problems encountered with conventional methods. First thing to do before applying a statistical method is to choose whether a model-based or data-driven approach should be used.

There are several advantages of using a model-based approach rather than a data-driven strategy for denoising VSD imaging data recorded on anesthetized animal. Most important signal sources such as heartbeat and respiration are monitored and synchronized during data acquisition. This makes it easier to estimate a realistic basis for source regressors. Eye fixation provides a repetitive acquisition on the same region with the same fixation and same stimulus onset and offset for all trials. Moreover, working on an anesthetized preparation provides elimination of intrinsic controls on visual perception such as attention. On the other hand, spatial profile of contributions of the signal sources is not taken into account with this approach, and unexpected sources are challenging to be estimated. These weak points should be kept in mind while applying a model-based approach.

First step of our denoising strategy consists of defining all possible signal sources that contribute to the recordings, and then to use GLM in order to find the contribution of each component to the raw data. Nature of signal sources and GLM procedure applied to VSD Imaging are explained in details in Chapter 4. Here we will explain the modifications that we made on the regressor basis proposed by Reynaud et al. (2010), in order to adapt their model to fit to our data.

The analysis is restricted to a region of interest (ROI) that is defined by highly fluorescent areas, centered on the areas 18 and/or 17. ROI included 2756±739 pixels that are highly fluorescent (pixels that contain min. >60% of maximum fluorescence) on about 2-3 mm to 3-6 mm of cortical sheet.

Reynaud et al. (2010) reported an oscillation related to the illumination noise that

occurs at harmonics of 10 Hz on phantom recordings. In our data, these oscillations were only visible after averaging of all the pixels and trials, and they were not detectable in the PSD of raw recordings on the cortex (data not shown). For this reason, we did not include harmonics of 10 Hz in the GLM regressor base. We only included a 50 Hz oscillation phase-fixed to the region outside the ROI in order to model the line noise which was the only instrumental noise that we observed. Absence of the harmonics of 10 Hz signal in our data may be due to the use of a CMOS camera instead of a CCD camera.

While bleaching component in stained phantom experiment on a piece of white paper could be fitted to a single exponential, in none of our experiments on cat cortex we could obtain a good fit by using only one exponential. Dye bleaching was better modeled with a double-exponential fit on the cortex. The model for two-step bleaching is:

$$B(t) = a_1 + a_2(1 - \exp^{\frac{-t}{\tau_1}}) + a_3(1 - \exp^{\frac{-t}{\tau_2}})$$

Relaxation times τ_1 and τ_2 are estimated by fitting the mean of all pixels on the ROI for average of all smoothed blank trials. a_1, a_2 and a_3 are estimated by least-squares fitting. For 7 of the recordings, τ_1 estimated as 127±24 ms, τ_2 as 614±72 ms and τ_1/τ_2 ratio was 4.94±0.7. For two other recordings, τ_1 was at a nearby range (140±19 ms) while τ_2 was almost one order of magnitude higher. In any case, double exponential fitting was significantly better than single exponential fitting. In cases where τ_2 was very high, we clamped τ_1 and τ_2 to the average obtained from other data. This gave an appropriate fitting with the same r^2 value as double-exponential fitting without clamping. We simply supposed baseline fluorescence to be additive to the rest of the regressors in order to provide better comparison to BS. We supposed all the fluorescence-related signals to be fixed. In this case, no contamination is expected with the neural-related signal, hence we did not include any of them in $Artefact_{GLM}$.

Frequency variations of the heartbeat are not very important for the first few cycles of heart activity, for this reason using a simple sine wave is enough (Reynaud et al., 2010). We modeled the heart-beat induced artefact as an oscillatory component with the frequency of the heartbeat calculated individually for each trial. Three harmonics of the heartbeat modeled as a sum of sine and cosine waves in order to detect the phase (Reynaud et al., 2010):

$$S_f(t) = a_1 \sin(2\pi f t) + a_2 \cos(2\pi f t)$$

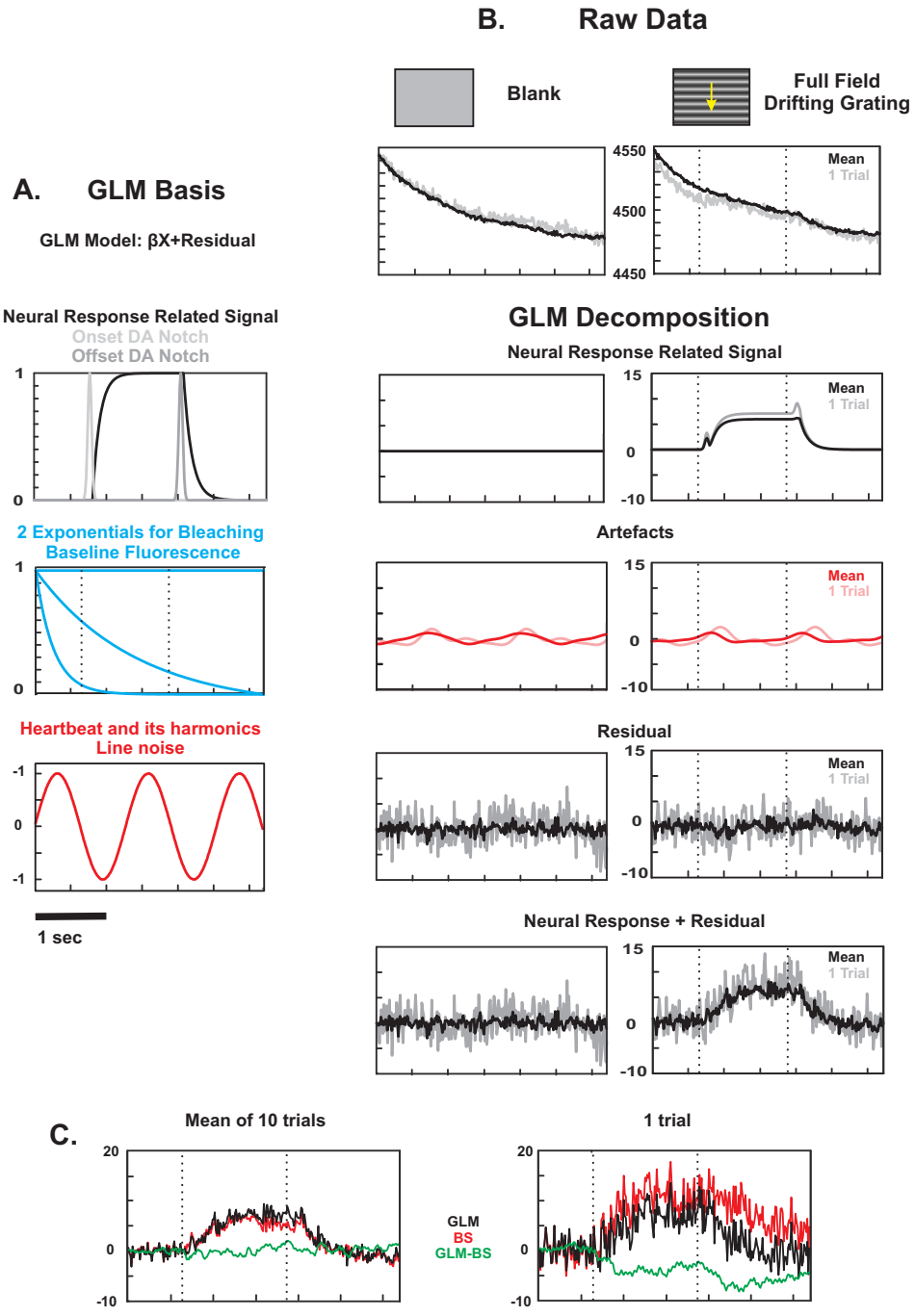

Figure 6.3 – Basis functions for the GLM, and resulting source separation. A: Neural response related basis functions are the global response that increases with response onset and decreases with response offset exponentially, the onset DA notch, and the offset DA notch. Fluorescence-related artefacts are baseline fluorescence, and bleaching which is modeled as two exponentials. Artefacts with free phase (red) are modeled as one sine and one cosine wave of the fundamental frequency of the oscillation, and their harmonics if present. These artefacts included the heartbeat related warping. B: Corresponding signal components revealed by GLM for blank and drifting grating responses. C: Blank subtracted temporal response compared to GLM on the same pixel.

This procedure is useful in order to detect the phase at each pixel, but it would remove all the signals around this frequency band including also neuronal-related signals. This was the main source of contamination between signals and artefacts.

We observed a strong oscillatory signal (12 Hz in average) at higher harmonics of the heartbeat frequency, with a spatial profile that looks like the heartbeat artefact. However, amplitude and frequency changed slightly from one period of oscillation to other, especially during neural response, making it impossible to be removed by GLM. This artefact was not always at the same frequency band or at same order of harmonics for all data. When we did not introduce this signal in the GLM basis, 2nd step of denoising by PCA could successfully remove this artefact as we will explain later. This signal is possibly related to the arterial pulse wave that results from the opening/closing of the arterial valves, revealed in the higher harmonics of the heartbeat frequency (Emilie Macé, personal communication). Opening and closing of valves introduce strong mechanical vibration to the surrounding tissue, which is captured by the camera.

50 Hz oscillation is introduced to the regressor base with the phase calculated by fast Fourier transform outside the ROI. This provides removal of only a particular phase of 50 Hz while avoiding removal of a possible gamma-range activity that may occur at this band. We considered this artefact to be fixed at the first step, and excluded its contribution right after GLM.

We modeled the stimulus-evoked neural signal as a component that increases rapidly after stimulus onset, and after following a plateau, fading out again gradually. Stimulus-dependent rise and decay of the response is modeled as an exponential change.

The model for the signal was:

$$\begin{aligned} V_c(t) &= V_{in}(t)\exp(\frac{t_{on}+\delta_{on}-t}{\tau_{on}}), t\epsilon[1, t_{off}+\delta_{off}-1) \\ V_c(t) &= V_{in}(t)\exp(\frac{t_{off}+\delta_{off}-t}{\tau_{off}}), t\epsilon[t_{off}+\delta_{off}, end] \end{aligned}$$

$V_{in}(t)$ is a step function with 1 between t_{off}+δ_{off} until the final point and 0 elsewhere. Model parameters were chosen by fitting the model to the blank-subtracted average response ($\delta_{on} = 55.6 \pm 19.5$ ms, $\delta_{off} = 17.1 \pm 5.2$ ms, $\tau_{on} = 33.1 \pm 10.6$ ms, $\tau_{off} = 41.3 \pm 8.4$ ms). DA notch (Sharon and Grinvald, 2002) was included if it was present in the beginning and at the end of neural response estimated by blank subtraction (in 5 out of 8 areas that were analyzed). The model for the notch was:

$$V_{notch_{on}}(t) = \exp((\frac{t_{on} + t_{notchpeak_{on}} - t}{\sigma_{notchpeak_{on}}})^2)$$
$$V_{notch_{off}}(t) = \exp((\frac{t_{on} + t_{notchpeak_{off}} - t}{\sigma_{notchpeak_{off}}})^2)$$

Notch parameters were obtained by fitting the signal together with the $V_c(t)$ ($t_{notchpeak_{on}} = 69 \pm 3.2$ ms, $t_{notchpeak_{off}} = 73 \pm 11.6$ ms, $\sigma_{notchpeak_{on}} = 17 \pm 2.4$ ms, $\sigma_{notchpeak_{off}} = 16 \pm 1.2$ ms). To sum up, our final vector base contained 1 or 3 components for neural signal, 2 exponential components for bleaching, 3 harmonics for heartbeat-induced artefact at the corresponding frequency for each trial, 50 Hz mains noise with fixed phase, and one unit vector for the baseline fluorescence. Neural response related signal is included in the regressor basis only for evoked responses, thus the blank response is modeled only by artefacts. Finally, contribution of each of these sources was estimated by applying a least-squares fitting to the regressor basis and to the raw data for each trial. Signal sources and resulting source separation are shown in Figure 6.3. Trials shown in this figure for blank and evoked responses are from the same trial stack (less than 8 acquisitions between). Even though the artefacts (red) are close for the trials of blank and evoked responses, there is still some difference. Similarly, mean of the artefacts for both blank and evoked states cannot capture all the artefact-related components observed in one trial.

GLM-cleaned signal is compared to the signal obtained by the classical method of blank subtraction in Figure 6.3C. Black trace stands for the GLM-cleaned trial, red for the BS-cleaned trial, and blue for the difference between these two traces. The main differences between the BS-cleaned and GLM-cleaned responses are the heartbeat-related signal which varies from one trial to another, line noise which is not synchronized among trials, and the drift in the response.

Even though GLM seems to separate correctly the neural response from the artefacts, the hypothesis behind the distinction of neural signal and artefacts may be misguiding. First of all, defining a particular frequency band as artefact may remove a part of neural signal, as the neural responses can be expressed in various frequency bands. Second, we may not know all signal sources from the beginning. Finally, defining a rigid shape for deterministic sensory-evoked response may not capture the response at one trial because of trial-by-trial variations of the evoked activity. Defining multiple components for neural response in order to get all the possible shapes is risky as the artefacts may converge to the irrelevant neural-response related components.

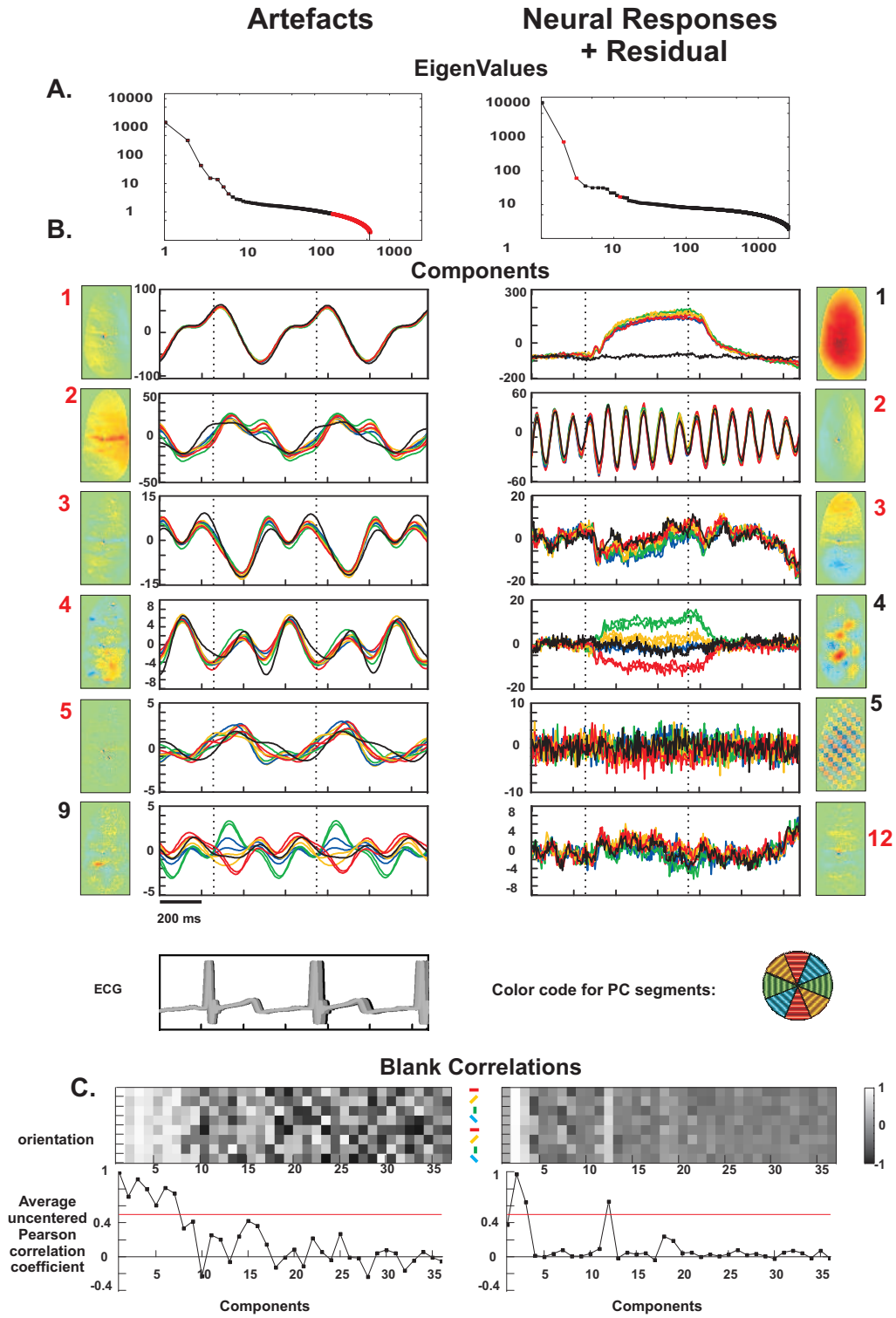

Figure 6.4 – PCA decomposition on artefacts and neural response + residual, revealed by GLM. A. Eigenvalues for the two groups of sources, in log-log scale. B. Eigenvectors (spatial maps) and principal components (shown as de-concatenated and superposed time plots). Principal components are de-concatenated and colored with respect to the corresponding stimulation. Artefacts that are detected by blank correlation in this step are indicated by red on the PC number, and on the eigenvalue plots in A. C: Blank correlation for artefact detection.

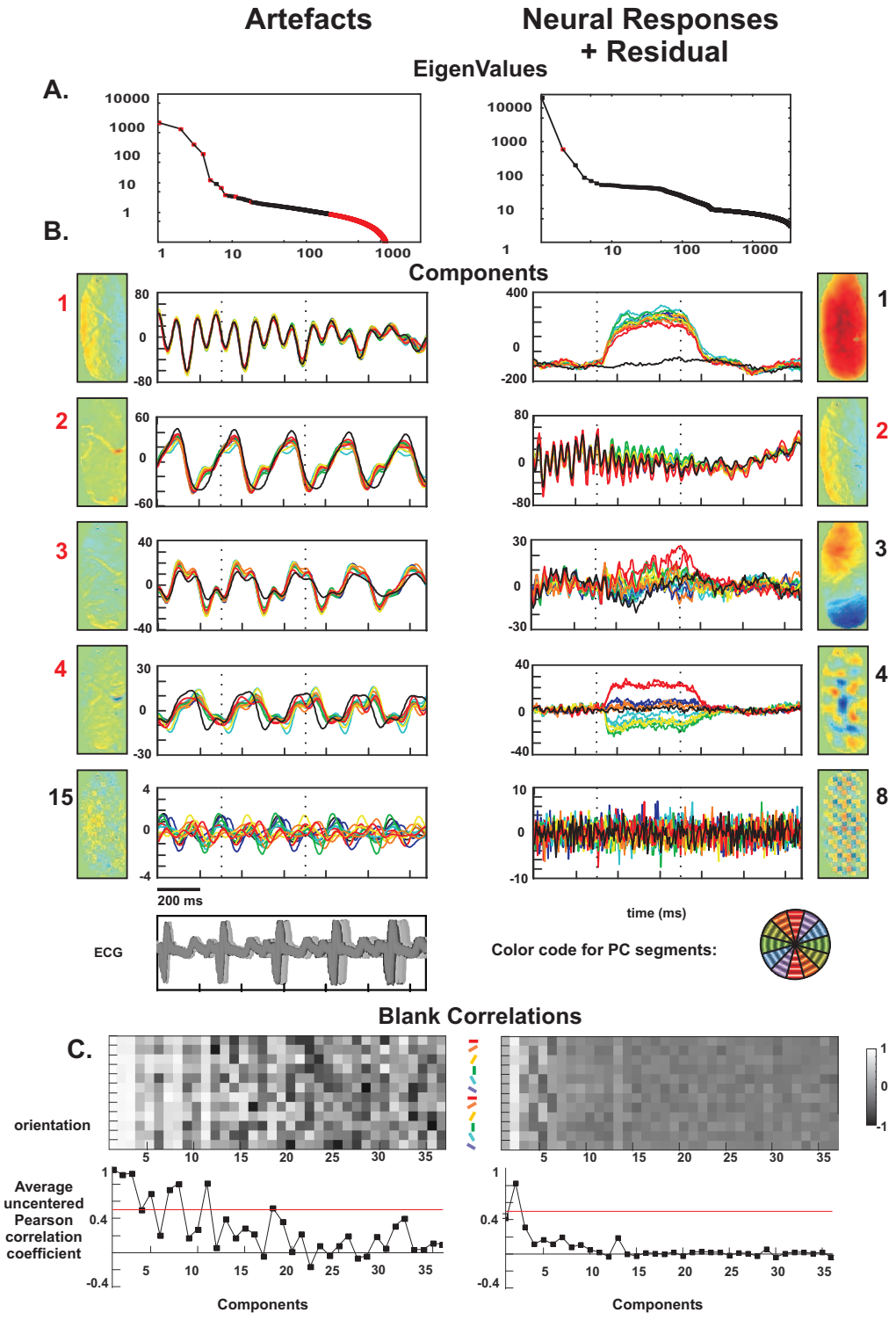

Figure 6.5 – Same as 6.4, for another data that consists of 6 orientation conditions.

In order to make sure that the neural response and artefacts are well separated, we applied a second step for better separation. In this second step, we used a data-driven approach to avoid the problems that arise from the original hypothesis for

data composition claimed by the model-based approach. This additional approach would take into account the correlation between the statistical distributions of the signal sources instead of their temporal activation profile.

Sources that are extracted by GLM are grouped into two sets that consist of the artefacts ($Artefact_{GLM}$) and the sum of sensory-evoked reproducible signal and residual ($Signal_{GLM}$+r) in order to take into account the neural variability, as suggested by Reynaud et al. (2010). For the next step, only artefacts with free phase are kept in $Artefact_{GLM}$. In our case, this corresponds to only the heartbeat-related signals. Once all the trials are analyzed with GLM, PCA was applied to concatenation of all trials and average response to all directions of drifting grating and the blank stimulus on both $Signal_{GLM}$+r and $Artefact_{GLM}$ sets, by calculating the eigenvectors of the covariance matrix. Concatenation of all evoked and blank responses provides a compromise between 'blank' and 'cocktail blank' control statements, taking into account correlations both with blank condition and among all stimulus conditions. We used temporal PCA instead of spatial PCA, not only because of the lower dimensionality of our concatenated data in space rather than in time, but also to keep the coherence of the hypothesis that each signal source has a temporal structure and that the mixtures are made by different recording channels, which are the pixels in case of VSD imaging. As PCA will extract groups of pixels that express the same temporal structure, spatial aspect is also taken into account.

PCA on $Artefact_{GLM}$ and on $Signal_{GLM}$+r revealed that GLM was not able to separate completely the neural response from artefacts. Two different examples are shown in Figure 6.4 and 6.5. Resulting eigenvectors are re-organized as spatial maps, and principle components which are temporal activation profiles are de-concatenated in order to distinguish the temporal structure corresponding to a stimulation that a trial is responding to. For each stimulation condition, average principal component segment is calculated among the trial segments. Uncentered Pearson correlation coefficient is calculated between the average segments of blank and each direction of movement of drifting grating. If average correlation coefficient was higher than 0.5, this principal component is considered as an artefact. For the examples shown in Figure 6.4 and Figure 6.5, all the components marked as red in the eigenvalues and principal component numbers are marked as artefacts. ECG traces are also shown in the Figures in order to provide a comparison to the artefacts. Note that for the example given in Figure 6.5, heartbeat is faster and more irregular than in the example in Figure 6.4. As a result of the irregularity in the heartbeat trace, higher harmonics of the heartbeat related artefacts become completely desynchronized, resulting in a flat profile at the end of the mean PC segments.

After the blank correlation, all the components that exhibit high correlation with blank are removed from $Signal_{GLM}$+r and added to $Artefact_{GLM}$ to obtain $Artefact_{GLM\text{-}PCA}$

and vice versa for the non-correlated components. PCA residual (after the first 200 principal components) of $Signal_{GLM}$+r set is kept with the reconstruction of components that were not correlated with blank, and the sum of these two groups is labeled as $Signal_{GLM\text{-}PCA}$. Residual of PCA on $Artefact_{GLM}$ is added to the blank-correlated components, and the resulting sum is labeled as $Artefact_{GLM\text{-}PCA}$.

This second step of denoising provided an acceptable separation of the signal of interest from the artefacts. For the example data shown in Figure 6.4, the first seven components for artefact set expressed a strong correlation between the blank and evoked responses. Average segments for the next 10-20 components were uncorrelated between blank and evoked responses. Doubling of the same orientation in the Figure is because of two different directions of drifting grating. Moreover, average segments for these principal components exhibited orientation selective structure: if the segment corresponding to a particular orientation had a positive sign, segment corresponding to the opposite orientation was negative. This is revealed in the anti-correlation between pairs of orthogonal orientations. For all the components that were marked to be neural-related (except the first global activation component), correlation coefficient for at least one orthogonal orientation pair was negative (data not shown). 12th principal component on Figure 6.4B is shown as an example for this observation. These neural-related components seem to be related to the response onset-offset variations that were not included in our regressor basis for GLM. The number of neural-related components was fairly high, but it should be noted that the total energy of all the stimulus-related components was only 9.5±4.2% of the total energy of the $Artefact_{GLM}$. First 200 components in $Artefact_{GLM}$ included 91.1±2.3% of all the variance.

On the other hand, PCA on $Signal_{GLM}$+r revealed that there are also some artefacts in neural related-response revealed by GLM. Only few components were marked as artefacts and represented 1.5±0.6% of total energy of $Signal_{GLM}$+r. First 200 components reflected 42±10.4% of all the variance in $Signal_{GLM}$+r.

This two-step denoising provided better separation by isolating the neural-related signal from the unwanted sources. Resulting clean signal and artefacts for the examples in Figures 6.4 and 6.5 are shown in Figures 6.6 and 6.7 respectively. Only one direction of each orientation and blank temporal responses are shown.

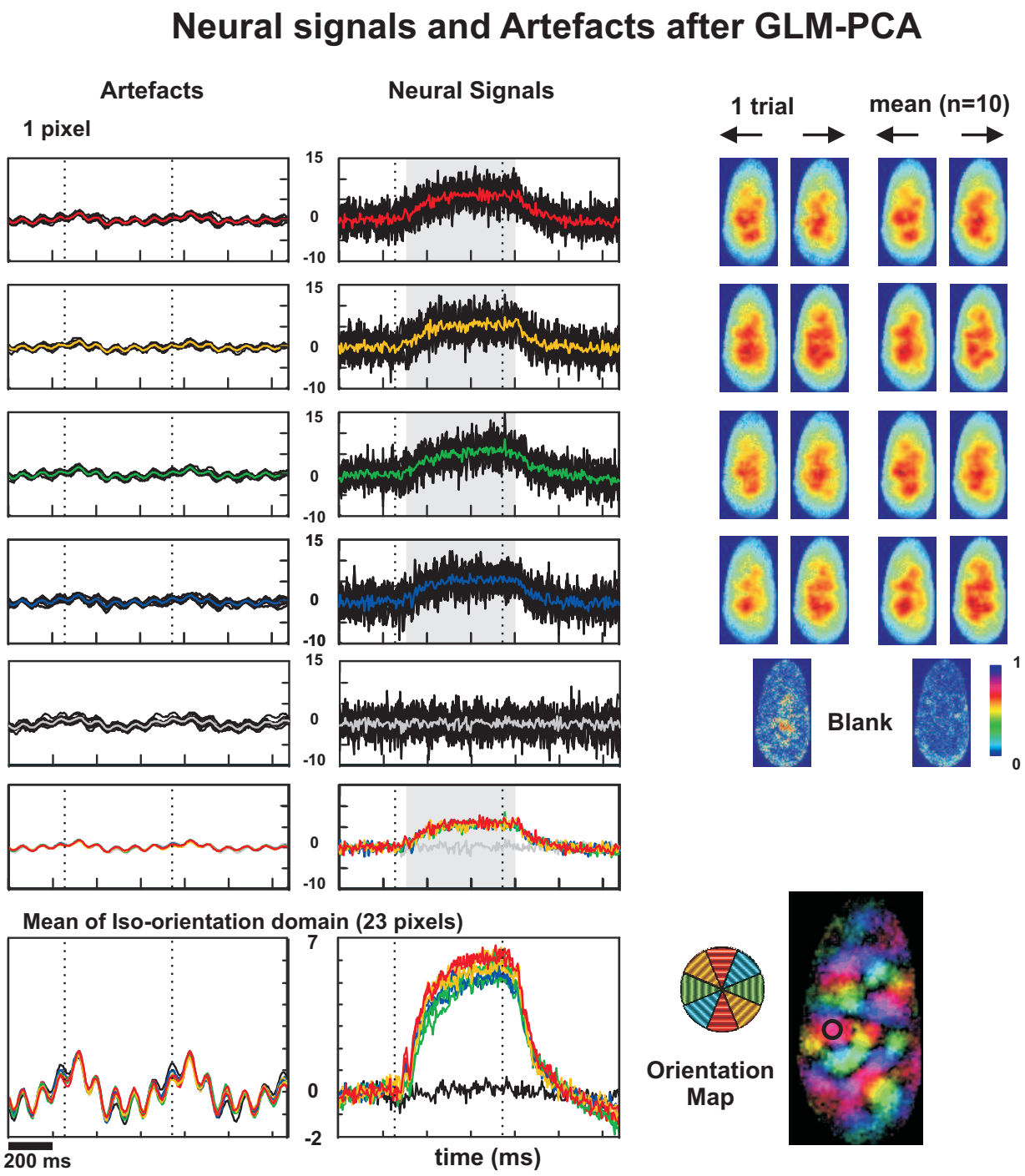

Figure 6.6 – Neural signals and artefacts after the hybrid two-step GLM-PCA denoising. Black traces are trials, and colored traces are mean trials in response to drifting gratings on a pixel shown on the orientation map (same pixel as in Figure 6.2A). Final trace is the superposition of all average traces. Spatial maps are for the neural signals calculated by taking the mean of all the frames in the shaded region shown on the temporal superposition.

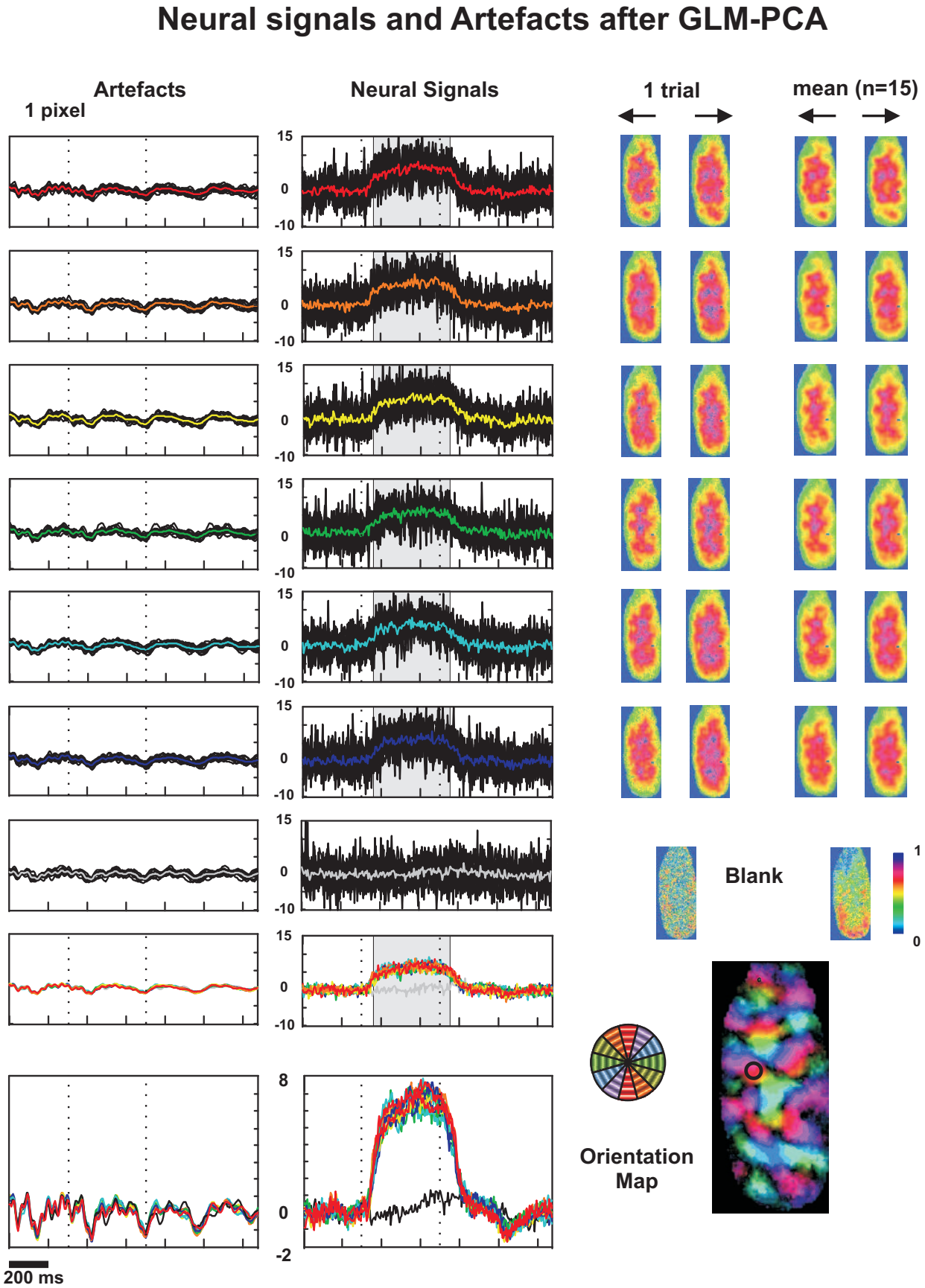

Figure 6.7 – Neural signals and artefacts for the data in response to the 6 orientation protocol.

Resulting artefacts were synchronized for different trials and stimulations, but still there is a trial-to-trial variability, showing why blank subtraction could not remove all these artefacts. The main components that could not be removed by BS are revealed to be the 50 Hz noise as a result of the non-reproducible nature of the signal, and the heart beat because of the variations of the heart beat frequency. Resulting artefact-free neural signals exhibited high variability; nevertheless selectivity of each pixel could be calculated on average response using the vector averaging method for orientation maps in order to find out the orientation selectivity of one pixel.

6.2.3 Variations of the Denoising Model

PCA after other preprocessing steps than GLM

We applied PCA on raw, bleaching-removed and blank-subtracted data in order to show that using a sophisticated denoising method such as GLM as a first step is necessary. All of these analyses are applied prior to baseline normalization explained above. We also analyzed the same data with ICA but ICA was not successful in any of the cases (data not shown). This is probably a result of the trial-to-trial variability of artefacts, which results in extraction of single-trial components by ICA.

PCA on raw data could not distinguish evoked neural response neither on concatenation of all trials (Figure 6.8), nor on single trial responses (data not shown but the problem is the same as for concatenation). The main problem was the bleaching being strongly correlated to the baseline neural activity, showing that bleaching and baseline fluorescence are not statistically independent from the neural signal. This is probably due to better diffusion on the cortex rather than on other tissue such as blood vessels. Focusing the camera on the region of interest on which neural response can be better visualized may also have an effect on this correlation. The 3D form of the cortex on the ROI is elevated on the center of the gyrus that contains areas 17 and 18; hence the periphery is more distant to the camera than the center. Consequently, the camera is not parallel to the cortex around the sulci. This would result in the loss of some light on the periphery, reflecting the incoming light outside of the focus of the camera. This could be a reason why we see more fluorescence and neural response on the center of the ROI rather than in the periphery.

In order to separate the fluorescence-related artefacts from the rest to avoid con-

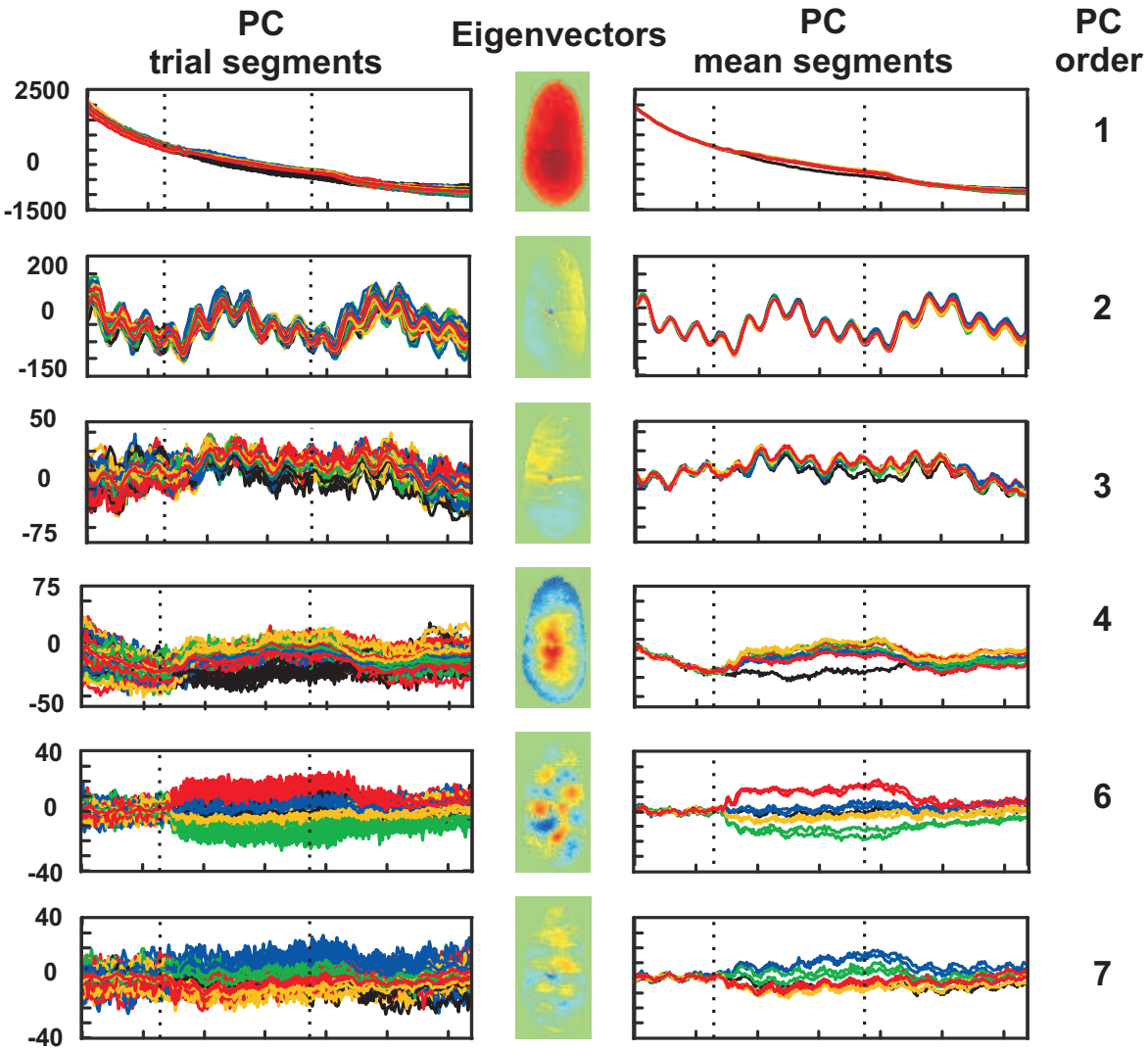

Figure 6.8 – PCA on raw data. Color codes are the same as in the Figure 6.4B.

tamination of neural-related response, we tried to apply PCA on bleaching-removed signals (Figure 6.9). PCA after removal of bleaching by a double exponential fit could not distinguish the heartbeat and pulsation artefacts from the neural response.

We also tried to apply PCA after BS in order to check if same kind of contamination as after GLM occurs for blank subtraction too (Figure 6.10). Resulting components included the 12 Hz signal. This means that this signal could not be removed by BS method. Moreover, there were drifts that change from one trial to other for most of the components. It was not obvious to mark all the components as signal or artefact, as the resulting components that were not observed by PCA after GLM (for example, components 3 and 4 in Figure 6.10) did not show any clear stimulus dependence.

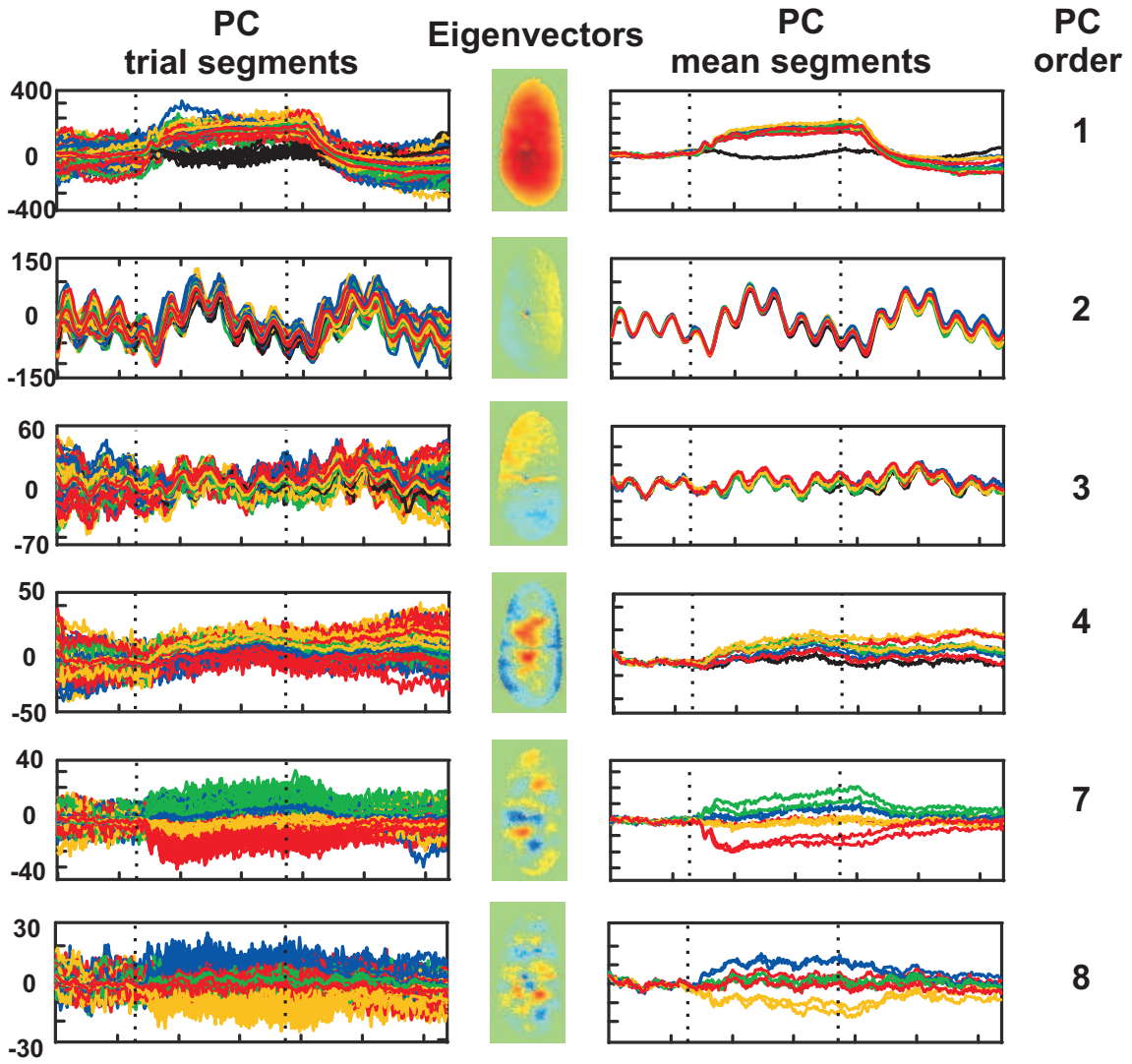

Figure 6.9 – PCA after removal of bleaching by a double-exponential fit.

Introducing the 12 Hz Signal in the Regressor Basis for GLM

Introducing the 12 Hz oscillation to the regressor basis was not enough to detect this source completely as artefact (Figure 6.11). In this case, PCA after GLM resulted in a component with the frequency of this signal on both $Signal_{GLM}$ and $Artefact_{GLM}$ groups. This was the reason why we excluded this signal from the regressor basis.

6.3 Discussion

VSD imaging recordings are high-dimensional and noisy. In this work, we introduced a hybrid source separation method for denoising single trials of VSD imaging

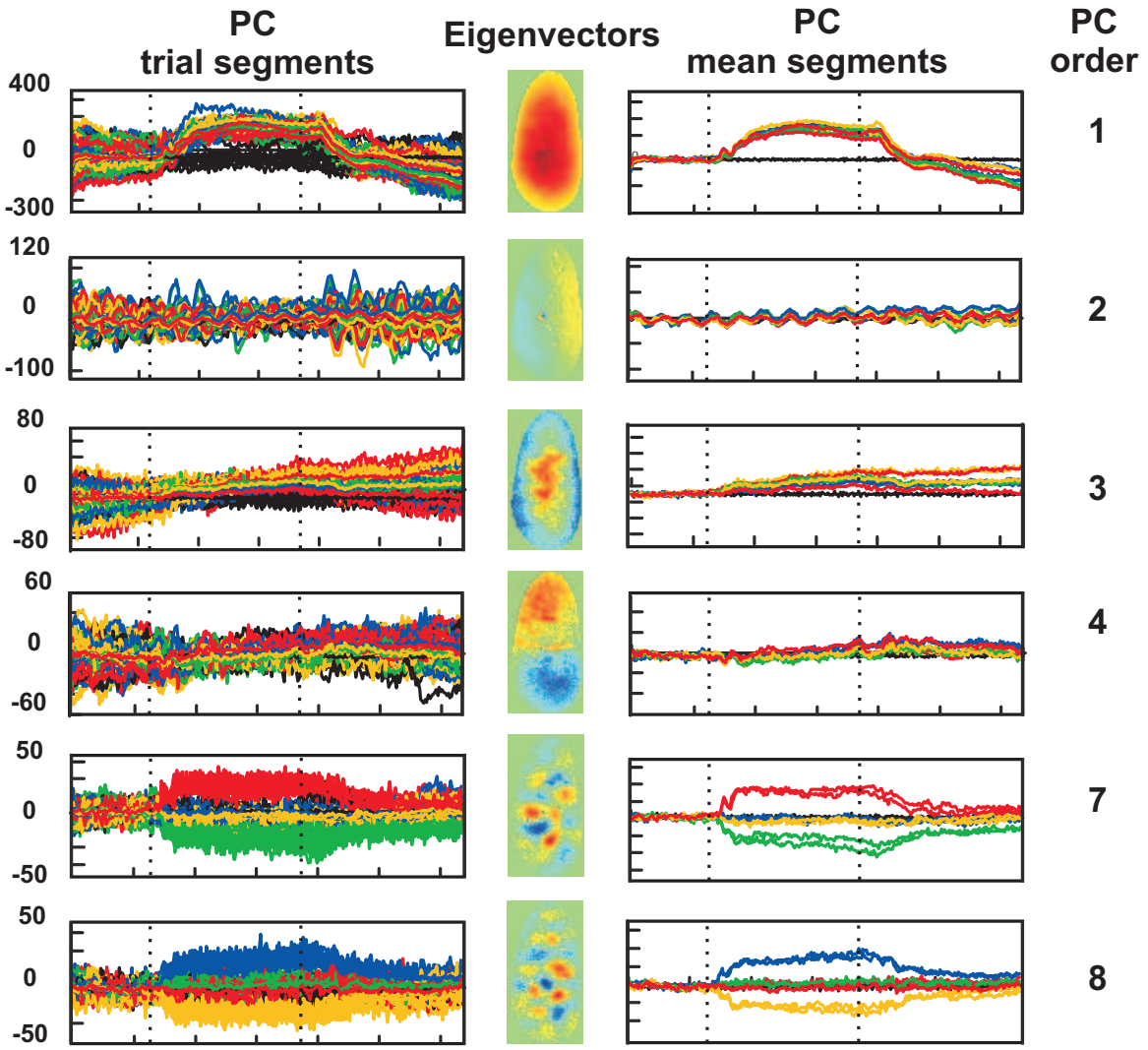

Figure 6.10 – PCA after blank subtraction.

data. This method involves performing PCA and ICA after GLM denoising; making use of both data-driven and model based approaches at the end.

When faced the source separation problem, one is exposed to numerous problems about the identification of sources contributing to the observed signal: What is the relationship between the sources? If there is a relationship, what is the nature of the dependence? Do we have prior information about the nature of the sources? How are the different sources "mixed" by different recording channels? Responses to these questions lie behind a good choice for source separation strategy. In our case, GLM, which is a model-based method, was more successful in identification of signal sources on the raw data than data-driven PCA. Yet this approach was not enough to separate the signal of interest from the rest. Combination of this method with the PCA as a second step provided better results for source separation.

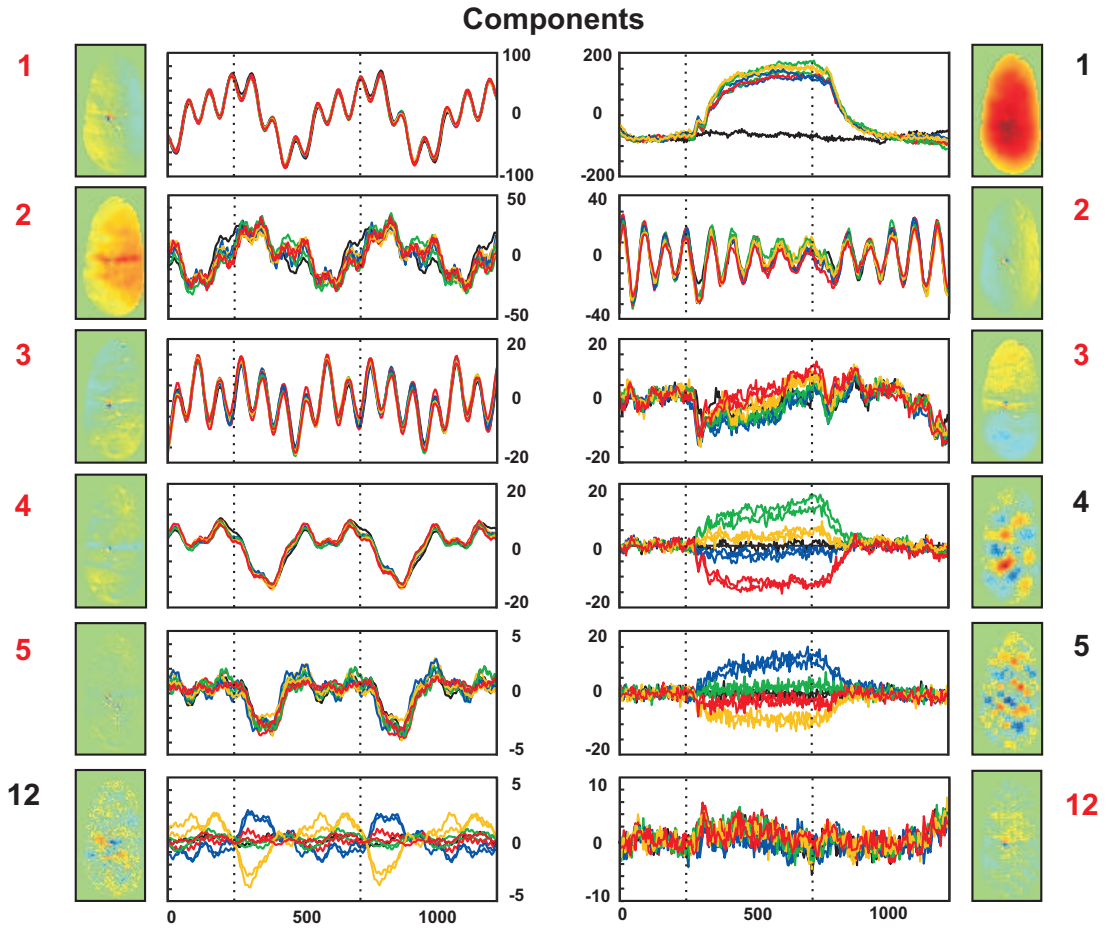

Figure 6.11 – GLM with 12 Hz signal.

Success and failure of different strategies may give information about the nature of signal sources. Data-driven strategies, which are also referred to as Blind Source Separation methods, namely PCA in our case was not sufficient to distinguish the neural signal from the noise, despite that some were reported to work for VSD Imaging on other animal models, or on data recorded by using different techniques. Identification of the pulsation signal was also a problem with GLM and this signal seems to be related to neural signal as well as the heartbeat artefact, because when a similar frequency signal was included in the GLM basis as artefact, second step PCA on $Signal_{GLM}$+r gave a strong principle component (most of the cases 2nd in the order) of this frequency band, which was suppressed during visual response. Pulsation signal fall into the same frequency band as alpha waves that decrease with an "active" brain state, which may involve in a possible mixing of the neural signal with the pulsation artefact in this type of preparation.

On the raw data, only the first component that standed for the fluorescence-related artefacts plus the neuronal nonselective response standed alone for more than 99% of the variance. This was a result of the fluorescence-related artefacts being much

stronger than the other components. In other cases that do not include these artefacts, number of significant components revealed by PCA was always very high. In order to keep ~90% of the variance of the bleaching-removed data, retaining thousands of components were needed. This was one of the limiting factors for using ICA directly to denoise the raw data, as ICA (at least in case of FastICA algorithm that we used) needs reduction of dimensionality before applying the ICA procedure. One reason for high dimensionality was the presence of non-deterministic but spatially coherent camera noise, which shows up as checkerboard patterns as indicated before.

Another reason for why data-driven approaches were unable to distinguish the neural signal from artefacts in VSD Imaging as good as in fMRI may be that in fMRI recordings there are regions that are explicitly dominant of noise and absent of neural-related signal, like ventricles and large blood vessels (Calhoun et al., 2003). In contrast, in optical imaging most of the region of interest includes both neural and artefactual signals, therefore signal and artefacts are 'mixed' in a similar way on each pixel, which leads to grouping of these signals under the same source.

Although it is tempting to do PCA on the domain that consist of smaller dimensionality, orthogonality assumptions may not hold for both spatial and temporal domains. We preferred to use temporal PCA as it is more coherent to consider signal sources to have a predictable structure in time rather than in space, as the artefacts are of oscillatory nature, and the neural response is expressed by the selectivity of cell populations that respond with a similar temporal structure. In our case, it is also advantageous to perform the analysis in the temporal rather than spatial domain, as the concatenation of all trials of all stimulus conditions results in a higher number of frames than the number of pixels.

In GLM we only introduced less than 10 components, but number of significant components revealed by PCA was always higher. This indicates that the decomposition made by GLM is very rough and does not take into account the rich nature of the VSD Imaging data. Nevertheless, GLM provided better separation than the other methods, because it provides removal of the most important artefact sources which are predictable up to a certain degree.

In GLM we used a different strategy to model the neural-related signal than the previously suggested GLM strategy (Reynaud et al., 2010). Using PCA to detect the latency and slope of the evoked response as they did results in Fourier-like decomposition of transient responses. If the number of components to define the signal is taken to be the maximum (this number was 64 in our case), we observed that GLM overfits the residual, resulting in a very flat residual on the transient responses (data not shown). Even when we took less than 10 components to model the signal,

some of the artefacts (especially heartbeat) converged to these signal components, and second-step PCA could not distinguish this contamination as good as it does for the method that we used. We preferred restricting the onset and the slope of the transient responses rather than letting it flexible. Flexibility of the neural response transient parameters was important for Reynaud et al. (2010) as they developed this method in order to analyze local stimulus responses that trigger traveling waves on the cortex. As we analyzed only full field drifting responses, this point was not as important for us. Our second step of denoising that involves PCA could successfully detect the variability of the transient responses. Another difference in our study compared to Reynaud et al. (2010) is that we did not aim to obtain a white residual. First of all, all the stimulus dependent response cannot be modeled explicitly with model-based methods. For example, retinotopic response to drifting gratings that occur as waves on the cortex (Onat et al., 2011b) are not taken into account in the model suggested by Reynaud et al. (2010). There may be other aspects of the evoked activity that are not known to date. Creating a regressor basis in order to obtain a white residual may result in convergence of this kind of evoked responses to irrelevant regressors. In fact, this kind of contamination would occur in any case, as it is impossible to predict all the components perfectly. This is why we opted to perform a second step of analysis that involves data-driven separation rather than using a purely model-based approach. Here we show that this second step of denoising is useful in order to detect unwanted contaminations that are resulted because of the insufficient conception of the regressor basis.

In order to detect contaminations in the signals and artefacts detected by GLM, we used the criterion of synchronization between blank and evoked response projection segments for the same component. In our case this was enough because even though the artefacts were not completely synchronized for single trials, comparison of average of blank to average of evoked conditions provided a fairly good synchrony of artefacts. Most of the variability of the artefacts come from the change of the rate of heartbeat during the experiment. This change was rather smooth than big shifts. We record stacks of randomized stimulus conditions, each containing one trial per each stimulus condition. Therefore, average of stimulus conditions contains trials with close heartbeat rates. This provides the averages to be synchronized. Other criteria such as coherence or cross-spectrum with the ECG signal and/or other measures of artefacts may be used in order to detect the artefactual components revealed by PCA for awake animal preparations, or in any case where the synchrony may not be achieved.

Our method provides a good denoising of single trials by using both model-based and data-driven approaches. Development of a recurrent method could provide an even better approach for denoising.

Chapter 7

Source Separation for Dimensionality Reduction of Neuronal Activity

Multichannel recordings provide observation of dynamics at multiple neuronal sites simultaneously. The number of pixels provided by the cameras used in optical imaging is very high. In our case, the camera recorded from 10000 pixels, and the region of interest was one-fourth to one-third of the recorded area. As a result, recorded signal is very high dimensional and it is difficult to analyze each channel individually.

A more convenient way to study this complex data would be to analyze patterns of activity instead of analyzing the channels one by one. In primary visual cortex, visual stimulation evokes responses in different neural populations which are clustered with respect to their preference for a particular stimulus feature, as explained in Chapter 2.3. The modular organization of the visual cortex indicates a spatial aspect of population coding. Identification of the stimulus-selective clusters and investigating their response dynamics would help us to understand how different populations cooperate in order to code for different features of the visual scenes. Statistical source separation methods are useful for extracting these patterns, as explained in Chapter 3.3.

After denoising our data with the GLM-PCA method explained in the previous Chapter, we applied PCA and ICA to the denoised drifting grating responses in order to extract spatio-temporal dynamics of neuronal activity in response to oriented dynamic stimulation.

7.1 PCA on Denoised Recordings

In order to apply PCA on denoised recordings, we concatenated all trials in response to all stimulation conditions, as well as the trials of responses to blank screen. Concatenation procedure is the same as in the PCA step of the GLM-PCA denoising. Concatenation of all stimulus responses would permit searching for components as a function of stimulus condition. In order to favor the stimulus-evoked deterministic response more than the single-trial responses, means of all trials of drifting grating responses as well as the mean of blank response are concatenated with the trials.

7.1.1 Stimulus selective and nonselective components revealed by PCA

PCA on drifting grating responses revealed three major components that were present in on all of the 10 cortices that we analyzed. Two examples are shown in Figures 7.1 and 7.2. The first example is for the analysis of the data obtained in response to the 4 orientation protocol, while second is obtained by the 6 orientation protocol. These two data are obtained on two different animals.

Resulting eigenvalues are shown in log-log scale in A. First four components with highest energy are shown in B. Projections of the trials on the spatially re-arranged eigenvectors (de-concatenated principal components) are shown on the left, and the stimulus-defined averages of these trials are shown at the right of the eigenvectors.

First component corresponded to the activation of the cortex in response to visual stimulation, regardless of the orientation of the drifting grating. This component was not uniform on the cortex: The amplitude of the component was stronger on the center of the recorded area than in periphery, with the same spatial profile as the “first frame”, or the baseline fluorescence component revealed by GLM. This shows that the overall amplitude of the neural activity is dependent on the fluorescent marking. The energy of this component reflected 26.8±8.7% of the overall variability.

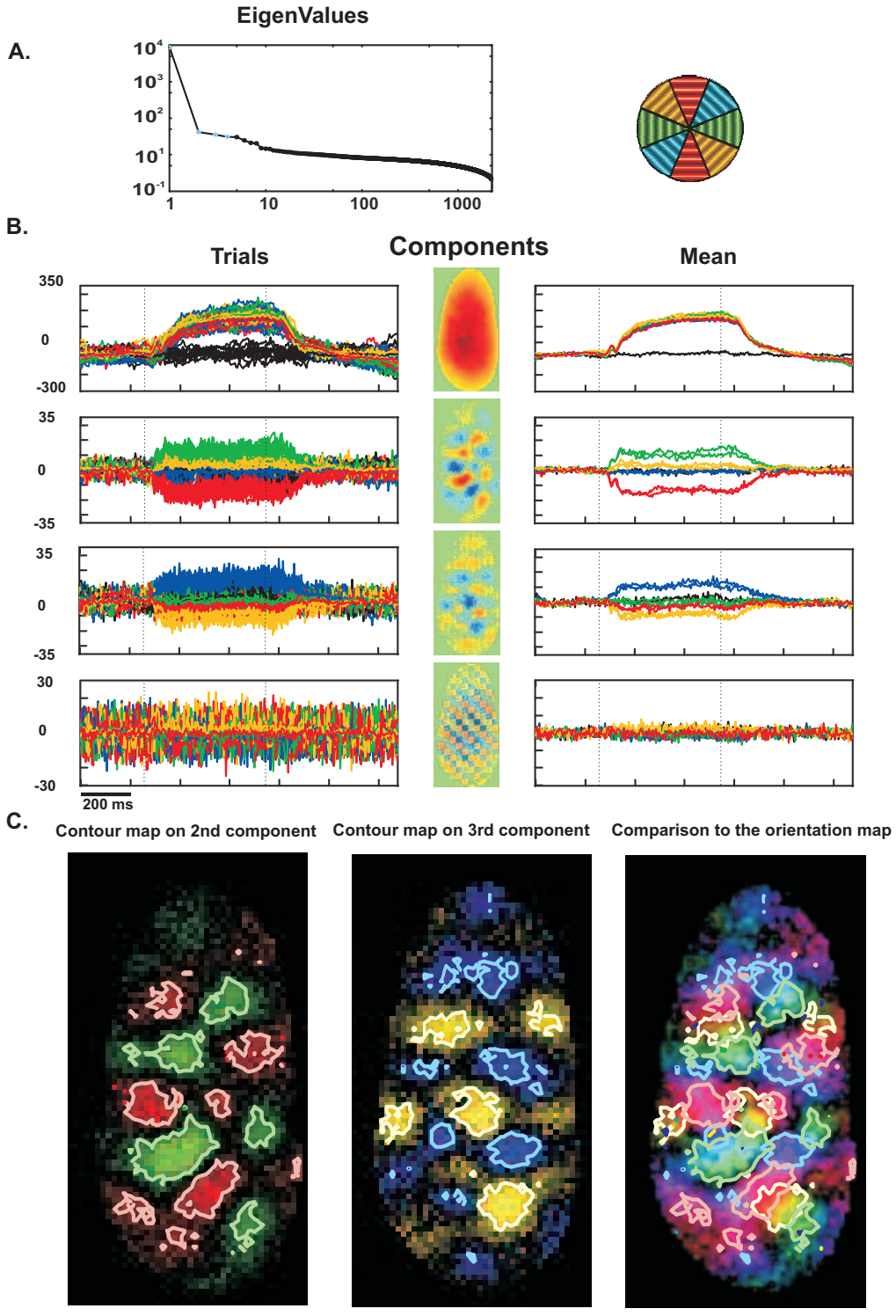

Figure 7.1 – PCA on concatenation of all trials after the GLM-PCA denoising for 4 orientation protocol. A: Eigenvalues. B: First four eigenvectors (arranged as spatial maps) and principal components (de-concatenated and superposed). Color code is given on the wheel above. C: Contour maps on 2nd and 3rd eigenvector maps and superposition of contour maps on the vectorial orientation map.

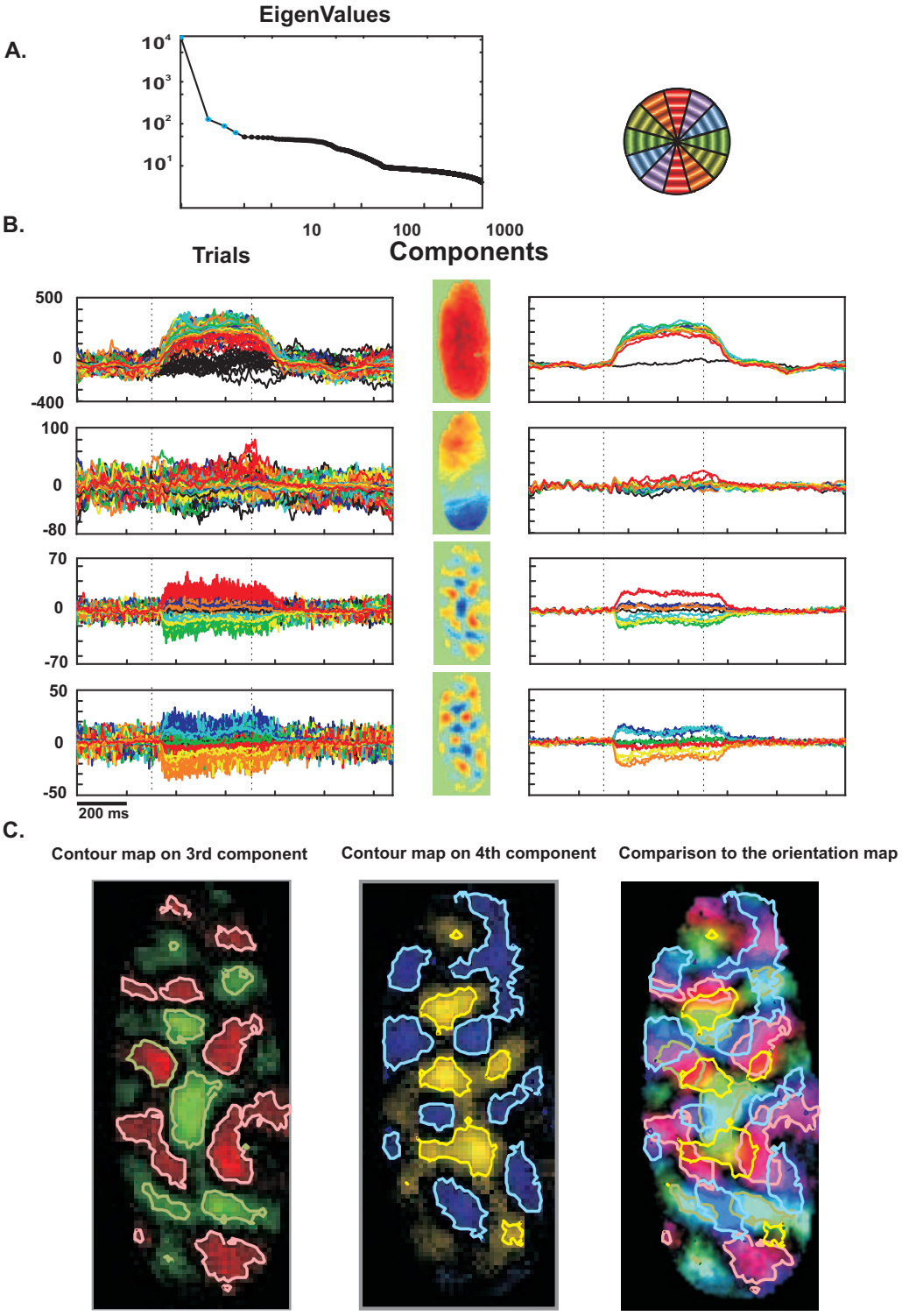

Figure 7.2 – Same as Figure 7.1 for 6 the orientation protocol.

Next components included two components which defined the orientation-selective eigenspace. All the evoked states in response to drifting gratings are found on a ring defined by two eigenvectors, in coherence with previous theoretical and intrin-

sic imaging studies (Ben-Yishai et al., 1995; Everson et al., 1998; Sirovich et al., 1996; Sornborger et al., 2005). One of the two orientation-selective components revealed the regions that are selective to horizontal versus vertical drifting gratings. In the eigenvector that represented the spatial profile of this component, the regions that are activated for horizontal drifting grating were of opposite sign for vertical, and vice versa. Second orientation-selective component had the same profile as the previous one, for 45° versus 135° drifting grating responses. Superposition of the eigenvector contour maps on the orientation map reveal that the stimulus-selective regions of the first component corresponded well to the regions that prefer horizontal versus vertical orientation (red vs. green), and for the second component corresponded to the regions that are selective to 45° versus 135° (Figures 7.1 and 7.2). We will refer to the component that separates horizontal-selective vs. vertical-selective regions as the cardinal component, and the other as the oblique component, but it should be noted that the real attractors are slightly shifted with respect to the principal component axes.

In 6 out of 10 maps, cardinal component had more energy than the oblique component. In only one map, oblique component had more energy than the cardinal component. On two other data, there were more than two components that coded for orientation and on one data, separation was more likely to separate 30°/120° and 75°/165° axis. Overall, the cardinal component expressed 0.28±0.04% of overall variance, while the oblique component expressed 0.24±0.04% of the total energy. Given that the evoked responses were present in less than half the total recording session, and that the variance in the blank response is also included in this energy, the variance expressed by the orientation-selective component in VSD recordings is in fact bigger than that. It should be noted that all the orientations evoke either positive or negative response on both orientation-selective components, even though the amplitude of projection was lower on one component than the other. Positive or negative response that is revealed on the orientation-selective components are added to the first component, which has a higher energy than the others, and therefore the overall observed neural response is always positive.

The example shown in Figure 7.2 included an additional component that expressed higher energy than the orientation-selective components. A possible explanation for this component may be the retinotopic response to drifting gratings that has been reported recently using similar analysis procedures (Onat et al., 2011b). The component that we see in Figure 7.2 had a stronger amplitude for horizontal drifting grating, with a phase shift for the two different directions of movement of the grating. The spatial representation of the eigenvector was indeed aligned with the retinotopic alignment of the horizontal grating. This kind of components was present in 6 of the 10 cortices, but most of the time they were very weak and the

energy was shared among multiple components.

Projection of the denoised data on the first nonselective and the next two orientation-selective components provided reduction of dimensionality to three dimensions that provide a visualization of the spatio-temporal dynamics of orientation selectivity. We will not consider the retinotopic components when reducing the dimensionality for analyzing orientation selectivity, but they will be taken into account for calculating the independent components later.

This 3-dimensional representation revealed a plane on which the visual response as a function of the orientation follows a slightly distorted circular shape. The attractor states were lined up on a ring, which may stand for a continuous ring attractor. This ring on the orientation-selective plane got activated by the nonselective component, which corresponded to the first principal component.

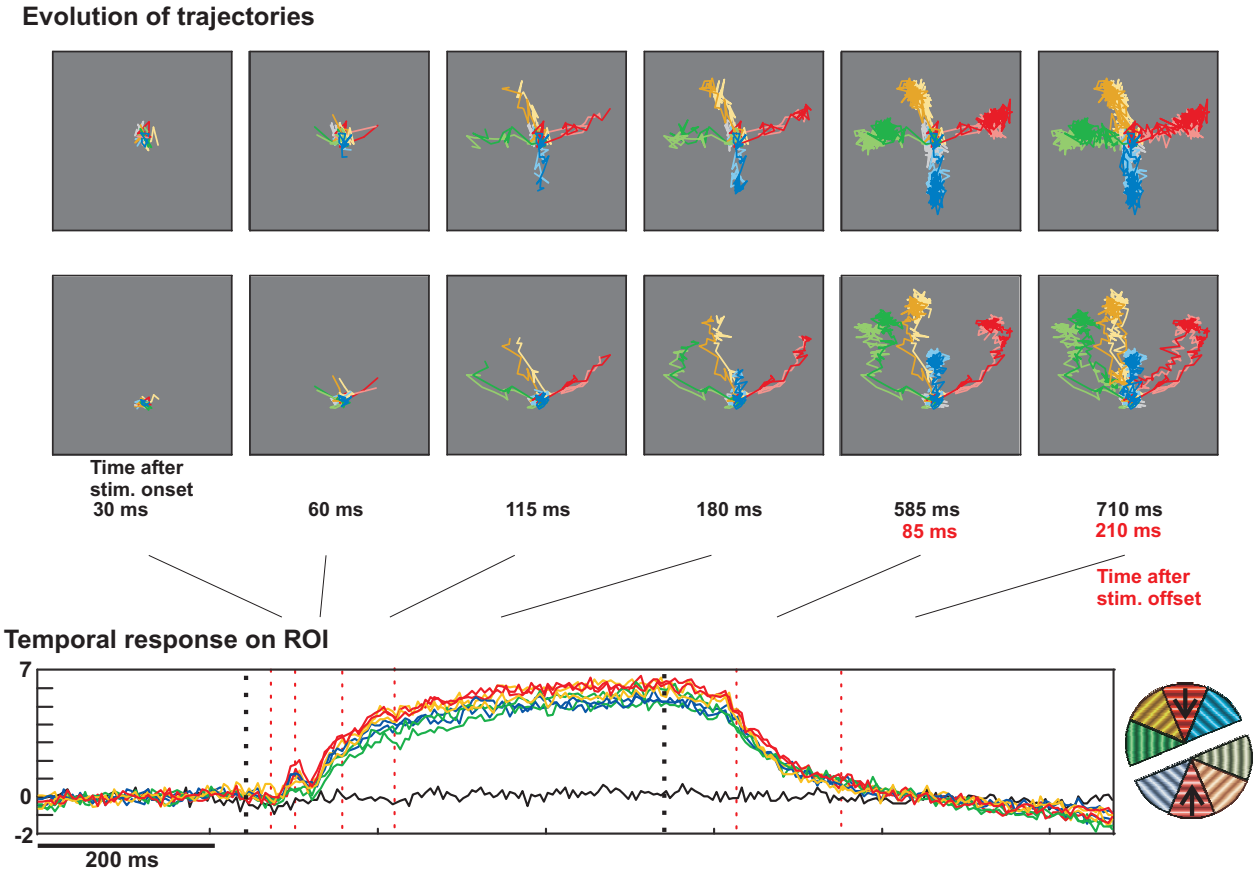

Figure 7.3 – Evolution of trajectories on 3D principal component space, for the data shown in Figure 7.1. Light and dark colors represent two directions of the same orientation.

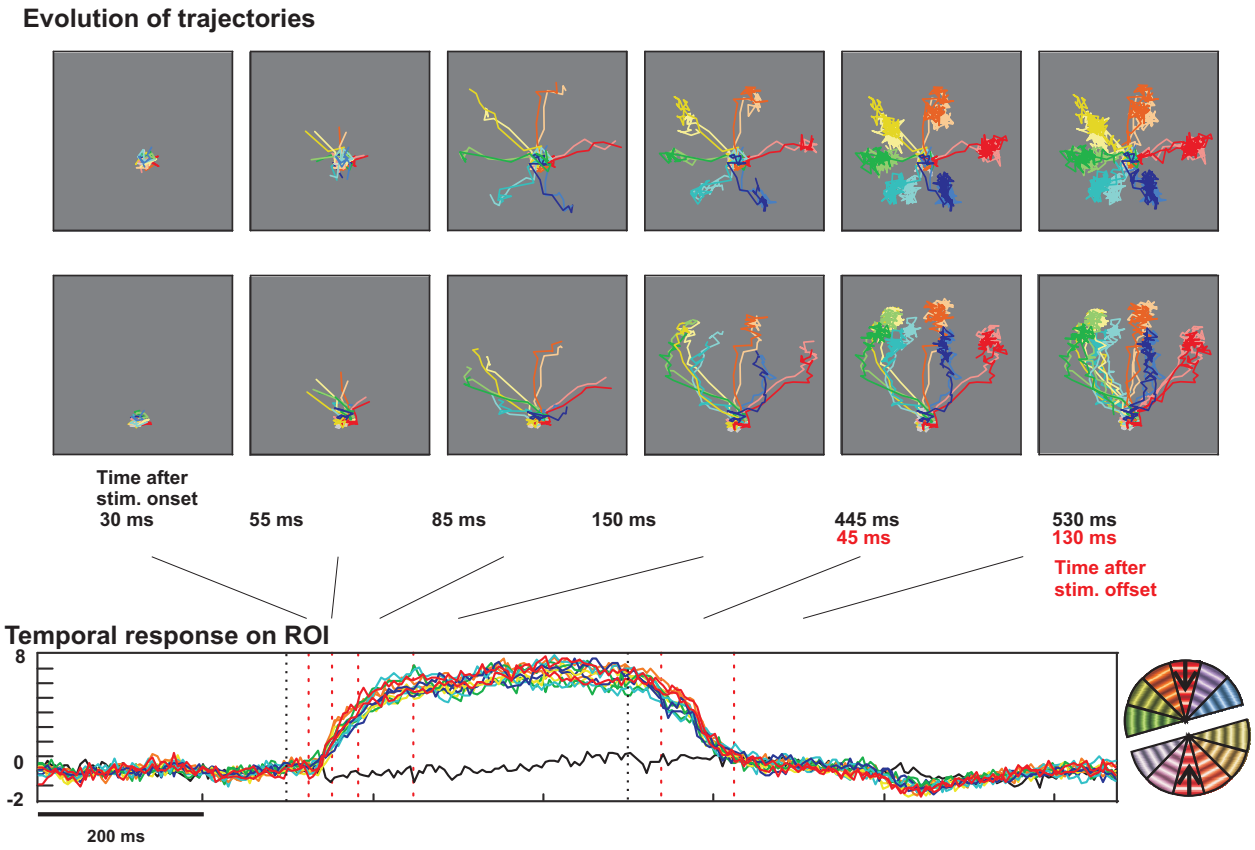

Figure 7.4 – Same as Figure 7.3 for the 6 orientation protocol example.

7.1.2 Dynamics of Orientation Selectivity on a 3-Dimensional Principal Component Space

3-Dimensional PC projection revealed several points about the dynamics of orientation selectivity that were not evident to see by conventional methods (Figures 7.3 and 7.4). Following the stimulus onset, cortical response converged rapidly to an attractor point on this ring, depending on the orientation of the stimulus. Separation of the orientation-selective states started 57±4 ms after stimulus onset, which corresponded to 12±4 ms after response onset. Orientation selectivity reached its maximum in the middle of the transient response at 80±18 ms after stimulus onset and started to decline slightly afterwards, while the response on the nonselective axis peaked around 118±37 ms after stimulus onset. These results indicate that discrimination of the stimulus orientation starts right at the beginning of the visual response, and the most efficient orientation discrimination is reached much before reaching the peak of the temporal signal. Even though there was a certain amount of variability for each trial, trials stayed in the vicinity of the attractor during visual response (Figures 7.5 and 7.6).

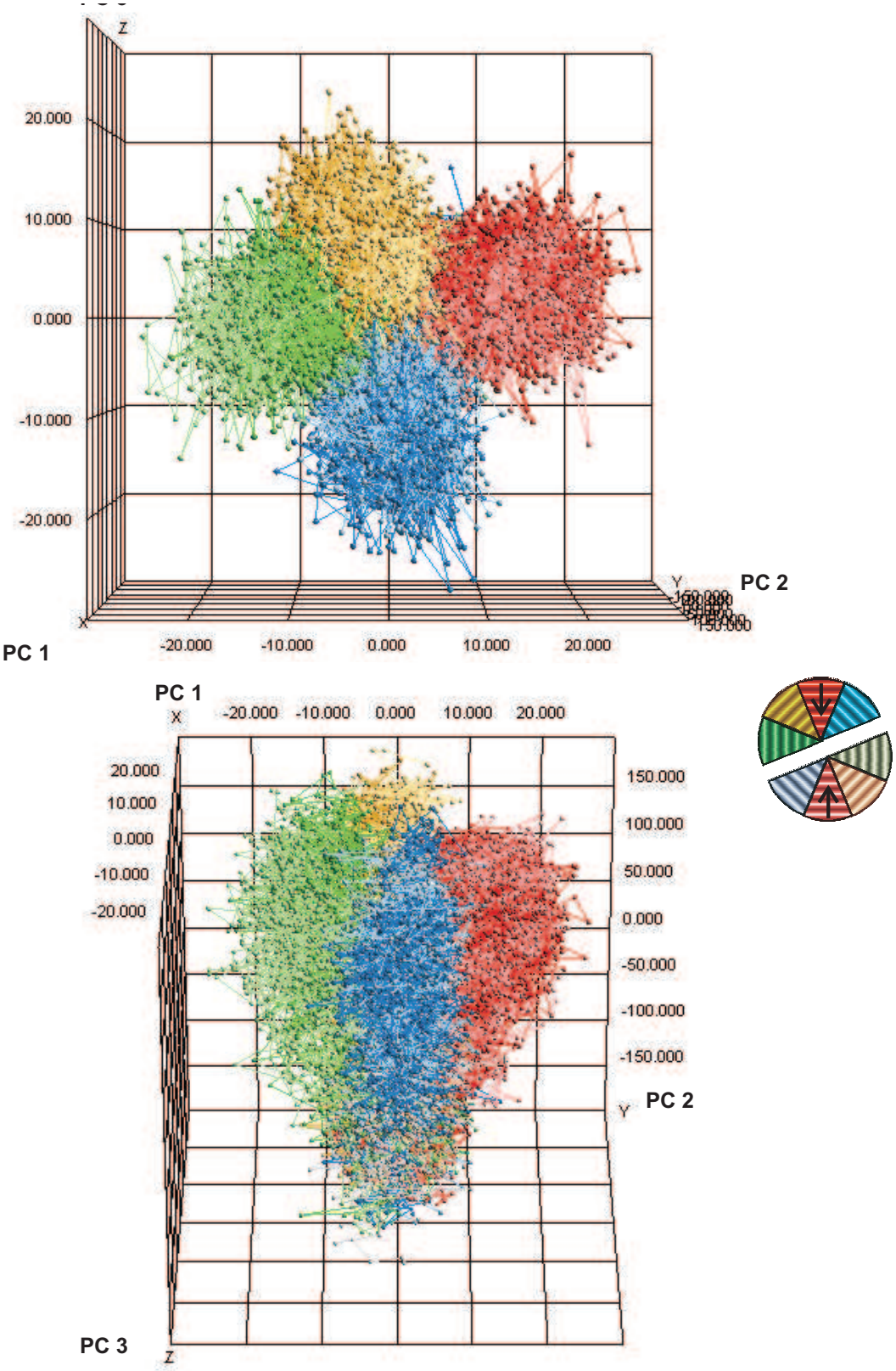

Figure 7.5 – Trajectories followed by all trials on the 3D eigenspace.

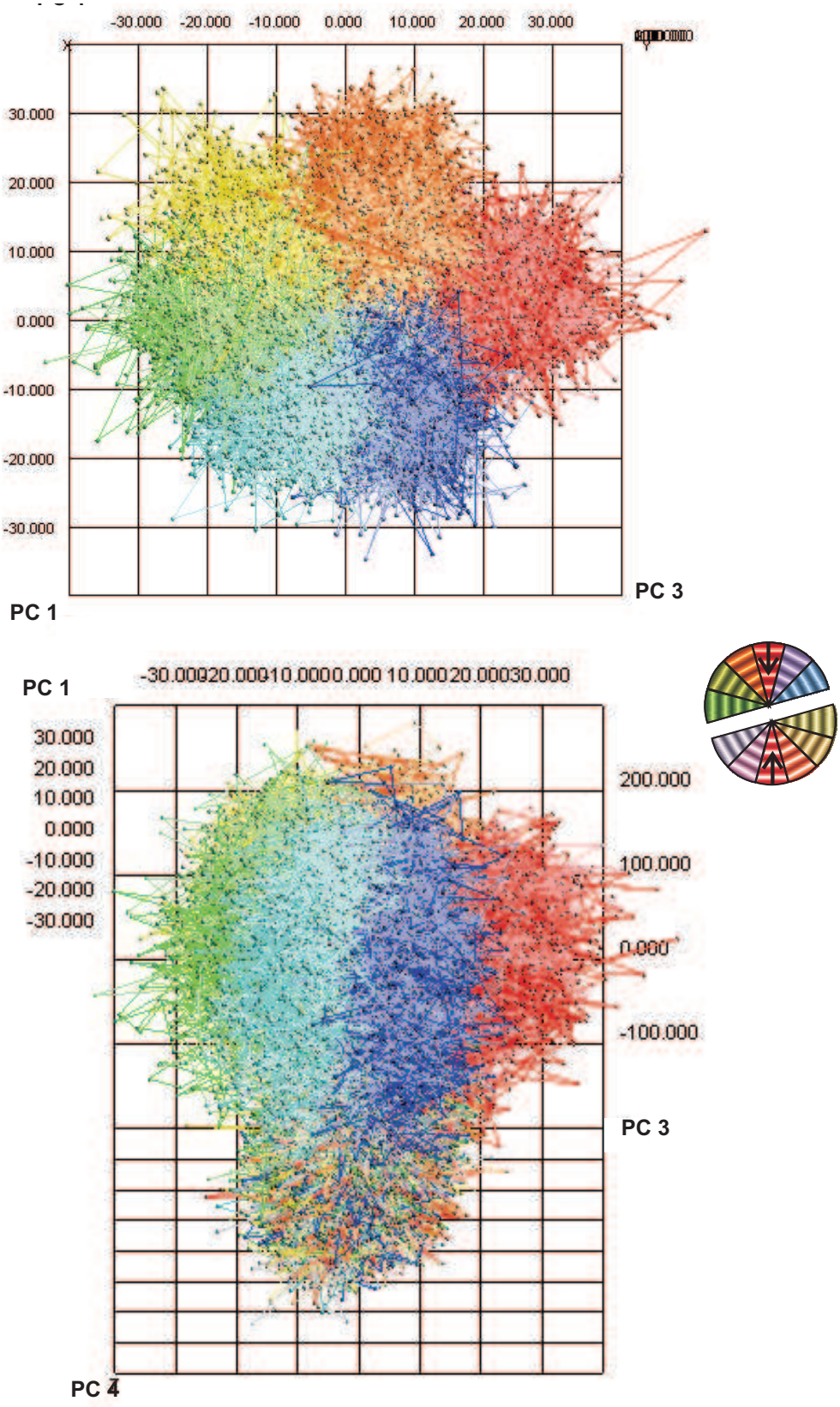

Figure 7.6 – Same as 7.5, for the 6 orientation protocol example.

The path that the trajectories followed on this space showed a hysteresis for the onset and the offset transients. While the onset trajectory was highly orientation-specific, offset trajectory followed a path that is closer to the no-stimulus attractor (the point of origin).

7.1.3 Anisotropies of the ring attractor

The first sign of anisotropy of the orientation preference revealed by PCA was the cardinal component having higher energy than the oblique component on 6 versus 1 cortical areas that included only 2 orientation-selective components. Other than that, when we aligned the two orientation-selective components to have horizontal-selective attractor to lie at 0° on the ring, we observed that the stimulus-selective response has a particular organization on the orientation-selective domain (Figure 7.7). The dots in the Figure represent the mean of all the time points that fall on the attractors for all data with successful separation for 4-orientation protocol (5 out of 7 data). The standard deviation on the two principal component axes is represented by the cross around the points. Orientation-selective attractors (on the left of each subfigure) are calculated by taking the mean of the attractors for two directions of movement (on the right).

The angle separating the attractor from the nearby attractors seem to be the highest for the horizontal-selective attractor. Moreover, distance of 0° attractor to the origin seem to be bigger than for the other attractors. This would probably indicate a stronger separability for the horizontally-oriented visual features than the other orientations, which may stand for an over-representation of the horizontal orientation selectivity in visual cortex, which is known as the oblique effect (Appelle, 1972; Li et al., 2003). However, while this effect could clearly be seen on the data with smaller standard deviation, the difference was not so clear when the standard deviation was high. More data and more sophisticated tools are needed in order to prove clearly the existence of this effect.

7.1.4 Orientation preference on the ring attractor compared to the orientation map

In order to verify if the ring on the two-dimensional orientation-selective eigenspace represents the continuity of all possible orientations, we calculated the linear combination of the two components with coordinates that correspond to 24 points on a circle centered at the origin. Then, we defined a mask with this linear combination, by setting the minimum amplitude of the pixels to 0 and the maximum to 1, and we multiplied this mask point by point with the orientation map.

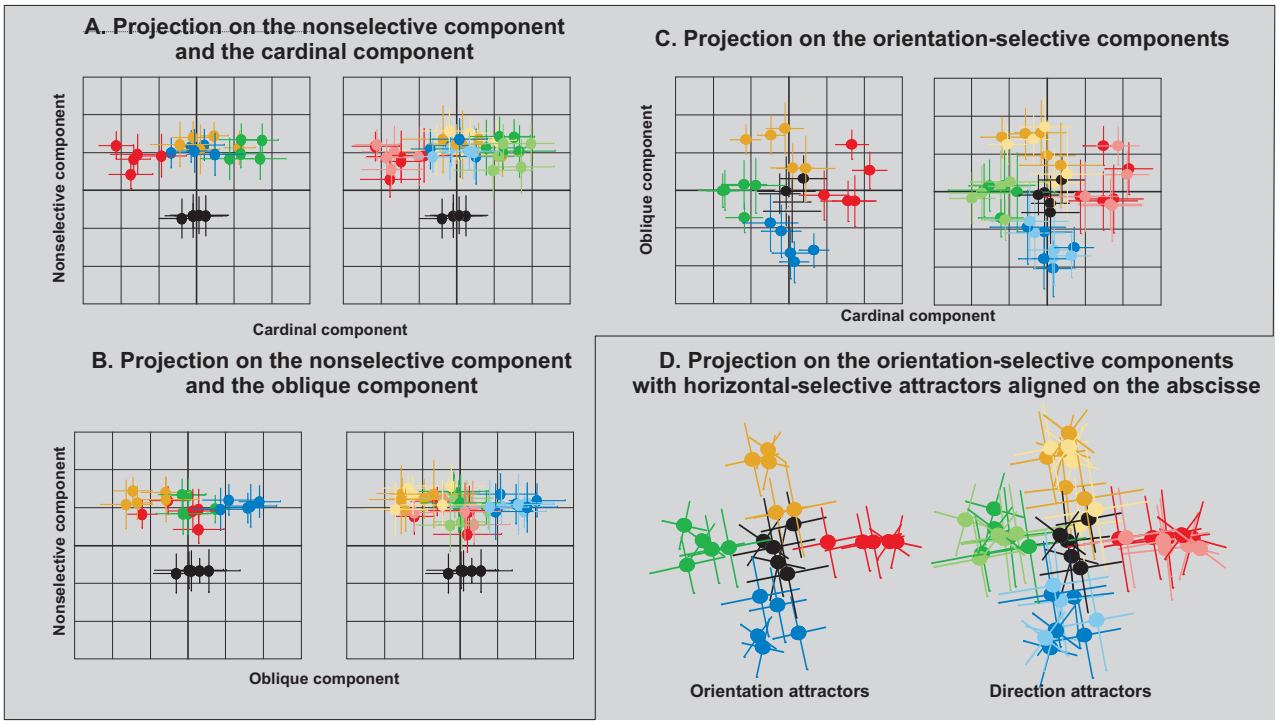

Figure 7.7 – Superposition of the mean of the normal principal component projections on the response plateau. Minimum of all the axis is -4 and maximum is 4. A, B, C correspond to the 2-dimensional projection of the data on principal components 1-2, 1-3, 2-3 respectively. D represents the same projection as in C, except that the horizontal-selective attractors (or the first direction of the horizontal orientation in case of direction-selective attractors) are aligned on the abscissa.

The resulting orientation maps masked by each of the 24 samples on the ring are shown in Figure 7.8A. The masking of the orientation map shows that the positive regions on the linear combination of the two eigenvectors on the ring corresponded well to the regions that prefer the orientation defined on the ring, which results in dominance of the regions that have an orientation preference represented by the color code of the ring (the same color code as the orientation phase map). Defining an alternative tuning curve for each pixel by sampling the circle on the orientation-selective principle components gives an orientation map (Figure 7.8C) which represents the same angular preference as in the orientation map calculated by the vectorial summation method on denoised data (Figure 7.8B). This alternative method for calculating the orientation map provides a smoother orientation map than Gaussian fit on individual pixels, as the ring attractor provides a higher sampling of the orientation domain than the actual number of orientations used in the protocol (24 compared to 4 points in case of the example in Figure 7.8). It should be noted that the anisotropies of the ring are not taken into account with this method. Moreover, even though the angular preference is preserved, the changes in selectivity between the pinwheels and iso-orientation domains was less smooth than it is observed on

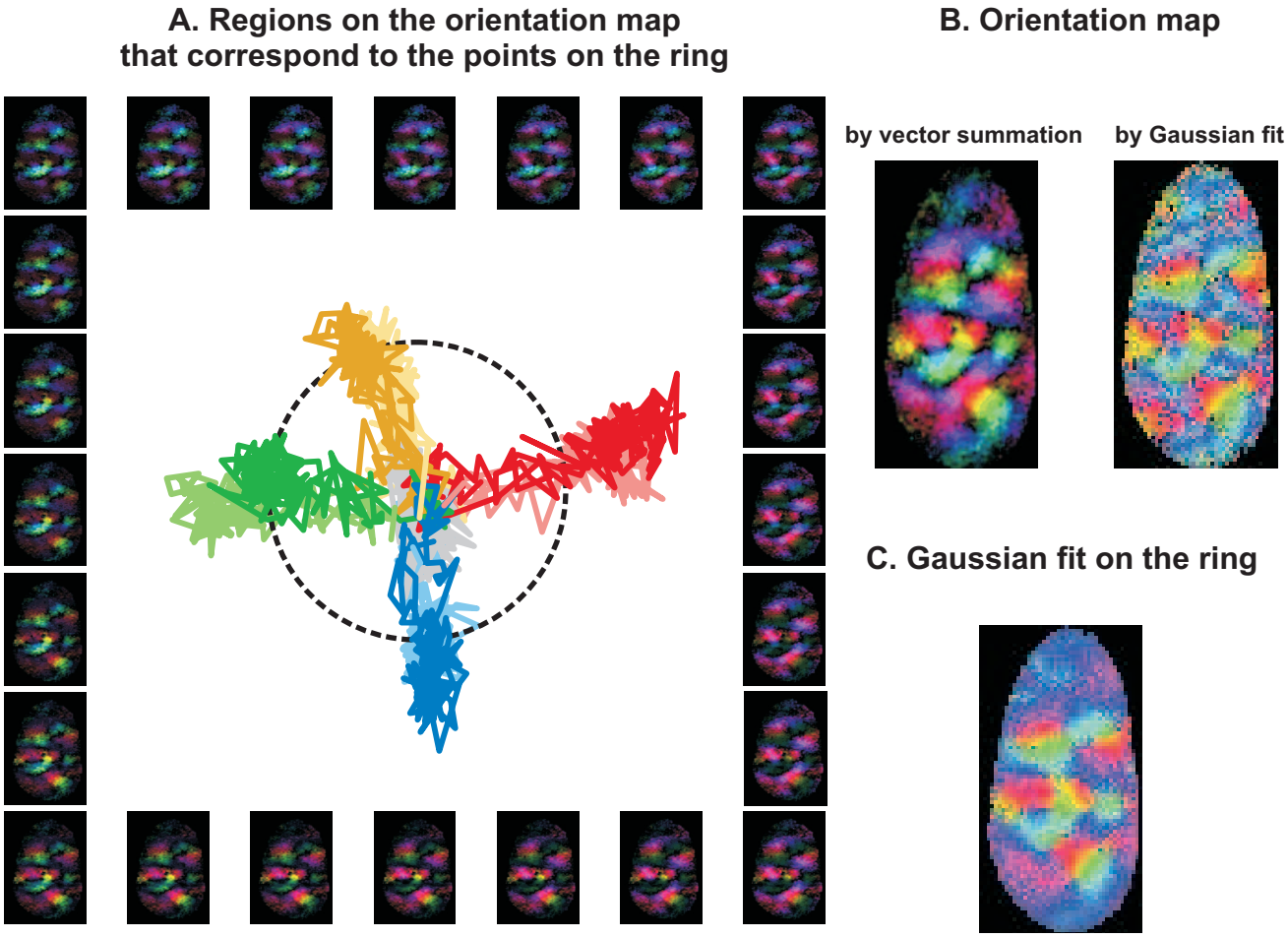

Figure 7.8 – Orientation map calculated on the ring defined by the two orientation-selective components. A: Orientation map multiplied point by point by the linear combination of two components with coordinates at equidistant angles on the ring. B. Orientation maps calculated by vector summation and Gaussian fit on the tuning curve. C: Orientation map calculated by a Gaussian fit on the artificially generated orientation maps represented in A.

the vectorial summation orientation map. This approach is not enough to replace the conventional methods for calculating the orientation maps. Nevertheless, calculating the orientation map from the principal components may help to find the orientation map on the regions that get activated locally, such as the orientation maps of areas 17 and 18 separately as we will see in the following section.

7.1.5 Detection of the Area 17/18 Border by PCA

When the analyzed regions contained both areas 17 and 18, PCA gave 4 orientation-selective components instead of 2, which represent two pairs of components, each coding for either area 17 or area 18 (Figure 7.9). This was the case for data from two animals. In the example shown in the Figure, separation of the two areas was

not clearly visible from the temporal activation profile of the pixels in the ROIs (A and B). When PCA is applied to this data, we could distinguish the border between the two cortical areas. The intersection of the two maps represents possibly the transition region. As it was suggested by Bonhoeffer et al. (1995), iso-orientation domains revealed by PCA were more similar to the 'linear zones' than circular blobs, and as it was suggested by Swindale (1996), these linear zones lied perpendicular to the area 17/18 border. Unfortunately, we did not perform another recording with a spatial frequency that would provide separation of the two cortical areas on this data.

As we observed this separation in the PCA, we re-analyzed this data by separating the two cortical areas. This provided a better separation, which provided components that were more similar to the examples presented previously.

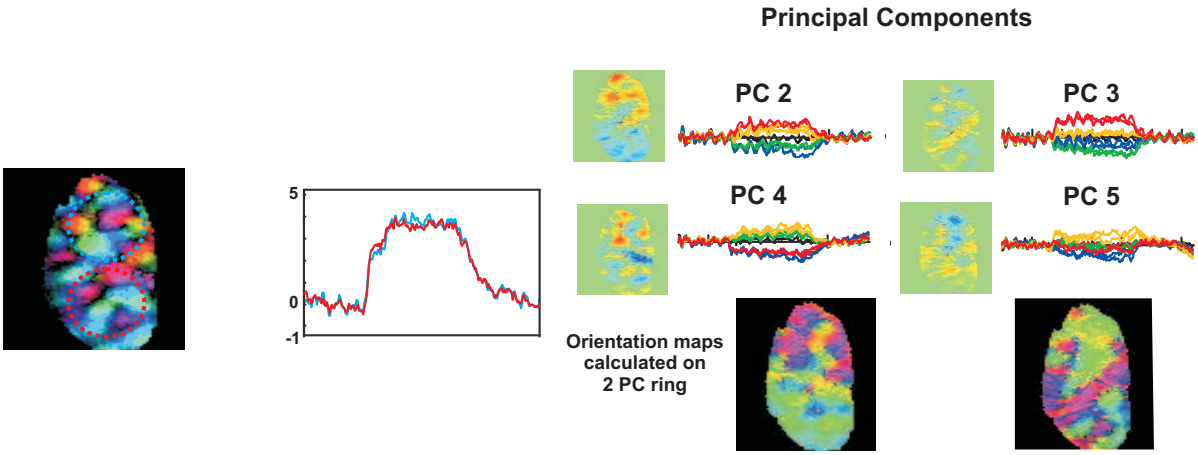

Figure 7.9 – Area 17/18 border detected by PCA. A: Orientation map and the two regions of interest for area 17(blue) and 18(red). B: Mean temporal response of all the pixels in the ROIs in A. C: Resulting principal components. D: Orientation maps for each PC couple shown in C, calculated by the method represented in Figure 7.8.

7.2 ICA on Denoised Recordings

The decomposition criterion in PCA is orthogonality of the sources, which is revealed by the eigenvectors of the covariance matrix of the data. However, this criterion may not be enough and it may even be restrictive. In our case, PCA could distinguish activity patterns that code for different orientations but it failed to separate different directions of movement of the same orientation. Nevertheless, with a careful look we can see that the direction-selective attractors do not project on the exact same location (see the direction-selective attractors in Figure 7.7). Direction-selective attractors were placed at very close regions in the principle component space, but no orthogonal axis could be assigned for coding of direction of movement.

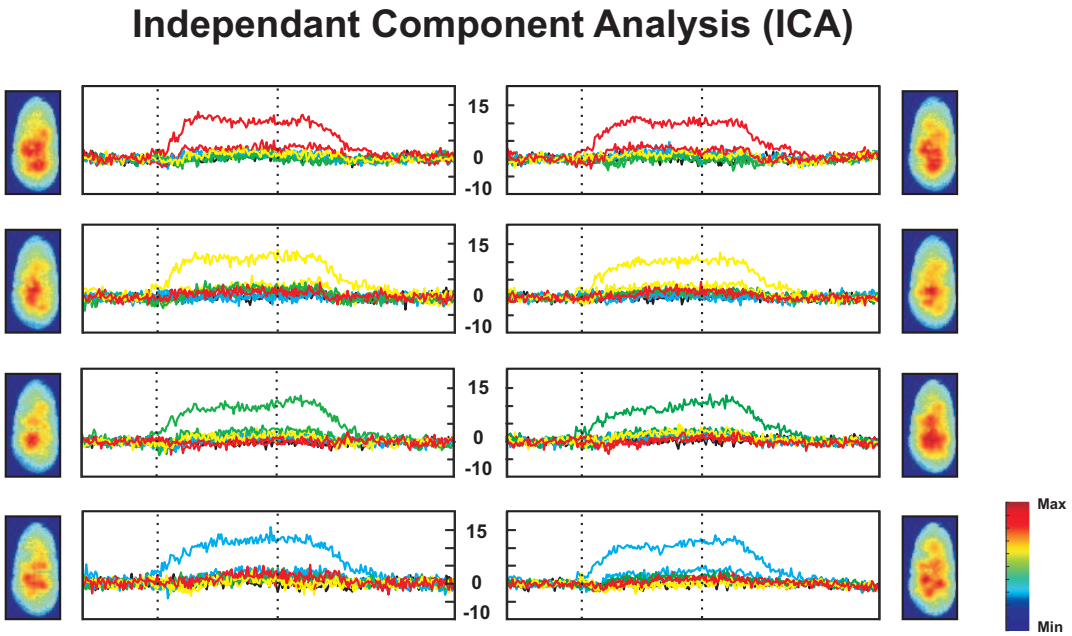

Figure 7.10 – ICA for 4 orientation 8 direction protocol on the data whitened by PCA as shown in Figure 7.1.

ICA provides a more sophisticated decomposition than PCA by taking into account the higher order statistics, as explained in details in Chapter 4.2.2. The FastICA algorithm (Hyvarinen, 1999) allows separation of non-Gaussian sources by taking into account the negentropy estimated by kurtosis, which is proportional to the fourth moment about the mean. Resulting independent components do not have to be orthogonal. Here, we show that ICA can discriminate direction-selective temporal activity patterns.

ICA is calculated on the first 200 principal components obtained by PCA on de-noised data as explained previously. FastICA algorithm is used with symmetric approach and *tanh* nonlinearity.

For the example with 4-orientation protocol shown in the previous figures, ICA revealed 8 direction selective components, each reflecting a weak orientation-dependent response (Figure 7.1). ICA was successful in 4 of 10 data for separating different directions of at least one orientation. On 3 out of 10 data, ICA separated individual orientations, and on the others ICA resulted in only camera pattern noise. The cases where ICA failed to discriminate direction-selective populations were mostly the data contaminated strongly by camera pattern noise.

7.3 Discussion

After denoising the data with our hybrid GLM-PCA method, we analyzed the artefact-free signal by PCA, and later by ICA in order to find statistically uncorrelated and independent neuronal response patterns. PCA revealed orientation selective patterns, while ICA could separate populations that responded to directions of movement of drifting gratings. We showed that the two opposite directions of drifting grating of the same orientation were placed on nearby but yet distinguishable two points in a two-dimensional eigenspace. Each evoked trajectory converged rapidly after the response onset to an attractor point that coded for the orientation of stimulus in this space.

First principal component that we observed stood for the visual response which is not selective to the orientation of the drifting grating. Sharon et al. (2007) reported that a local oriented visual stimulation evokes a plateau of activity which is largely independent of stimulus orientation. We show that this plateau adds up linearly to the orientation-selective response pattern. This kind of first principal component that does not discriminate stimulus-specific information was also reported in an electrophysiological study of prefrontal cortex of monkeys during frequency discrimination task (Machens et al., 2010). In V1, both simple and complex cells elicit membrane potential depolarization in response to nonselective orientation (Carandini and Ferster, 2000; Gillespie et al., 2001). Moreover, it is known since the earliest intrinsic imaging studies that any stimulus evokes a metabolic response in a way that is not stimulus-specific in the visual cortex (Blasdel and Salama, 1986; Blasdel, 1992a). Under these evidences, this signal may be at least partially of cortical origin. It is possible that this signal originates from decoupling of soma and dendrites due to shunting inhibition. Another possible candidate is the activation of the inhibitory neurons. Taken into account the smaller number of inhibitory cells with respect to excitatory cells, the latter argument cannot explain the high energy of the nonselective component. Taking into account the spatial profile of the signal, one may conclude that this nonselective profile of the evoked activity is amplified by the baseline fluorescence.

Sornborger et al. (2005) reported that the average response among drifting gratings contains 100 times the power (10 times the signal amplitude) of the differential response in intrinsic imaging, which we confirm to be at the same level on VSD imaging data in response to full-field drifting grating stimulation. This is the reason why differential imaging is preferred by optical imaging community if only spatial attributes of the evoked activity are investigated. On the other hand, if anisotropies of the ring attractor exist, differential imaging strategy may be misleading as orthogonal orientations may not be exactly 180° apart on the ring.

We show that when the orientation-selective response and the nonselective response are considered separately, orientation-selective pattern emerges more rapidly than the nonselective component. Early peak of orientation selectivity followed by a decline was reported earlier by Sharon and Grinvald (2002). Our results confirm their observations which were obtained by the analysis of the shape of the tuning curve on regions that prefer a particular orientation. As Sharon and Grinvald (2002) claimed, decline of orientation selectivity indicates intracortical modification of orientation tuning. Analysis of the dynamics of stimulus-selective and nonselective components may provide information about how different mechanisms involve in tuning of visual cortical responses.

We observed the DA notch to be present both on orientation selective and nonselective components. This signal probably represents the cortical response to the flash of the visual stimulation, while the slower global activation corresponds to the response to the drifting of the grating.

Fast dynamics of the stimulus-selective response components was comparable to the observations of Mazor and Laurent (2005) about the fast odor discrimination by locust antennal lobe projection neurons during transient states and the study of Briggman et al. (2005) on faster decision making of neuronal populations than single cells in leech nervous system, in the sense that population responses discriminated different orientations during the early transient responses. These results indicate that the transient response is more efficient than stationary fixed point response in terms of coding, and given that the two previous study and our work are performed on different systems, this effect may be universal for neuronal coding.

On the other hand, attractor states that are observed after tens of milliseconds of visual stimulation onset would help maintaining the persistent activity in the cortex during stimulus response (Brody et al., 2003). We observed that attractor state dynamics are achieved in response to drifting gratings about 80 ms following stimulus onset. This type of attractor state coding would provide investigation of stimulus after-effects in future studies using appropriate protocols.

Following the stimulus offset, trajectories followed a path which was less orientation-selective than the onset trajectory. This is probably a consequence of the decrease in orientation selectivity during visual responses. Following a less stimulus-selective trajectory at the response offset may be a strategy to converge more easily towards a new attractor state in case of incoming stimulus.

A recent study by Onat et al. (2011b) showed that PCA could separate the orientation-selective component from the retinotopic response to the drifting grating. In our data, 6 out of 10 recordings seemed to include this kind of components. The main reason for why this component was not present for all of the data and for all stimu-

lus conditions is possibly the difference between the analysis design between their approach and our approach. Our analysis is aimed to separate orientation-selective response patterns among a complete set of orientations, and to investigate their transient and fixed response dynamics. Onat et al. (2011b) excluded the transient response (first 400 ms of the visual response) from their analysis, which eliminates the strong change in the amplitude of the fluorescent signal due to the onset of the visual response. The authors pointed out that inclusion of the transients in their analysis reduced the sensitivity of the method to the oscillatory response that occurred lately in the signal. This late part of the signal was not present in our data as we restricted the stimulus duration to only 500 ms. Moreover, the authors noted that they could not observe these components in all the cases neither: it was possible to extract this signal only when the VSD signal was very clean. Given all these differences in the protocol design between the two studies, our method is expected to be less sensitive to the retinotopic waves which explains why we did not always observe this component.

PCA on denoised data revealed a first component that stood for the nonselective component of the evoked activity, and following components coded for orientation selectivity. This means that the nonselective activity is uncorrelated with the orientation-selective activity. On the other hand, ICA resulted in components that were selective for direction of the stimulus, which resulted in individual components corresponding to each direction of movement of each orientation. Even though all directions could not be extracted for all data, there was no nonselective component revealed by ICA: this component was shared between each direction-selective component. Therefore, independent components represented a mixture of both nonselective and selective parts, and probably some other components (such as retinotopic responses to gratings) as there were no other components with a particular spatial profile. This means that the nonselective activity may be uncorrelated with the stimulus-selective response, but these two are not statistically independent.

The failure of PCA for discriminating direction-selective attractors indicate that direction selectivity is not orthogonal to the orientation selectivity as suggested before (Goldberg et al., 2004). However, it should be noted that in our protocol direction of movement was dependent on orientation. More appropriate protocols may be needed to evaluate the dependence between orientation and direction selectivity.

When the checkerboard-pattern camera noise was very strong in the recordings, ICA after our GLM-PCA denoising gave components that reveal this camera noise, instead of direction selective components. ICA is known to be sensitive to outliers, therefore this approach should be carefully used in this case.

Our blind source separation analysis for discrimination of functional neural popu-

lations on denoised data shows that statistics shared by neuronal sub-populations can be revealed by source separation on VSD imaging data. Since PCA was shown to separate efficiently the orientation preference domains, we conclude that orientation selectivity coding can be retrieved from the sole study of variance of responses. Since ICA, which is based on 4th order moment about the mean, revealed direction selectivity preference, we conclude that higher order statistics in the VSD Imaging signal are necessary to extract computations in the visual cortex linking motion and orientation. We speculate that the discrimination of the orientation-selective and direction-selective patterns by using 2nd order and 4th order statistics respectively may also be one of the strategies how the discrimination of the motion and form is implemented in the visual system: Higher order areas may extract statistics of their interest from the populations that they see in the lower area in the hierarchy. In our case, we may speculate that the 4th order statistics would be transmitted to the motion pathway while 2nd order statistics would be extracted by the form pathway.

Chapter 8

Analysis of VSD Imaging Recordings in Response to Stimuli with Different Statistics

In this chapter, we will briefly introduce possible strategies for analysis of VSD imaging data in response to longer and more complicated visual stimulation protocols, and we will present some preliminary results.

8.1 Denoising of Long Recordings

Recording of long exposure and stimulation durations implicate more complicated source components in the recordings. We extended our denoising strategy in order to analyze long recordings (longer than 2 seconds; in our case 5120 ms of recording and 4 s of visual stimulation). At this temporal range, intrinsic signal arises as a result of the metabolic changes of the neural tissue, respiration artefact starts to be significant, and heartbeat synchronization is lost. A long recording example and resulting GLM source separation is shown in Figure 8.1. This recording is performed on the same cortex as the example shown in Figure 6.3.

As the heartbeat frequency may change over the recording, it is not reliable to use simple sine waves in the GLM regressor base for the heartbeat-induced artefact model in long recordings. Instead, we developed a heart-triggered average method to be used in GLM. After removing the bleaching by using a double-exponential fit, mean heartbeat window among all trials is calculated for each pixel by averaging windows of blank activity centered on each heartbeat; and this window is filtered above 30 Hz. This set of heartbeat windows is then analyzed by PCA.

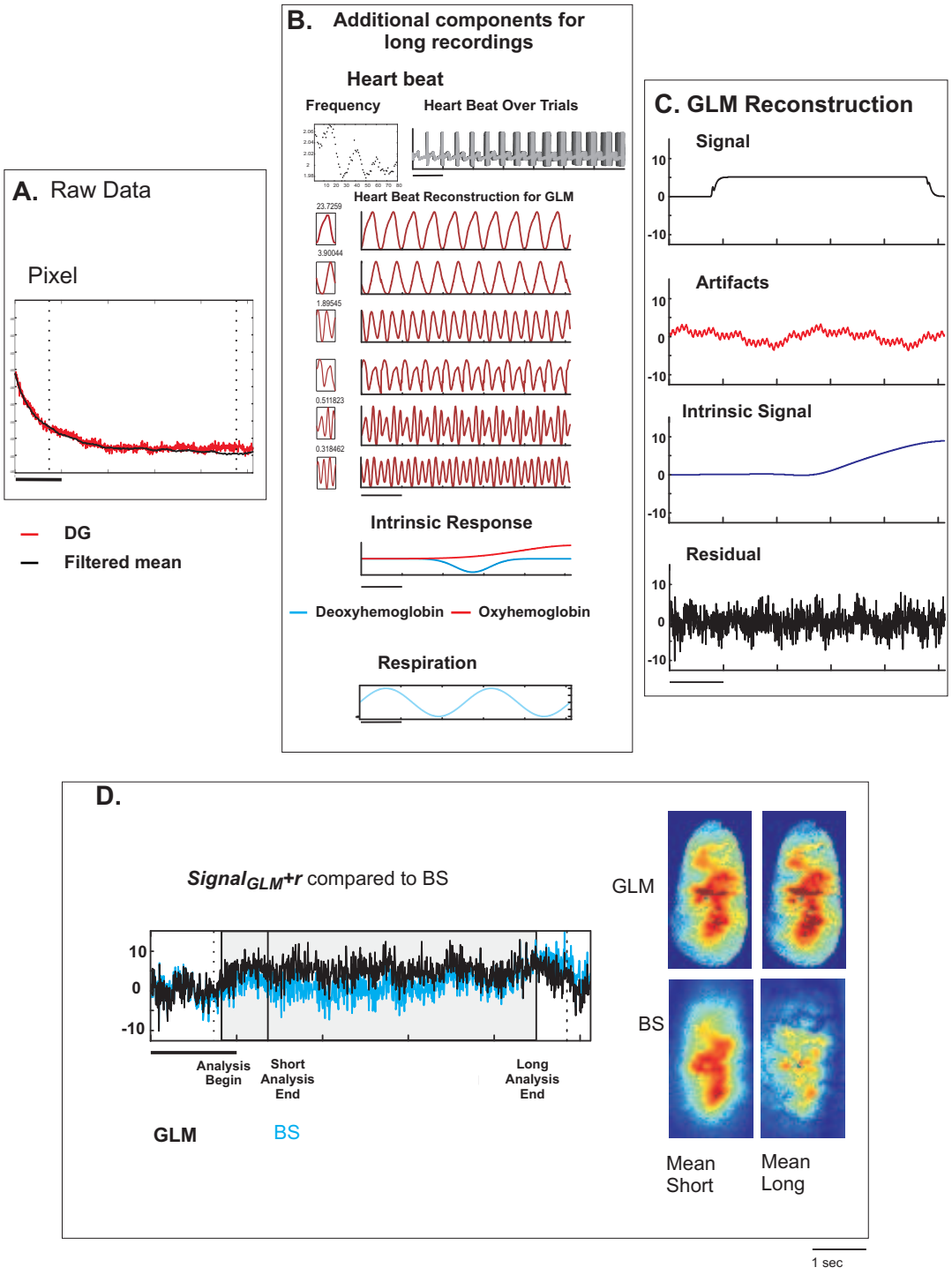

Figure 8.1 – Problems encountered while separating the sources involving long recordings, and additional GLM regressors developed to remedy this problem. A: Temporal response on a pixel on the raw data, and the filtered mean blank response that is used for blank subtraction. B: Components that occur for long recordings, and how the corresponding regressors are modeled. C: Source separation by GLM. Resulting $Signal_{GLM}$+r is the black trace and BS-cleaned response is the blue trace. Maps correspond to the mean spatial response on the short and long temporal windows specified on the temporal response window.

Decomposition of heartbeat windows on all the pixels with PCA revealed components that are relevant with Fourier decomposition; reflecting the phase and harmonics of the heartbeat. Resulting components were closer to the blood pressure signals than simple sine waves (Figure 8.1B). To reconstruct the heartbeat induced artefact, only the components that reflect up to 3rd harmonics of the heartbeat (6-8 components) were included in the reconstruction. For each of these components a heartbeat trace was constructed by centering the average window on each heartbeat of the recording of interest. On the overlapping windows, the mean of the tails of the two windows is taken into account.

Respiration artefact starts to be significant for recordings longer than two seconds. We introduced 2 harmonics of respiration in the GLM base for long recordings.

We modeled the neural-response related signal the same way as for short recordings. We included the notch components only for drifting gratings, as we did not observe the notch signal for natural image and dense noise responses.

Another modification to the model is to take into account the slow intrinsic signal, which we modeled with 2 components, reflecting the oxyhemoglobin and deoxyhemoglobin change Vanzetta and Grinvald (1999):

$$- a_4 \exp(\frac{(t_{onset} + peak_1 - t)^2}{{\sigma_1}^2}) \tag{8.1.1}$$

and

$$a_5 \exp(\frac{(t_{onset} + peak_2 - t)^2}{{\sigma_2}^2}) \tag{8.1.2}$$

where $peak_1 = 2000ms$ is the peak of deoxyhemoglobin, $peak_2 = 4500ms$ is the peak of oxyhemoglobin concentration. These values are estimated from the blank subtracted response. σ_1 is estimated to be 120 and $\sigma_2$to be 370 from the intrinsic change observed on the average drifting grating response. Resulting regressor vectors are shown in Figure 8.1B.

Resulting GLM source separation compared to BS on one pixel is shown in Figure 8.1D. Mean maps on short and long segments obtained after GLM denoising were similar, while BS cleaned response vanished in time and space. These results suggest that GLM could successfully remove the intrinsic response.

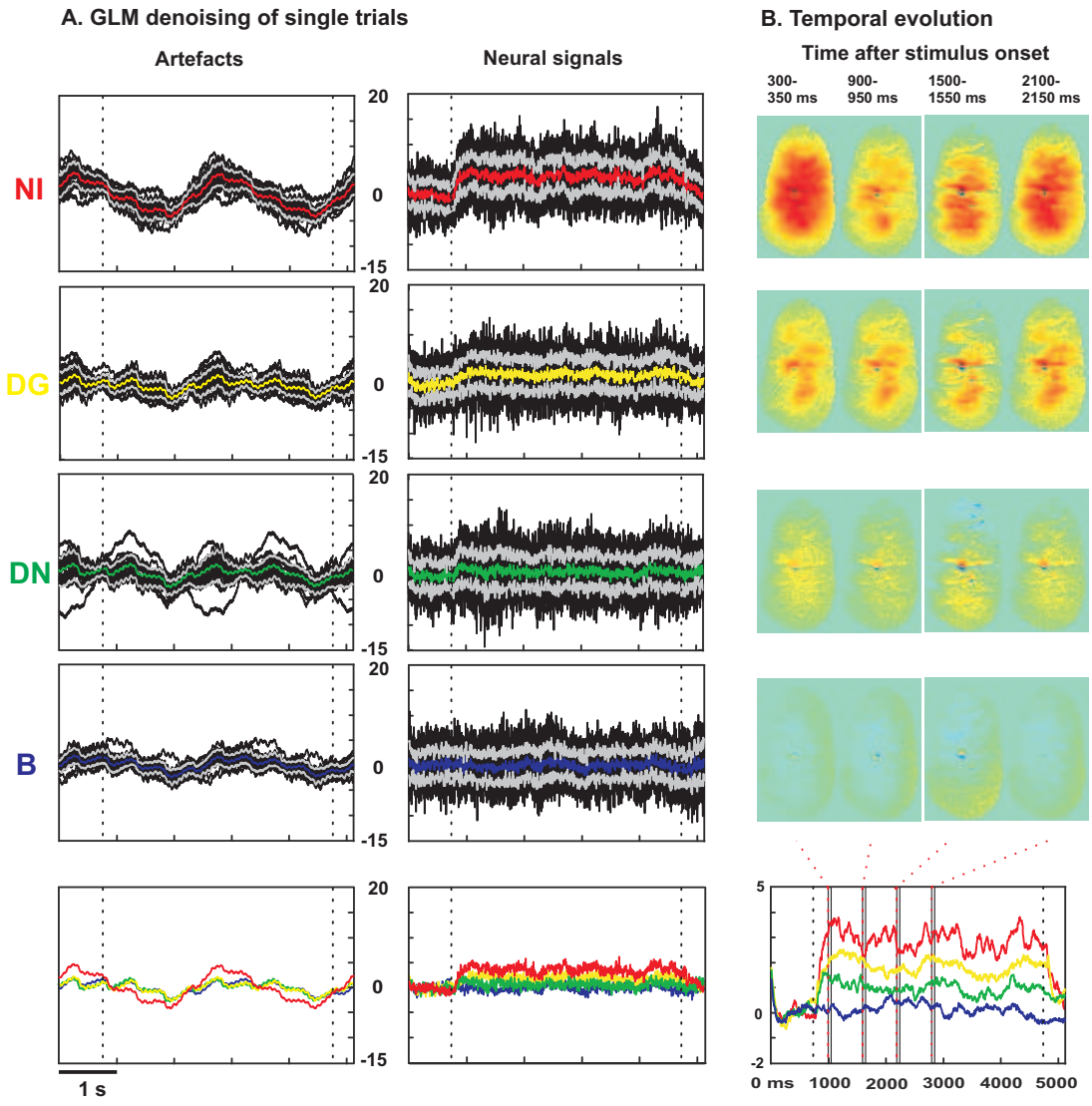

Figure 8.2 – Neural signals and artefacts revealed by GLM on long recordings in response to natural images animated with eye movements (red), horizontal grating drifting downwards (yellow), dense noise (green) and blank (blue). A. Superposition of all trials (black traces) and their means (colored traces). Superposition of means of all stimulus responses is shown at the bottom. B. Temporal evolution of the spatial responses.

Results of GLM denoising on all trials of responses to natural image animated with artificial eye movements, horizontal drifting grating, dense noise and blank are shown in Figure 8.2. Extracted artefacts and resulting neural-related signals for each trial are shown in A. Here we see that the GLM could successfully extract most of the artefacts, with some exaggeration of the respiration artefact for the natural image responses and one out-of-phase artefact extraction for dense noise. Nevertheless, the temporal profile of the responses was free of the intrinsic responses. Examples of the mean spatial profile of 10 frames triggered at four time points of the recording are shown in B. We see that the spatial profile of the drifting grating response stays stable while natural image response is more global on the cortex and visits different spatial regions. Dense noise evoked very weak response on all over the cortex. Temporal response shown below the maps represents the mean of all trials in the ROI that includes all the pixels analyzed by GLM.

8.2 Variability of Neural Population Activity in Response to Different Stimulus Statistics

Stimulus-dependency of the trial-to-trial variability of VSD imaging signal is evaluated by applying a stimulus-locked frequency-time wavelet analysis similar to the one practiced on intracellular recordings (Baudot et al., submitted).

The time-frequency wavelet analysis developed by Baudot et al. (submitted) provides both the reliability of the rate code which is mostly revealed in the low frequency bands, and of the spike timing code which is revealed in high frequencies. This analysis, when applied to VSD imaging recordings, gives a 4-dimensional representation of the trial-to-trial variability (as a function of time, frequency, 2-dimensional pixel space), allowing us to study the response reliability as a function of network structure for different time and frequency ranges. As a result of the nature of VSD recordings, only low frequency components were observed on our data.

The advantage of VSD imaging is multichannel recording of population dynamics. This permits us to record responses to a visual stimulation simultaneously on multiple channels, providing means to investigate spatial aspect of trial-to-trial variability. In order to check for time-frequency signal to noise ratio of population responses as a function of orientation selectivity, we divided the pixels in five groups

as a function of their localization in pinwheel or orientation center. 4 orientation domains are considered (0°, 45°, 90° and 135°).

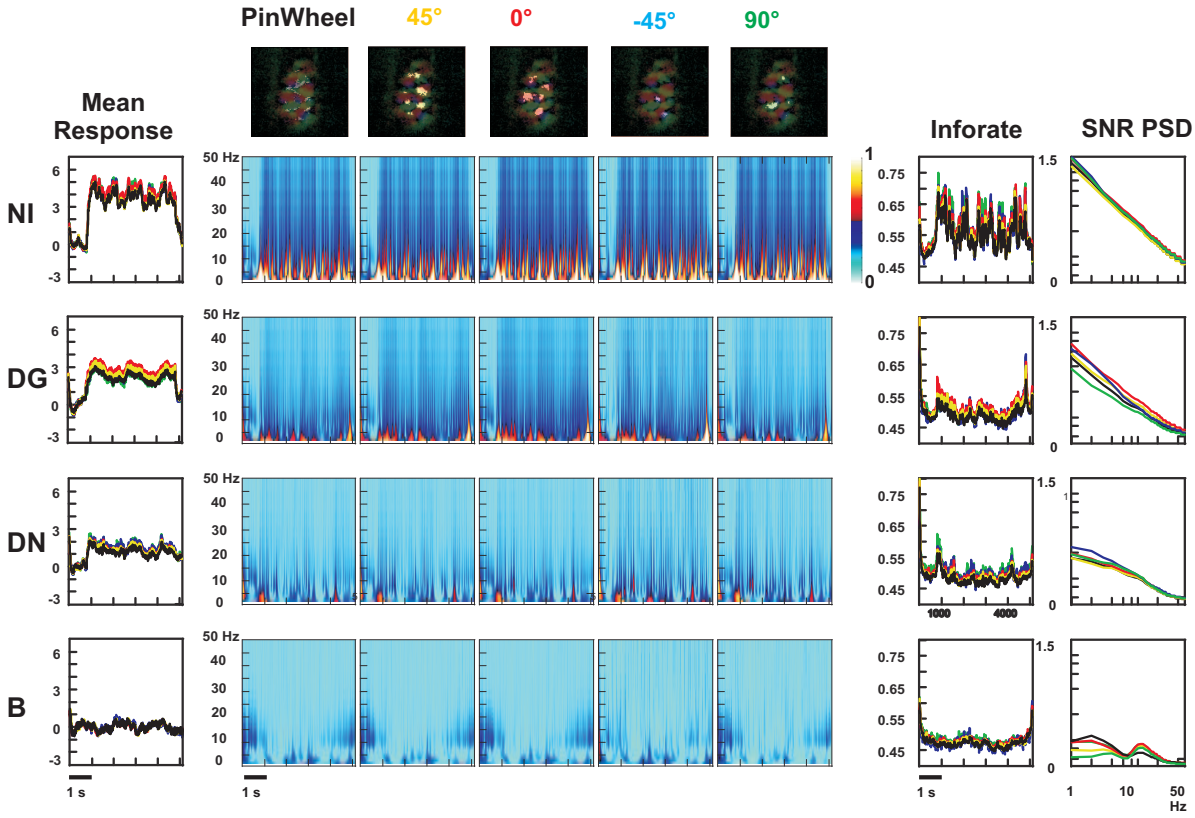

Figure 8.3 – Stimulus dependency of trial-to-trial variability on five functional population groups revealed by stimulus-locked wavelet analysis.

Preliminary results show that the SNR increases with ecological relevance of stimulus statistics, in coherence with the previous studies from our lab (Baudot et al., submitted; Frégnac et al., 2005; Marre et al., 2009; El Boustani et al., 2009). Signal-to-Noise Ratio was higher for natural image responses, creating an almost homogeneous response on each orientation-selective group. Drifting gratings evoked strong SNR on the pixels that prefer the orientation of the grating, with a decreasing SNR as a function of orientation preference on the rest of the map. Peak of the SNR was at the onset and offset of evoked responses. Dense noise resulted in lower SNR than natural image and drifting grating responses in low frequencies.

8.3 PCA on Natural Image Response

We applied PCA on the concatenation of 20 trials of natural image responses in order to extract uncorrelated spatiotemporal patterns that are involved in coding of natural images.

As it was the case for drifting gratings, the first component corresponded to the global activation of the cortex. This principal component corresponded to the main fluctuations of the membrane potential observed on all the cortex. Unlike drifting gratings, natural image responses could be separated into a number of local patches (for example, components 11 and 12 in Figure 8.4). As a result of these functional components, dimensionality of the signal was very high.

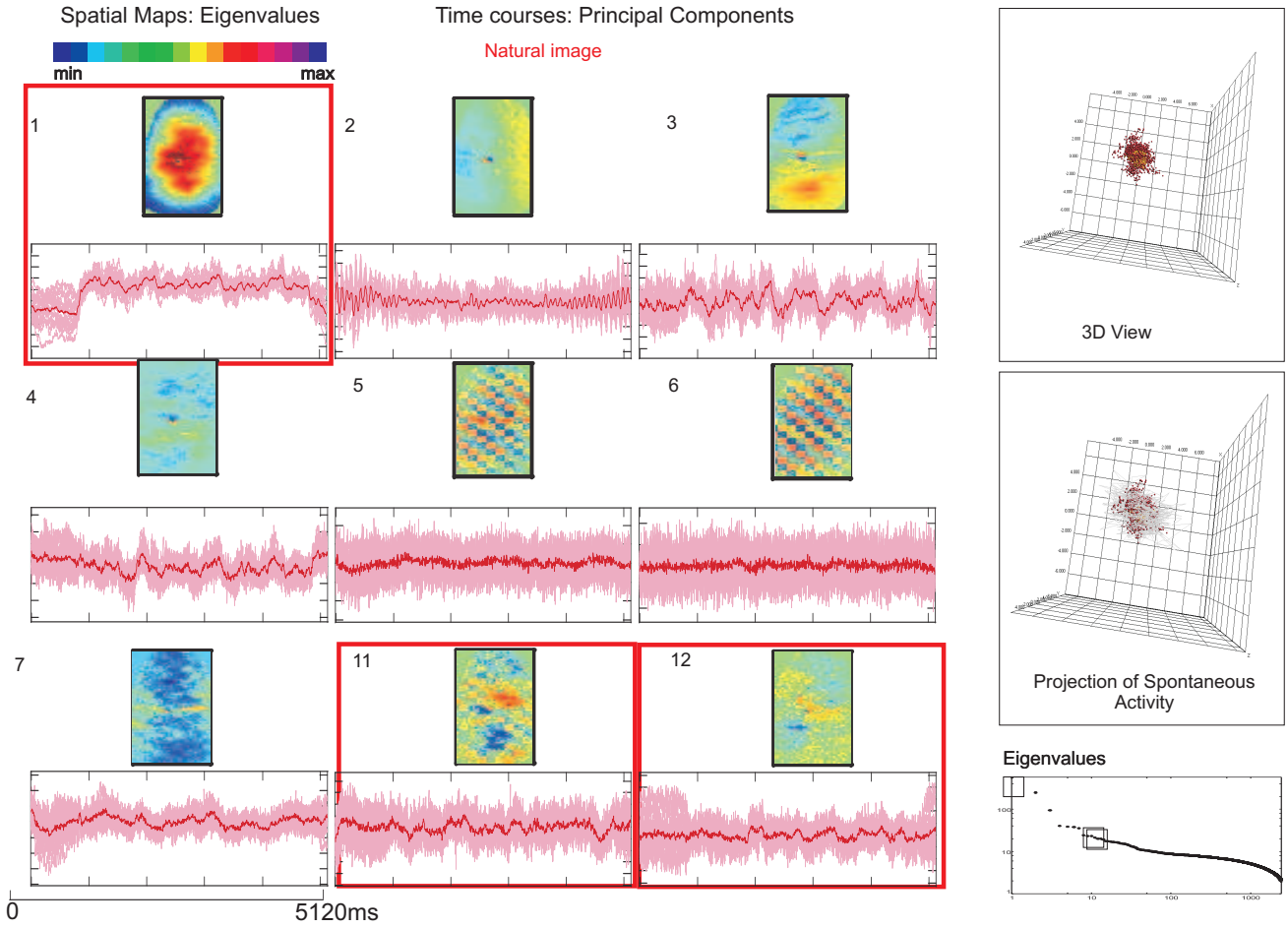

Figure 8.4 – PCA on concatenation of trials of natural image responses.

8.4 Discussion

Long recordings are much more complex than the short ones, partially as a result of some possible nonlinear interactions that occur in this time scale. Blood volume

change is difficult to be estimated a priori; therefore this metabolic change is not included in the model. Horizontal stripes on the GLM response map in Figure 8.1D are aligned with blood vessels, showing that the model could not completely separate the vessels from the neural response. In addition to these problems, second step PCA with blank correlation for artefact detection would not work in this case because the intrinsic response related signal is not present in the blank response. More sophisticated tools are needed to compare membrane potential related signal, intrinsic signal, and artefacts.

Another problem for GLM on long recordings is the neural response being more complex than short duration simple stimulus. Especially in case of natural images, modeling the neural response as a simple step function underestimates the contribution of the fluctuations created by the changes in the subthreshold membrane potential to the signal. Estimation of source vectors by analysis of local luminance and contrast of the visual stimulus can be useful for a more realistic modeling of the neuronal responses. Another possibility may be to use response signals deduced from LFP recordings with appropriate methods.

Stimulus locked time-frequency analysis revealed that the signal to noise ratio of neuronal responses increases with stimulus complexity, in coherence with earlier intracellular studies (Baudot et al., submitted) . In addition, we could study the signal to noise ratio as a function of orientation preference. We observed that animated natural image stimulation evoked high SNR on all the map including pinwheels, while horizontal drifting grating evoked maximum SNR on regions that prefer horizontal orientation and minimum on vertical-selective regions and pinwheels. In any case, SNR of natural image response was higher than SNR of drifting grating response on all regions. These results show that on low frequencies trial-to-trial variability in population responses share the same stimulus dependent profiles as intracellular recordings.

PCA on denoised natural image responses revealed that the dimensionality of this signal is much higher than the short drifting grating responses, as it was suggested by Onat et al. (2011a). On the other hand, contrary to the observations of Onat et al. (2011a), we observed the excitation levels in response to animated natural images to be higher than drifting grating responses. This is probably a consequence of the differences between the natural images sequences that are used in the studies. We used a single image animated with artificial eye movements with 1/f statistics both in space and time, while they used natural images recorded by a camera that is head-fixed to the freely moving cats in the forest. This type of stimulation discards the importance of the eye movements, resulting in a relatively static recording of the environment. Moreover, with a closer look to their Figure 2 we can see that the natural image response starts to be as strong as the drifting grating response

when low spatial frequency features appear and move in the visual scene. Another important reason may be that in our case natural image animation evoked activity on a wide region on the cortex, while drifting gratings only activate the regions that are selective to the presented stimulation.

Part IV

Conclusion

In this thesis, we claimed that statistical source separation methods can be applied to VSD imaging data both for denoising of recordings from unwanted sources, and for extraction of functional patterns of activity. We investigated application of data-driven and model-based strategies to VSD imaging data. We developed a hybrid denoising method that could successfully clean the neural-related response from the artefacts better than only a data-driven or model-based method alone. Following the hybrid denoising, we performed data-driven source separation analysis which revealed that the neuronal populations in response to full field drifting gratings are statistically separable as a function of their stimulus preference. We then introduced a strategy to denoise longer recordings which involve intrinsic response and more complicated heartbeat dynamics. This denoising strategy let us analyze data obtained by the protocol that involves 4 second long responses to animated natural images, drifting gratings, dense noise and blank. Preliminary analysis showed that the trial-to-trial variability as a function of stimulus complexity is comparable to the results obtained in in-vivo intracellular recordings in low frequencies, while high frequency reliability is lost in VSD recordings. Reliability of the drifting gratings depended on the orientation preference of the pixels, resulting in a higher SNR on the regions that prefer the presented stimulus. PCA on natural images resulted in higher dimensionality and weaker space-time separability than drifting gratings. These results provide information about certain limits of linear source separation on VSD recordings.

Comparison of denoising methods

As we indicated in Chapter 6, appropriateness of a certain source separation strategy depends strictly on the nature of the signal of interest and the prior knowledge about the signal sources.

We observed that data-driven denoising with PCA and ICA on raw data could not distinguish evoked neural response from the artefacts. The main problem was the bleaching being strongly correlated to the nonselective neuronal activity. PCA after removal of bleaching by a double exponential fit could not distinguish the heartbeat and heart pulsation noise from the neuronal response. In any case, number of significant components was always very high, which makes it impossible to decrease the dimensionality of the responses, which is a necessary step to perform ICA.

A reason why ICA on VSD recordings does not work as good as it does on fMRI recordings is the simultaneous presence of signals and artefacts at the same regions VSD recordings, in contrast to fMRI recordings. Another major problem for PCA and ICA was the bleaching having a very dominant contribution to the observed

mixture. As a result of this, PCA would first extract the bleaching component and then search for other orthogonal vectors that may not explicitly represent neuronal response.

Another reason for why PCA and ICA does not provide good source separation may be that the signal sources are not really statistically independent, as the microvasculature is spatially organized to support neurons, and dye diffusion is correlated with the areas that include neural cells. Indeed, the heart pulsation signal which occurs at higher harmonics of the heartbeat frequency could not be separated from the neuronal response completely. Hence, this signal does not seem to be independent or uncorrelated of the neuronal response in the sense that is taken into account by blind source separation.

PCA orders the principal components with respect to their energy. Often, first components represent most of the variance expressed in the data; therefore it is convenient to discard components which have lower energy. This provides a compression of the data by decreasing the dimensionality to the number of first significant components. When we consider the total energy expressed in the recordings, PCA on VSD imaging data both for denoising and population analysis aspects resulted in a very high number of components. The first cut-off for the eigenvalues was observed just after the orientation selective and retinotopic components (3-5 components). These components corresponded to less than 30% of the total variance. For the following components, even though a spatio-temporal structure remained in the principal components, there was no obvious cut-off. Nevertheless, even though the energy decreased very slowly, we observed that the spatial and temporal structure starts to be meaningless after a few hundred components. This rich nature of the signal is partially a result of the complexity of the neuronal responses. It is also a consequence of the noisy nature of the VSD imaging signal.

GLM provided better means for signal denoising than PCA and ICA on our data. While doing VSD imaging on anesthetized and paralyzed cat, prior information about the most important artefacts such as heart beat and bleaching can be obtained by additional measures. This facilitates the application of GLM on VSD data. Even though GLM was successful up to a point, there were still some components that could not be clearly distinguished. To remedy this problem, we developed a method that benefits the advantages of both method-based and data-driven strategies. Addition of a second step of denoising that uses a data-driven approach provided an acceptable denoising by extracting the stimulus dependent response from the rest of the sources. We are also currently collaborating with Hugo Raguet and Gabriel Peyré for development of a more flexible GLM algorithm that would also take into account spatial correlations between sources.

Hybrid model for denoising of VSD Imaging data

The first aim of our work was to develop an appropriate denoising approach that would permit single-trial analysis. We tried both data-driven (PCA and ICA) and model-based (GLM) approaches. GLM provided a successful denoising at the first step, but it could not separate fully the neural-related signal from the artefacts. Having prior information about the nature of the most of the artefacts permitted us to define an appropriate regressor base. However, it is not easy to predict the exact profile of the neural response in time. This was the limiting factor for the GLM method. Nevertheless, we were able to detect the components that could not be extracted by GLM by applying PCA on all dataset in order to detect common spatiotemporal patterns among all trials of all stimulation and no-stimulation conditions. This provided a compromise between using blank or cocktail-blank control conditions. While comparison of the activity to blank condition would reveal any neural 'responsibility', comparison to cocktail blank would reveal rather 'selectivity' of the neural responses. Indeed, PCA could reveal one major component that reveals responsive but not selective neural activity pattern, while the following components were stimulus selective.

Data-driven and model-based approaches are based on different and complementary hypothesis about the nature of the mixture that is measured by the observer. Hybrid models are shown to be more successful than using only one approach alone in fMRI and intrinsic imaging recordings (McKeown, 2000; Zheng et al., 2001; Calhoun et al., 2005; Hu et al., 2005). By combining carefully these two approaches, one can avoid the disadvantages of claiming strong hypothesis about the nature of individual sources or their mixtures.

Doing PCA and ICA after GLM denoising can be considered as a hybrid method, as we use both data-driven and model-based approaches at the end. By using both methods, we minimize disadvantages of using either only data-driven or model-based methods. Furthermore, even if GLM provides better decomposition, the fact that in GLM we only introduce less than 20 components, number of significant components revealed by PCA was always higher and therefore the decomposition made by GLM is very rough and does not take into account the rich nature of the VSD Imaging data.

Development of source separation strategies are heavily influenced by the way the brain solves the cocktail party problem. Development of ICA was initiated by the discussion about how the simple cells code sparse representations of the world (Barlow, 1995). Researchers then searched for algorithms that would separate sparse representations observed in a mixture. Indeed, ICA algorithms that use higher order statistics are accepted to solve the cocktail party problem efficiently

(Comon, 1994; Bell and Sejnowski, 1997, 1995). A recent fMRI study showed that the brain solves the source separation problem by using both data-driven and model-based approaches in parallel in decision making (Daw et al., 2011). Understanding these mechanisms and development of parallel hybrid models with knowledge from neuroscience could provide a more realistic approach for source separation. Reciprocally, development of hybrid methods inspired by the brain would be useful in increasing the efficiency of the biologically inspired artificial systems for solving pattern recognition and decision making problems.

Dynamics of stimulus-driven responses in V1 in a low dimensional space

There are several advantages of using source separation methods that provide dimensionality reduction of visual cortical dynamics revealed by VSD imaging.

First of all, VSD imaging provides simultaneous recording of thousands of neurons on the superficial layers of the cortex, providing good means for investigating the cooperative behavior arising from the lateral connectivity linking neural populations. Thanks to the modular organization of the primary visual cortex, neurons that share common statistics are clustered together on the cortical sheet. This organization provides emergence of smooth spatial representations, which can then be extracted by source separation.

Our second advantage was the use of drifting grating protocol which evoked different profiles of selectivity by providing a complete basis of neural response patterns. Classification of neuronal populations by this method would permit studying more complicated neural dynamics such as natural image responses, waves of activity evoked by spatially localized visual stimulations as well as the spontaneous activity.

PCA on denoised recordings revealed spatio-temporal dynamics of orientation selective stimulus-driven responses. Extraction of spatio-temporal patterns that correspond to each orientation indicates space-time separability of orientation selective responses.

In response to drifting gratings, neural populations converged to corresponding attractor states right after the response offset. This indicates that even though the VSD responses of single pixels have very slow dynamics, stimulus-selective population responses are indeed very fast and efficient. PCA could separate the non-selective activity from the stimulus-selective activity, and permitted to investigate the dynamics of each component one by one. Our results indicate that global pop-

ulation dynamics are more informative about the neuronal dynamics observed on small populations.

Future directions

Previous studies suggested different interplay between stimulus-selective and non-selective components as a function of stimulus size (Sharon and Grinvald, 2002; Sharon et al., 2007; Chavane et al., 2011). Application of our method to data obtained with different sizes of oriented stimulus can help better understanding of the dynamics of orientation selectivity as a function of stimulus size.

It would be interesting to investigate how the cortical network will be activated if the starting point of the response would be different than the point of no-stimulus origin. Attractor-state coding would reveal this kind of activity which may reflect adaptation or stimulus aftereffects. Design of adequate stimulus protocols would permit using this type of analysis in order to investigate these phenomena. This kind of protocols would also reveal whether the ring attractor of orientation selectivity is continuous or not.

A common belief in visual neuroscience is that the evoked activity sums up linearly with the preceding spontaneous activity (Arieli et al., 1996; Azouz and Gray, 1999). Studies that evaluated this correlation usually take the response onset as the reference point for preceding spontaneous activity. Here we showed that in response to drifting gratings, evoked patterns were stimulus selective right at the beginning of the response. Our results indicate that the high correlation observed in the previous studies may be due to a misjudgment of the response onset as a result of the slow amplitude of transient responses. Moreover, Arieli and colleagues conducted their experiments on animals that are deeply anesthetized by pentothal. This anesthetizer is from barbiturate family, which is known for enhancement of inhibition. This may result in a strong transient inhibition right before the excitation, which could evoke a spatio-temporal pattern of inhibitory activity in the cortex. Another important point is the sensitivity of the recordings to artefacts. Presence of an artefact may be considered by mistake as the ongoing activity, which would result in a high correlation of the ongoing and evoked activities. Arieli and colleagues used the red dye which is much more sensitive to heartbeat related artefacts. Our denoising method provides a better cleaning of the data from the unwanted signal contributions; therefore we expect to obtain more coherent results.

We provided an attractor-state coding scheme for orientation and direction selectivity, which are the most prominent features of V1. We showed that direction-selective responses are not separable with PCA, even though different clusters can

be observed for the two directions. Introducing the higher order moments in the analysis by ICA could solve this problem. This is probably a consequence of the orthogonality restriction in PCA. Protocols that permit mapping of direction-selective populations on the cortex independently of orientation selectivity, such as moving dots or motion clouds, could provide independent analysis of direction and orientation selectivity in V1.

Another possibility to investigate stimulus-dependent features would be to search for common components for other combinations. We searched the components that would code for orientation and direction selectivity by searching the common spatiotemporal patterns in response to a full set of stimulus orientations and directions. Onat et al. (2011b) performed PCA on only one stimulus condition, and succeeded to extract retinotopic-related responses to drifting grating, and corresponding orientation-selective responses. Using a single stimulus condition would provide a more detailed decomposition of components that correspond to a stimulus. On the other hand, searching common components in response to a complete set of stimulus helps us to understand how the cortex is organized in order to code for a stimulus feature. It is also possible to compare the cortical organization corresponding to different receptive field properties, as Everson et al. (1998) did for orientation selectivity compared to spatial frequency organization in space. One step further may be to combine all these conditions, and perform PCA on a dataset that contains responses to stimuli that favor multiple receptive field properties. This kind of approach could also reveal the interplay between different selectivity map structures in the cortex.

Finally, projection of non-classical stimulus responses on the ring attractor may help better understanding of how orientation selectivity is involved in neural coding under more complex stimulus scenarios, including natural image responses. Projection of the blank response on the orientation-selective ring attractor would also provide quantification of the occurrence of orientation-selective patterns in spontaneous activity (Kenet et al., 2003; Goldberg et al., 2004).

Bibliography

Abbott, L., Dayan, P., 1999. The effect of correlated variability on the accuracy of a population code. Neural Computation 11 (1), 91–101.

Abeles, M., 1982. Local cortical circuits: An electrophysiological study. Springer-Verlag New York.

Abeles, M., 1991. Corticonics: Neural circuits of the cerebral cortex. Cambridge Univ Pr.

Adams, D., Horton, J., 2003. Capricious expression of cortical columns in the primate brain. Nature neuroscience 6 (2), 113–114.

Albus, K., 1975. A quantitative study of the projection area of the central and the paracentral visual field in area 17 of the cat. Experimental Brain Research 24 (2), 159–179.

Angelucci, A., Bressloff, P., 2006. Contribution of feedforward, lateral and feedback connections to the classical receptive field center and extra-classical receptive field surround of primate v1 neurons. Progress in Brain Research 154, 93–120.

Angelucci, A., Levitt, J., Walton, E., Hupé, J., Bullier, J., Lund, J., 2002. Circuits for local and global signal integration in primary visual cortex. The Journal of Neuroscience 22 (19), 8633–8646.

Angelucci, A., Sainsbury, K., 2006. Contribution of feedforward thalamic afferents and corticogeniculate feedback to the spatial summation area of macaque v1 and lgn. The Journal of comparative neurology 498 (3), 330–351.

Appelle, S., 1972. Perception and discrimination as a function of stimulus orientation: The" oblique effect" in man and animals. Psychological bulletin 78 (4), 266.

Arieli, A., Shoham, D., Hildesheim, R., Grinvald, A., 1995. Coherent spatiotemporal patterns of ongoing activity revealed by real-time optical imaging coupled with

single-unit recording in the cat visual cortex. Journal of Neurophysiology 73 (5), 2072–2093.

Arieli, A., Sterkin, A., Grinvald, A., Aertsen, A., 1996. Dynamics of ongoing activity: explanation of the large variability in evoked cortical responses. Science 273 (5283), 1868–1871.

Atick, J., 1992. Could information theory provide an ecological theory of sensory processing? Network: Computation in neural systems 3 (2), 213–251.

Atick, J., Redlich, A., 1992. What does the retina know about natural scenes? Neural Computation 4 (2), 196–210.

Attneave, F., 1954. Some informational aspects of visual perception. Psychological review 61 (3), 183.

Azouz, R., Gray, C., 1999. Cellular mechanisms contributing to response variability of cortical neurons in vivo. The Journal of neuroscience 19 (6), 2209–2223.

Bacci, A., Huguenard, J., 2006. Enhancement of spike-timing precision by autaptic transmission in neocortical inhibitory interneurons. Neuron 49 (1), 119–130.

Bak, P., Tang, C., Wiesenfeld, K., 1987. Self-organized criticality: An explanation of the 1/f noise. Physical Review Letters 59 (4), 381–384.

Barlow, H., 1961. Possible principles underlying the transformation of sensory messages. Sensory communication, 217–234.

Barlow, H., 1972. Single units and sensation: a neuron doctrine for perceptual psychology. Perception 1 (4), 371–394.

Barlow, H., 1995. The neuron doctrine in perception.

Basole, A., White, L., Fitzpatrick, D., 2003. Mapping multiple features in the population response of visual cortex. Nature 423 (6943), 986–990.

Bassett, D., Gazzaniga, M., 2011. Understanding complexity in the human brain. Trends in cognitive sciences.

Bathellier, B., Van De Ville, D., Blu, T., Unser, M., Carleton, A., 2007. Wavelet-based multi-resolution statistics for optical imaging signals: application to automated detection of odour activated glomeruli in the mouse olfactory bulb. Neuroimage 34 (3), 1020–1035.

Baudot, P., Levy, M., Marre, O., Monier, C., Frégnac, Y., submitted. Animation of natural scene by virtual eye movements evokes high precision and low noise in v1 neurons.

Bednar, J., 2012. Building a mechanistic model of the development and function of the primary visual cortex. Journal of Physiology-Paris.

Beggs, J., Plenz, D., 2003. Neuronal avalanches in neocortical circuits. The Journal of neuroscience 23 (35), 11167–11177.

Bell, A., Sejnowski, T., 1995. An information-maximization approach to blind separation and blind deconvolution. Neural computation 7 (6), 1129–1159.

Bell, A., Sejnowski, T., 1997. The 'independent components' of natural scenes are edge filters. Vision research 37 (23), 3327–3338.

Ben-Yishai, R., Bar-Or, R., Sompolinsky, H., 1995. Theory of orientation tuning in visual cortex. Proceedings of the National Academy of Sciences 92 (9), 3844.

Benucci, A., Frazor, R., Carandini, M., 2007. Standing waves and traveling waves distinguish two circuits in visual cortex. Neuron 55 (1), 103–117.

Berger, T., Borgdorff, A., Crochet, S., Neubauer, F., Lefort, S., Fauvet, B., Ferezou, I., Carleton, A., Lüscher, H., Petersen, C., 2007. Combined voltage and calcium epifluorescence imaging in vitro and in vivo reveals subthreshold and suprathreshold dynamics of mouse barrel cortex. Journal of neurophysiology 97 (5), 3751–3762.

Berkes, P., Orbán, G., Lengyel, M., Fiser, J., 2011. Spontaneous cortical activity reveals hallmarks of an optimal internal model of the environment. Science 331 (6013), 83.

Blasdel, G., 1992a. Differential imaging of ocular dominance and orientation selectivity in monkey striate cortex. The Journal of Neuroscience 12 (8), 3115–3138.

Blasdel, G., 1992b. Orientation selectivity, preference, and continuity in monkey striate cortex. The Journal of Neuroscience 12 (8), 3139–3161.

Blasdel, G., Salama, G., 1986. Voltage-sensitive dyes reveal a modular organization in monkey striate cortex. Nature 321 (6070), 579–585.

Bonhoeffer, T., Grinvald, A., 1991. Iso-orientation domains in cat visual cortex are arranged in pinwheel-like patterns. Nature 353 (6343), 429–431.

Bonhoeffer, T., Grinvald, A., 1993. The layout of iso-orientation domains in area 18 of cat visual cortex: optical imaging reveals a pinwheel-like organization. The Journal of neuroscience 13 (10), 4157–4180.

Bonhoeffer, T., Kim, D., Malonek, D., Shoham, D., Grinvald, A., 1995. Optical imaging of the layout of functional domains in area 17 and across the area 17/18 border in cat visual cortex. European Journal of Neuroscience 7 (9), 1973–1988.

Borg-Graham, L., Monier, C., Fregnac, Y., 1998. Visual input evokes transient and strong shunting inhibition in visual cortical neurons. Nature 393 (6683), 369–372.

Bosking, W., Crowley, J., Fitzpatrick, D., 2002. Spatial coding of position and orientation in primary visual cortex. Nature neuroscience 5 (9), 874–882.

Bosking, W., Zhang, Y., Schofield, B., Fitzpatrick, D., 1997. Orientation selectivity and the arrangement of horizontal connections in tree shrew striate cortex. The Journal of Neuroscience 17 (6), 2112–2127.

Bressloff, P., Cowan, J., 2002a. So (3) symmetry breaking mechanism for orientation and spatial frequency tuning in the visual cortex. Physical review letters 88 (7), 78102.

Bressloff, P., Cowan, J., 2002b. The visual cortex as a crystal. Physica D: Nonlinear Phenomena 173 (3-4), 226–258.

Briggman, K., Abarbanel, H., 2006. From crawling to cognition: analyzing the dynamical interactions among populations of neurons. Current opinion in neurobiology 16 (2), 135–144.

Briggman, K., Abarbanel, H., Kristan Jr, W., 2005. Optical imaging of neuronal populations during decision-making. Science 307 (5711), 896–901.

Bringuier, V., Chavane, F., Glaeser, L., Frégnac, Y., 1999. Horizontal propagation of visual activity in the synaptic integration field of area 17 neurons. Science 283 (5402), 695–699.

Brody, C., Romo, R., Kepecs, A., 2003. Basic mechanisms for graded persistent activity: discrete attractors, continuous attractors, and dynamic representations. Current opinion in neurobiology 13 (2), 204–211.

Broome, B., Jayaraman, V., Laurent, G., 2006. Encoding and decoding of overlapping odor sequences. Neuron 51 (4), 467–482.

Brown, G., Yamada, S., Sejnowski, T., 2001. Independent component analysis at the neural cocktail party. TRENDS in Neurosciences 24 (1), 54–63.

Brunel, N., 2000. Dynamics of networks of randomly connected excitatory and inhibitory spiking neurons. Journal of Physiology-Paris 94 (5-6), 445–463.

Bullinaria, J., 2007. Understanding the emergence of modularity in neural systems. Cognitive science 31 (4), 673–695.

Buxhoeveden, D., Casanova, M., 2002. The minicolumn hypothesis in neuroscience. Brain 125 (5), 935–951.

Buzás, P., Volgushev, M., Eysel, U., Kisvárday, Z., 2003. Independence of visuotopic representation and orientation map in the visual cortex of the cat. European Journal of Neuroscience 18 (4), 957–968.

Buzsáki, G., Anastassiou, C., Koch, C., 2012. The origin of extracellular fields and currentsŮeeg, ecog, lfp and spikes. Nature Reviews Neuroscience 13 (6), 407–420.

Cafaro, J., Rieke, F., 2010. Noise correlations improve response fidelity and stimulus encoding. Nature 468 (7326), 964–967.

Calhoun, V., Adali, T., Hansen, L., Larsen, J., Pekar, J., 2003. Ica of functional mri data: an overview. In: in Proceedings of the International Workshop on Independent Component Analysis and Blind Signal Separation. Citeseer.

Calhoun, V., Adali, T., Stevens, M., Kiehl, K., Pekar, J., 2005. Semi-blind ica of fmri: A method for utilizing hypothesis-derived time courses in a spatial ica analysis. Neuroimage 25 (2), 527–538.

Calvin, W., 1996. The cerebral code: Thinking a thought in the mosaics of the mind. The MIT Press.

Carandini, M., Ferster, D., 2000. Membrane potential and firing rate in cat primary visual cortex. The Journal of Neuroscience 20 (1), 470–484.

Chakraborty, S., Sandberg, A., Greenfield, S., 2007. Differential dynamics of transient neuronal assemblies in visual compared to auditory cortex. Experimental Brain Research 182 (4), 491–498.

Chavane, F., Sharon, D., Jancke, D., Marre, O., Frégnac, Y., Grinvald, A., 2011. Lateral spread of orientation selectivity in v1 is controlled by intracortical cooperativity. Frontiers in Systems Neuroscience 5.

Chemla, S., Chavane, F., 2010a. A biophysical cortical column model to study the multi-component origin of the vsdi signal. NeuroImage 53 (2), 420–438.

Chemla, S., Chavane, F., 2010b. Voltage-sensitive dye imaging: Technique review and models. Journal of Physiology-Paris 104 (1-2), 40–50.

Chen, Y., Geisler, W., Seidemann, E., 2008. Optimal temporal decoding of neural population responses in a reaction-time visual detection task. Journal of neurophysiology 99 (3), 1366–1379.

Chklovskii, D., Koulakov, A., 2000. A wire length minimization approach to ocular dominance patterns in mammalian visual cortex. Physica A: Statistical Mechanics and its Applications 284 (1), 318–334.

Churchland, M., Yu, B., Sahani, M., Shenoy, K., 2007. Techniques for extracting single-trial activity patterns from large-scale neural recordings. Current opinion in neurobiology 17 (5), 609–618.

Churchland, P., Sejnowski, T., 1988. Perspectives on cognitive neuroscience. Science 242 (4879), 741.

Civillico, E., Contreras, D., 2012. Spatiotemporal properties of sensory responses in vivo are strongly dependent on network context. Frontiers in Systems Neuroscience 6.

Clemens, M., ????
URL http://necsi.edu/projects/mclemens/cs_char.gif

Comon, P., 1994. Independent component analysis, a new concept? Signal processing 36 (3), 287–314.

Croner, L., Purpura, K., Kaplan, E., 1993. Response variability in retinal ganglion cells of primates. Proceedings of the National Academy of Sciences 90 (17), 8128–8130.

Dakin, S., Frith, U., 2005. Vagaries of visual perception in autism. Neuron 48 (3), 497–507.

Das, A., Gilbert, C., 1997. Distortions of visuotopic map match orientation singularities in primary visual cortex. Nature 387 (6633), 594–597.

Daw, N., Gershman, S., Seymour, B., Dayan, P., Dolan, R., 2011. Model-based influences on humans' choices and striatal prediction errors. Neuron 69 (6), 1204–1215.

Dean, A., 1981. The variability of discharge of simple cells in the cat striate cortex. Experimental Brain Research 44 (4), 437–440.

DeAngelis, G., Ghose, G., Ohzawa, I., Freeman, R., 1999. Functional microorganization of primary visual cortex: receptive field analysis of nearby neurons. The Journal of Neuroscience 19 (10), 4046–4064.

DeFelipe, J., Alonso-Nanclares, L., Arellano, J., 2002. Microstructure of the neocortex: comparative aspects. Journal of neurocytology 31 (3), 299–316.

DiCarlo, J., Zoccolan, D., Rust, N., 2012. How does the brain solve visual object recognition? Neuron 73 (3), 415–434.

Douglas, R., Martin, K., 2004. Neuronal circuits of the neocortex. Annu. Rev. Neurosci. 27, 419–451.

Durbin, R., Mitchison, G., 1990. A dimension reduction framework for understanding cortical maps. Nature 343 (6259), 644–647.

Ecker, A., Berens, P., Keliris, G., Bethge, M., Logothetis, N., Tolias, A., 2010. Decorrelated neuronal firing in cortical microcircuits. Science 327 (5965), 584–587.

Eggeling, C., Widengren, J., Rigler, R., Seidel, C., 1998. Photobleaching of fluorescent dyes under conditions used for single-molecule detection: Evidence of two-step photolysis. Analytical Chemistry 70 (13), 2651–2659.

El Boustani, S., Marre, O., Béhuret, S., Baudot, P., Yger, P., Bal, T., Destexhe, A., Frégnac, Y., 2009. Network-state modulation of power-law frequency-scaling in visual cortical neurons. PLoS computational biology 5 (9), e1000519.

Eriksson, D., Wunderle, T., Schmidt, K., 2012. Visual cortex combines a stimulus and an error-like signal with a proportion that is dependent on time, space, and stimulus contrast. Frontiers in Systems Neuroscience 6.

Everson, R., Knight, B., Sirovich, L., 1997. Separating spatially distributed response to stimulation from background. i. optical imaging. Biological cybernetics 77 (6), 407–417.

Everson, R., Prashanth, A., Gabbay, M., Knight, B., Sirovich, L., Kaplan, E., 1998. Representation of spatial frequency and orientation in the visual cortex. Proceedings of the National Academy of Sciences 95 (14), 8334.

Fekete, T., Omer, D., Naaman, S., Grinvald, A., 2009. Removal of spatial biological artifacts in functional maps by local similarity minimization. Journal of neuroscience methods 178 (1), 31–39.

Ferezou, I., Bolea, S., Petersen, C., 2006. Visualizing the cortical representation of whisker touch: voltage-sensitive dye imaging in freely moving mice. Neuron 50 (4), 617–629.

Field, D., 1994. What is the goal of sensory coding? Neural computation 6 (4), 559–601.

Field, G., Chichilnisky, E., 2007. Information processing in the primate retina: circuitry and coding. Annu. Rev. Neurosci. 30, 1–30.

Fontanini, A., Katz, D., 2008. Behavioral states, network states, and sensory response variability. Journal of neurophysiology 100 (3), 1160–1168.

Fournier, J., Monier, C., Pananceau, M., Frégnac, Y., 2011. Adaptation of the simple or complex nature of v1 receptive fields to visual statistics. Nature Neuroscience 14 (8), 1053–1060.

Frégnac, Y., Baudot, P., Levy, M., Marre, O., 2005. An intracellular view of time coding and sparseness of cortical representation in v1 neurons during virtual oculomotor exploration of natural scenes. Cosyne (http://www. cosyne. org/program05/main. html).

Frégnac, Y., Blatow, M., Changeux, J., de Felipe, J., Lansner, A., Maass, W., McCormick, D., Michel, C., Monyer, H., Szathmary, E., 2006. Neocortical microcircuits: Ups and downs in cortical computation.

Friston, K., 1997. Transients, metastability, and neuronal dynamics. Neuroimage 5 (2), 164–171.

Friston, K., 1998. Modes or models: a critique on independent component analysis for fmri. Trends Cogn. Sci 2 (10), 373–375.

Friston, K., Kilner, J., Harrison, L., 2006. A free energy principle for the brain. Journal of Physiology-Paris 100 (1-3), 70–87.

Friston, K., Tononi, G., Sporns, O., Edelman, G., 1995. Characterising the complexity of neuronal interactions. Human Brain Mapping 3 (4), 302–314.

Fröhlich, F., McCormick, D., 2010. Endogenous electric fields may guide neocortical network activity. Neuron 67 (1), 129–143.

Frostig, R., Lieke, E., Ts'o, D., Grinvald, A., 1990. Cortical functional architecture and local coupling between neuronal activity and the microcirculation revealed by in vivo high-resolution optical imaging of intrinsic signals. Proceedings of the National Academy of Sciences 87 (16), 6082.

Gabbay, M., Brennan, C., Kaplan, E., Sirovich, L., 2000. A principal components-based method for the detection of neuronal activity maps: application to optical imaging. NeuroImage 11 (4), 313–325.

Galuske, R., Schmidt, K., Goebel, R., Lomber, S., Payne, B., 2002. The role of feedback in shaping neural representations in cat visual cortex. Proceedings of the National Academy of Sciences 99 (26), 17083.

Gavrilyuk, S., Polyutov, S., Jha, P., Rinkevicius, Z., Ågren, H., Gel'Mukhanov, F., 2007. Many-photon dynamics of photobleaching. The Journal of Physical Chemistry A 111 (47), 11961–11975.

Geisler, W., Albrecht, D., 1997. Visual cortex neurons in monkeys and cats: detection, discrimination and identification. Visual neuroscience 14, 897–920.

Gilbert, C., Wiesel, T., 1989. Columnar specificity of intrinsic horizontal and corticocortical connections in cat visual cortex. The Journal of Neuroscience 9 (7), 2432–2442.

Gillespie, D., Lampl, I., Anderson, J., Ferster, D., et al., 2001. Dynamics of the orientation-tuned membrane potential response in cat primary visual cortex. Nature neuroscience 4, 1014–1019.

Goldberg, J., Rokni, U., Sompolinsky, H., 2004. Patterns of ongoing activity and the functional architecture of the primary visual cortex. Neuron 42 (3), 489–500.

Gollisch, T., Meister, M., 2010. Eye smarter than scientists believed: neural computations in circuits of the retina. Neuron 65 (2), 150–164.

Gray, C., 1999. The temporal correlation hypothesis review of visual feature integration: still alive and well. Neuron 24, 31–47.

Gray, C., König, P., Engel, A., Singer, W., 1989. Oscillatory responses in cat visual cortex exhibit inter-columnar synchronization which reflects global stimulus properties. Nature 338 (6213), 334–337.

Gray, C., Singer, W., 1989. Stimulus-specific neuronal oscillations in orientation columns of cat visual cortex. Proceedings of the National Academy of Sciences 86 (5), 1698.

Grinvald, A., 2005. Imaging input and output dynamics of neocortical networks in vivo: exciting times ahead. Proceedings of the National Academy of Sciences of the United States of America 102 (40), 14125.

Grinvald, A., Hildesheim, R., 2004. Vsdi: a new era in functional imaging of cortical dynamics. Nature Reviews Neuroscience 5 (11), 874–885.

Grinvald, A., Lieke, E., Frostig, R., Hildesheim, R., 1994. Cortical point-spread function and long-range lateral interactions revealed by real-time optical imaging of macaque monkey primary visual cortex. The Journal of neuroscience 14 (5), 2545–2568.

Grinvald, A., Shoham, D., Shmuel, A., Glaser, D., Vanzetta, I., Shtoyerman, E., Slovin, H., Wijnbergen, C., Hildesheim, R., Sterkin, A., 1999. In-vivo optical imaging of cortical architecture and dynamics.

Gross, C., 2002. Genealogy of the Ş grandmother cellŤ. The Neuroscientist 8 (5), 512–518.

Gross, C., Rocha-Miranda, C., Bender, D., 1972. Visual properties of neurons in inferotemporal cortex of the macaque. Journal of Neurophysiology 35 (1), 96–111.

Grossberg, S., 1976. Adaptive pattern classification and universal recoding: Ii. feedback, expectation, olfaction, illusions. Biological cybernetics 23 (4), 187–202.

Gupta, A., Wang, Y., Markram, H., 2000. Organizing principles for a diversity of gabaergic interneurons and synapses in the neocortex. Science 287 (5451), 273–278.

Gur, M., Beylin, A., Snodderly, D., 1997. Response variability of neurons in primary visual cortex (v1) of alert monkeys. The Journal of neuroscience 17 (8), 2914–2920.

Gur, M., Snodderly, D., 2006. High response reliability of neurons in primary visual cortex (v1) of alert, trained monkeys. Cerebral Cortex 16 (6), 888–895.

Haider, B., Krause, M., Duque, A., Yu, Y., Touryan, J., Mazer, J., McCormick, D., 2010. Synaptic and network mechanisms of sparse and reliable visual cortical activity during nonclassical receptive field stimulation. Neuron 65 (1), 107–121.

Hammond, P., 1974. Cat retinal ganglion cells: size and shape of receptive field centres. The Journal of Physiology 242 (1), 99.

Han, F., Caporale, N., Dan, Y., 2008. Reverberation of recent visual experience in spontaneous cortical waves. Neuron 60 (2), 321–327.

Harris, C., 1980. Insight or out of sight? two examples of perceptual plasticity in the human adult. Visual coding and adaptability, 95–149.

Harsch, A., Robinson, H., 2000. Postsynaptic variability of firing in rat cortical neurons: the roles of input synchronization and synaptic nmda receptor conductance. The Journal of Neuroscience 20 (16), 6181–6192.

Hebb, D., 1949. The organization of behavior: A neuropsychological approach. NewYork: John Wiley & Sons. Hinton, GE (1989). Deterministic Boltzmann learning performs steepest descent in weightspace. Neural Computation 1, 143–150.

Heggelund, P., Albus, K., 1978. Response variability and orientation discrimination of single cells in striate cortex of cat. Experimental Brain Research 32 (2), 197–211.

Hilgetag, C., O'Neill, M., Young, M., Van Essen, D., Felleman, D., 1996. Indeterminate organization of the visual systemon hierarchies: Response to hilgetag et al. rejoinder: Further commentary: Determinate or indeterminate organization. Science 271 (5250), 776–776.

Hirsch, J., Alonso, J., Reid, R., Martinez, L., 1998. Synaptic integration in striate cortical simple cells. The Journal of neuroscience 18 (22), 9517–9528.

Horton, J., Adams, D., 2005. The cortical column: a structure without a function. Philosophical Transactions of the Royal Society B: Biological Sciences 360 (1456), 837–862.

Hu, D., Yan, L., Liu, Y., Zhou, Z., Friston, K., Tan, C., Wu, D., 2005. Unified spm-ica for fmri analysis. Neuroimage 25 (3), 746–755.

Huang, J., Wang, C., Dreher, B., 2007. The effects of reversible inactivation of postero-temporal visual cortex on neuronal activities in cat's area 17. Brain research 1138, 111–128.

Hubel, D., Wiesel, T., 1959. Receptive fields of single neurones in the cat's striate cortex. The Journal of physiology 148 (3), 574–591.

Hubel, D., Wiesel, T., 1962. Receptive fields, binocular interaction and functional architecture in the cat's visual cortex. The Journal of physiology 160 (1), 106–154.

Hubel, D., Wiesel, T., 1963. Shape and arrangement of columns in cat's striate cortex. The Journal of physiology 165 (3), 559–568.

Hubel, D., Wiesel, T., 1968. Receptive fields and functional architecture of monkey striate cortex. The Journal of physiology 195 (1), 215–243.

Hubel, D., Wiesel, T., 1969. Anatomical demonstration of columns in the monkey striate cortex. Nature 221 (5182), 747.

Hubel, D., Wiesel, T., 1974. Sequence regularity and geometry of orientation columns in the monkey striate cortex. The Journal of comparative neurology 158 (3), 267–293.

Hubel, D., Wiesel, T., 1977. Ferrier lecture: Functional architecture of macaque monkey visual cortex. Proceedings of the Royal Society of London. Series B, Biological Sciences, 1–59.

Hübener, M., Shoham, D., Grinvald, A., Bonhoeffer, T., 1997. Spatial relationships among three columnar systems in cat area 17. The journal of neuroscience 17 (23), 9270–9284.

Hyvarinen, A., 1999. Fast and robust fixed-point algorithms for independent component analysis. Neural Networks, IEEE Transactions on 10 (3), 626–634.

Issa, N., Rosenberg, A., Husson, T., 2008. Models and measurements of functional maps in v1. Journal of neurophysiology 99 (6), 2745–2754.

Issa, N., Trepel, C., Stryker, M., 2000. Spatial frequency maps in cat visual cortex. The Journal of Neuroscience 20 (22), 8504–8514.

Izhikevich, E., 2006. Polychronization: Computation with spikes. Neural computation 18 (2), 245–282.

Jancke, D., Chavane, F., Naaman, S., Grinvald, A., 2004. Imaging cortical correlates of illusion in early visual cortex. Nature 428 (6981), 423–426.

Johnson, R., Burkhalter, A., 1996. Microcircuitry of forward and feedback connections within rat visual cortex. The Journal of comparative neurology 368 (3), 383–398.

Jones, H., Andolina, I., Oakely, N., Murphy, P., Sillito, A., 2000. Spatial summation in lateral geniculate nucleus and visual cortex. Experimental Brain Research 135 (2), 279–284.

Jones, H., Grieve, K., Wang, W., Sillito, A., 2001. Surround suppression in primate v1. Journal of Neurophysiology 86 (4), 2011–2028.

Jones, L., Fontanini, A., Sadacca, B., Miller, P., Katz, D., 2007. Natural stimuli evoke dynamic sequences of states in sensory cortical ensembles. Proceedings of the National Academy of Sciences 104 (47), 18772.

Jung, T., Makeig, S., McKeown, M., Bell, A., Lee, T., Sejnowski, T., 2001. Imaging brain dynamics using independent component analysis. Proceedings of the IEEE 89 (7), 1107–1122.

Kara, P., Reinagel, P., Reid, R., 2000. Low response variability in simultaneously recorded retinal, thalamic, and cortical neurons. Neuron 27 (3), 635–646.

Kelso, J., 1995. Dynamic patterns: The self-organization of brain and behavior. The MIT Press.

Kelso, J., 2012. Multistability and metastability: understanding dynamic coordination in the brain. Philosophical Transactions of the Royal Society B: Biological Sciences 367 (1591), 906–918.

Kenet, T., Bibitchkov, D., Tsodyks, M., Grinvald, A., Arieli, A., 2003. Spontaneously emerging cortical representations of visual attributes. Nature 425 (6961), 954–956.

Kisvarday, Z., Toth, E., Rausch, M., Eysel, U., 1997. Orientation-specific relationship between populations of excitatory and inhibitory lateral connections in the visual cortex of the cat. Cerebral Cortex 7 (7), 605–618.

Koch, C., Laurent, G., 1999. Complexity and the nervous system. Science 284 (5411), 96–98.

Koulakov, A., Chklovskii, D., 2001. Orientation preference patterns in mammalian visual cortex:: A wire length minimization approach. Neuron 29 (2), 519–527.

Kremkow, J., Perrinet, L., Masson, G., Aertsen, A., 2010. Functional consequences of correlated excitatory and inhibitory conductances in cortical networks. Journal of computational neuroscience 28 (3), 579–594.

Kuffler, S., 1953. Discharge patterns and functional organization of mammalian retina. J Neurophysiol 16 (1), 37–68.

Lampl, I., Reichova, I., Ferster, D., 1999. Synchronous membrane potential fluctuations in neurons of the cat visual cortex. Neuron 22 (2), 361–374.

Lee, D., Port, N., Kruse, W., Georgopoulos, A., 1998. Variability and correlated noise in the discharge of neurons in motor and parietal areas of the primate cortex. The Journal of neuroscience 18 (3), 1161–1170.

Lee, T., Mumford, D., 2003. Hierarchical bayesian inference in the visual cortex. JOSA A 20 (7), 1434–1448.

Lengyel, I., Epstein, I., 1991. Modeling of turing structures in the chlorite-iodide-malonic acid-starch reaction system. Science 251 (4994), 650–652.

LeVay, S., Voigt, T., 1990. Retrograde transneuronal transport of wheat-germ agglutinin to the retina from visual cortex in the cat. Experimental Brain Research 82 (1), 67–76.

Leventhal, A., Thompson, K., Liu, D., Zhou, Y., Ault, S., 1995. Concomitant sensitivity to orientation, direction, and color of cells in layers 2, 3, and 4 of monkey striate cortex. The Journal of neuroscience 15 (3), 1808–1818.

Li, B., Peterson, M., Freeman, R., 2003. Oblique effect: A neural basis in the visual cortex. Journal of Neurophysiology 90 (1), 204–217.

Lippert, M., Takagaki, K., Xu, W., Huang, X., Wu, J., 2007. Methods for voltage-sensitive dye imaging of rat cortical activity with high signal-to-noise ratio. Journal of neurophysiology 98 (1), 502–512.

Litvak, V., Sompolinsky, H., Segev, I., Abeles, M., 2003. On the transmission of rate code in long feedforward networks with excitatory–inhibitory balance. The Journal of neuroscience 23 (7), 3006–3015.

Logothetis, N., Wandell, B., 2004. Interpreting the bold signal. Annu. Rev. Physiol. 66, 735–769.

Lorente de No, R., 1938. Architectonics and structure of the cerebral cortex. In: Fulton, J. (Ed.), Physiology of the nervous system. Oxford University Press, pp. 291–330.

Luczak, A., Barthó, P., Harris, K., 2009. Spontaneous events outline the realm of possible sensory responses in neocortical populations. Neuron 62 (3), 413–425.

Maass, W., Natschläger, T., Markram, H., 2002. Real-time computing without stable states: A new framework for neural computation based on perturbations. Neural computation 14 (11), 2531–2560.

Machens, C., Romo, R., Brody, C., 2010. Functional, but not anatomical, separation of 'what' and 'when' in prefrontal cortex. The Journal of Neuroscience 30 (1), 350–360.

Maeda, S., Inagaki, S., Kawaguchi, H., Song, W., 2001. Separation of signal and noise from in vivo optical recording in guinea pigs using independent component analysis. Neuroscience letters 302 (2-3), 137–140.

Mainen, Z., Sejnowski, T., 1995. Reliability of spike timing in neocortical neurons. Science 268 (5216), 1503–1506.

Mainzer, K., 2007. The emergence of mind and brain: an evolutionary, computational, and philosophical approach. Progress in brain research 168, 115–132.

Makeig, S., Debener, S., Onton, J., Delorme, A., 2004. Mining event-related brain dynamics. Trends in cognitive sciences 8 (5), 204–210.

Maldonado, P., Gödecke, I., Gray, C., Bonhoeffer, T., 1997. Orientation selectivity in pinwheel centers in cat striate cortex. Science 276 (5318), 1551.

Malonek, D., Grinvald, A., 1996. Interactions between electrical activity and cortical microcirculation revealed by imaging spectroscopy: implications for functional brain mapping. Science 272 (5261), 551–554.

Mante, V., Carandini, M., 2005. Mapping of stimulus energy in primary visual cortex. Journal of neurophysiology 94 (1), 788–798.

Marre, O., Yger, P., Davison, A., Frégnac, Y., 2009. Reliable recall of spontaneous activity patterns in cortical networks. The Journal of Neuroscience 29 (46), 14596–14606.

Mazor, O., Laurent, G., 2005. Transient dynamics versus fixed points in odor representations by locust antennal lobe projection neurons. Neuron 48 (4), 661–673.

McCormick, D., 1999. Spontaneous activity: Signal or noise? Science 285 (5427), 541–543.

McKeown, M., 2000. Detection of consistently task-related activations in fmri data with hybrid independent component analysis. NeuroImage 11 (1), 24–35.

McKeown, M., Makeig, S., Brown, G., Jung, T., Kindermann, S., Bell, A., Sejnowski, T., 1998. Analysis of fmri data by blind separation into independent spatial components. Human Brain Mapping 6, 160–188.

McLaughlin, D., Shapley, R., Shelley, M., Wielaard, D., 2000. A neuronal network model of macaque primary visual cortex (v1): Orientation selectivity and dynamics in the input layer 4cα. Proceedings of the National Academy of Sciences 97 (14), 8087.

Mennerick, S., Chisari, M., Shu, H., Taylor, A., Vasek, M., Eisenman, L., Zorumski, C., 2010. Diverse voltage-sensitive dyes modulate gabaareceptor function. The Journal of Neuroscience 30 (8), 2871–2879.

Mikkulainen, R., 2005. Computational maps in the visual cortex. Springer Verlag.

Miller, K., Keller, J., Stryker, M., 1989. Ocular dominance column development: Analysis and simulation. Science 245 (4918), 605–615.

Milner, P., 1974. A model for visual shape recognition. Psychological Review 81 (6), 521.

Mioche, L., Singer, W., 1989. Chronic recordings from single sites of kitten striate cortex during experience-dependent modifications of receptive-field properties. Journal of neurophysiology 62 (1), 185–197.

Mishkin, M., Ungerleider, L., Macko, K., 1983. Object vision and spatial vision: Two cortical pathways. Trends in neurosciences 6, 414–417.

Mitra, P., Pesaran, B., 1999. Analysis of dynamic brain imaging data. Biophysical journal 76 (2), 691–708.

Monier, C., Chavane, F., Baudot, P., Graham, L., Frégnac, Y., 2003. Orientation and direction selectivity of synaptic inputs in visual cortical neurons:: A diversity of combinations produces spike tuning. Neuron 37 (4), 663–680.

Monyer, H., Markram, H., 2004. < i> interneuron diversity series</i>: Molecular and genetic tools to study gabaergic interneuron diversity and function. Trends in neurosciences 27 (2), 90–97.

Mountcastle, V., 1957. Modality and topographic properties of single neurons of cat's somatic sensory cortex. j. Neurophysiol 20 (4), 408–434.

Mountcastle, V., 1997. The columnar organization of the neocortex. Brain 120 (4), 701–722.

Movshon, J., Adelson, E., Gizzi, M., Newsome, W., 1985. The analysis of moving visual patterns. Pattern recognition mechanisms 54, 117–151.

Muller, L., Destexhe, A., 2012. Propagating waves in thalamus, cortex and the thalamocortical system: experiments and models. Journal of Physiology-Paris.

Nassi, J., Callaway, E., 2009. Parallel processing strategies of the primate visual system. Nature Reviews Neuroscience 10 (5), 360–372.

Nauhaus, I., Benucci, A., Carandini, M., Ringach, D., 2008. Neuronal selectivity and local map structure in visual cortex. Neuron 57 (5), 673–679.

Obermayer, K., Blasdel, G., 1993. Geometry of orientation and ocular dominance columns in monkey striate cortex. The Journal of neuroscience 13 (10), 4114–4129.

Ohki, K., Chung, S., Ch'ng, Y., Kara, P., Reid, R., 2005. Functional imaging with cellular resolution reveals precise micro-architecture in visual cortex. Nature 433 (7026), 597–603.

Ohki, K., Chung, S., Kara, P., Hübener, M., Bonhoeffer, T., Reid, R., 2006. Highly ordered arrangement of single neurons in orientation pinwheels. Nature 442 (7105), 925–928.

Olshausen, B., Field, D., 2004. Sparse coding of sensory inputs. Current opinion in neurobiology 14 (4), 481–487.

Olshausen, B., Field, D., 2005. How close are we to understanding v1? Neural computation 17 (8), 1665–1699.

Onat, S., K
"onig, P., Jancke, D., 2011a. Natural scene evoked population dynamics across

cat primary visual cortex captured with voltage-sensitive dye imaging. Cerebral Cortex.

Onat, S., Nortmann, N., Rekauzke, S., Konig, P., Jancke, D., 2011b. Independent encoding of grating motion across stationary feature maps in primary visual cortex visualized with voltage-sensitive dye imaging. Neuroimage.

Payne, B., Peters, A., 2002. The concept of cat primary visual cortex. In: Payne, B., Peters, A. (Eds.), The cat primary visual cortex. Academic Press, pp. 1–108.

Peterka, D., Takahashi, H., Yuste, R., 2011. Imaging voltage in neurons. Neuron 69 (1), 9–21.

Petitot, J., 2003. The neurogeometry of pinwheels as a sub-riemannian contact structure. Journal of Physiology-Paris 97 (2-3), 265–309.

Polyak, S., 1941. The retina: the anatomy and the histology of the retina in man, ape, and monkey, including the consideration of visual functions, the history of physiological optics, and the histological laboratory technique.

Poulet, J., Petersen, C., 2008. Internal brain state regulates membrane potential synchrony in barrel cortex of behaving mice. Nature 454 (7206), 881–885.

Prechtl, J., Cohen, L., Pesaran, B., Mitra, P., Kleinfeld, D., 1997. Visual stimuli induce waves of electrical activity in turtle cortex. Proceedings of the National Academy of Sciences 94 (14), 7621.

Quiroga, R., Reddy, L., Kreiman, G., Koch, C., Fried, I., 2005. Invariant visual representation by single neurons in the human brain. Nature 435 (7045), 1102–1107.

Rabinovich, M., Huerta, R., Varona, P., Afraimovich, V., 2008. Transient cognitive dynamics, metastability, and decision making. PLoS computational biology 4 (5), e1000072.

Rakic, P., 1988. Specification of cerebral cortical areas. Science 241 (4862), 170–176.

Reidl, J., Starke, J., Omer, D., Grinvald, A., Spors, H., 2007. Independent component analysis of high-resolution imaging data identifies distinct functional domains. Neuroimage 34 (1), 94–108.

Reynaud, A., Takerkart, S., Masson, G., Chavane, F., 2010. Linear model decomposition for voltage-sensitive dye imaging signals: Application in awake behaving monkey. Neuroimage.

Ringach, D., 2009. Spontaneous and driven cortical activity: implications for computation. Current opinion in neurobiology 19 (4), 439–444.

Ruderman, D., Bialek, W., 1994. Statistics of natural images: Scaling in the woods. Physical Review Letters 73 (6), 814–817.

Rudolph, M., Destexhe, A., 2001. Do neocortical pyramidal neurons display stochastic resonance? Journal of Computational Neuroscience 11, 19–42, 10.1023/A:1011200713411.
URL http://dx.doi.org/10.1023/A:1011200713411

Salinas, E., Sejnowski, T., 2000. Impact of correlated synaptic input on output firing rate and variability in simple neuronal models. The Journal of Neuroscience 20 (16), 6193–6209.

Scannell, J., Blakemore, C., Young, M., 1995. Analysis of connectivity in the cat cerebral cortex. The Journal of Neuroscience 15 (2), 1463–1483.

Scannell, J., Young, M., 2002. Primary visual cortex within the cortico-corticothalamic network. In: Payne, B., Peters, A. (Eds.), The cat primary visual cortex. Academic Press, pp. 609–654.

Schießl, I., Stetter, M., Mayhew, J., McLoughlin, N., Lund, J., Obermayer, K., 2000. Blind signal separation from optical imaging recordings with extended spatial decorrelation. Biomedical Engineering, IEEE Transactions on 47 (5), 573–577.

Schiller, P., Finlay, B., Volman, S., 1976. Short-term response variability of monkey striate neurons. Brain Research 105 (2), 347–349.

Schmidt, K., Goebel, R., Löwel, S., Singer, W., 1997. The perceptual grouping criterion of colinearity is reflected by anisotropies of connections in the primary visual cortex. European Journal of Neuroscience 9 (5), 1083–1089.

Schummers, J., Cronin, B., Wimmer, K., Stimberg, M., Martin, R., Obermayer, K., Koerding, K., Sur, M., 2007. Dynamics of orientation tuning in cat v1 neurons depend on location within layers and orientation maps. Frontiers in neuroscience 1 (1), 145.

Schummers, J., Mariño, J., Sur, M., 2002. Synaptic integration by v1 neurons depends on location within the orientation map. Neuron 36 (5), 969–978.

Schwartz, E., 1977. Spatial mapping in the primate sensory projection: analytic structure and relevance to perception. Biological cybernetics 25 (4), 181–194.

Schwartz, O., Simoncelli, E., 2001. Natural signal statistics and sensory gain control. Nature neuroscience 4 (8), 819–825.

Seriès, P., Lorenceau, J., Frégnac, Y., 2003. The 'silent' surround of v1 receptive fields: theory and experiments. Journal of physiology-Paris 97 (4-6), 453–474.

Shadlen, M., Britten, K., Newsome, W., Movshon, J., 1996. A computational analysis of the relationship between neuronal and behavioral responses to visual motion. The Journal of neuroscience 16 (4), 1486–1510.

Shadlen, M., Newsome, W., 1998. The variable discharge of cortical neurons: implications for connectivity, computation, and information coding. The Journal of Neuroscience 18 (10), 3870–3896.

Sharon, D., Grinvald, A., 2002. Dynamics and constancy in cortical spatiotemporal patterns of orientation processing. Science 295 (5554), 512–515.

Sharon, D., Jancke, D., Chavane, F., Na'aman, S., Grinvald, A., 2007. Cortical response field dynamics in cat visual cortex. Cerebral Cortex 17 (12), 2866–2877.

Shatz, C., Stryker, M., 1988. Prenatal tetrodotoxin infusion blocks segregation of retinogeniculate afferents. Science 242 (4875), 87–89.

Shmuel, A., Grinvald, A., 1996. Functional organization for direction of motion and its relationship to orientation maps in cat area 18. The Journal of Neuroscience 16 (21), 6945–6964.

Shmuel, A., Grinvald, A., 2000. Coexistence of linear zones and pinwheels within orientation maps in cat visual cortex. Proceedings of the National Academy of Sciences 97 (10), 5568.

Shoham, D., Glaser, D., Arieli, A., Kenet, T., Wijnbergen, C., Toledo, Y., Hildesheim, R., Grinvald, A., 1999. Imaging cortical dynamics at high spatial and temporal resolution with novel blue voltage-sensitive dyes. Neuron 24 (4), 791–802.

Shoham, D., Hübener, M., Schulze, S., Grinvald, A., Bonhoeffer, T., 1997. Spatio–temporal frequency domains and their relation to cytochrome oxidase staining in cat visual cortex. Nature 385 (6616), 529–533.

Shtoyerman, E., Arieli, A., Slovin, H., Vanzetta, I., Grinvald, A., 2000. Long-term optical imaging and spectroscopy reveal mechanisms underlying the intrinsic signal and stability of cortical maps in v1 of behaving monkeys. The Journal of Neuroscience 20 (21), 8111–8121.

Sillito, A., 1979. Inhibitory mechanisms influencing complex cell orientation selectivity and their modification at high resting discharge levels. The Journal of physiology 289 (1), 33–53.

Simoncelli, E., Olshausen, B., 2001. Natural image statistics and neural representation. Annual review of neuroscience 24 (1), 1193–1216.

Sirovich, L., 1987. Turbulence and the dynamics of coherent structures. part i: Coherent structures. Quarterly of applied mathematics 45 (3), 561–571.

Sirovich, L., Everson, R., Kaplan, E., Knight, B., O'Brien, E., Orbach, D., 1996. Modeling the functional organization of the visual cortex. Physica D: Nonlinear Phenomena 96 (1-4), 355–366.

Sirovich, L., Kaplan, E., 2002. Analysis methods for optical imaging. In: in: Frostig, RD (Ed.), In Vivo Optical Imaging of Brain Function, CRC Press, Boca Raton, FL. Citeseer.

Sornborger, A., Sailstad, C., Kaplan, E., Sirovich, L., 2003. Spatiotemporal analysis of optical imaging data. Neuroimage 18 (3), 610–621.

Sornborger, A., Yokoo, T., Delorme, A., Sailstad, C., Sirovich, L., 2005. Extraction of the average and differential dynamical response in stimulus-locked experimental data. Journal of neuroscience methods 141 (2), 223–229.

Sporns, O., Kötter, R., 2004. Motifs in brain networks. PLoS Biology 2 (11), e369.

Stetter, M., Schiessl, I., Otto, T., Sengpiel, F., Hübener, M., Bonhoeffer, T., Obermayer, K., 2000. Principal component analysis and blind separation of sources for optical imaging of intrinsic signals. NeuroImage 11 (5), 482–490.

Stone, J., 2002. Independent component analysis: an introduction. Trends in cognitive sciences 6 (2), 59–64.

Stopfer, M., Jayaraman, V., Laurent, G., 2003. Intensity versus identity coding in an olfactory system. Neuron 39 (6), 991–1004.

Stryker, M., Harris, W., 1986. Binocular impulse blockade prevents the formation of ocular dominance columns in cat visual cortex. The Journal of neuroscience 6 (8), 2117–2133.

Sur, M., Leamey, C., 2001. Development and plasticity of cortical areas and networks. Nature Reviews Neuroscience 2 (4), 251–262.

Swindale, N., 1980. A model for the formation of ocular dominance stripes. Proceedings of the Royal Society of London. Series B. Biological Sciences 208 (1171), 243–264.

Swindale, N., 1996. The development of topography in the visual cortex: a review of models. Network: Computation in neural systems 7 (2), 161–247.

Swindale, N., 2000. How many maps are there in visual cortex? Cerebral cortex 10 (7), 633–643.

Swindale, N., Matsubara, J., Cynader, M., 1987. Surface organization of orientation and direction selectivity in cat area 18. The Journal of neuroscience 7 (5), 1414–1427.

Swindale, N., Shoham, D., Grinvald, A., Bonhoeffer, T., Hubener, M., 2000. Visual cortex maps are optimized for uniform coverage. nature neuroscience 3, 822–826.

Swindale, N. V., Grinvald, A., Shmuel, A., 2003. The spatial pattern of response magnitude and selectivity for orientation and direction in cat visual cortex. Cerebral Cortex 13 (3), 225–238.
URL http://cercor.oxfordjournals.org/content/13/3/225.abstract

Tanaka, K., 1983. Cross-correlation analysis of geniculostriate neuronal relationships in cats. Journal of Neurophysiology 49, 1303–1316.

Tanaka, S., Ribot, J., Imamura, K., Tani, T., 2006. Orientation-restricted continuous visual exposure induces marked reorganization of orientation maps in early life. Neuroimage 30 (2), 462–477.

Tolhurst, D., Movshon, J., Dean, A., 1983. The statistical reliability of signals in single neurons in cat and monkey visual cortex. Vision research 23 (8), 775–785.

Tononi, G., Sporns, O., Edelman, G., 1994. A measure for brain complexity: relating functional segregation and integration in the nervous system. Proceedings of the National Academy of Sciences 91 (11), 5033.

Tootell, R., Hamilton, S., Silverman, M., Switkes, E., 1988a. Functional anatomy of macaque striate cortex. i. ocular dominance. The Journal of Neuroscience 8 (5), 1500–1530.

Tootell, R., Silverman, M., De Valois, R., 1981. Spatial frequency columns in primary visual cortex. Science 214 (4522), 813–815.

Tootell, R., Switkes, E., Silverman, M., Hamilton, S., 1988b. Functional anatomy of macaque striate cortex. ii. retinotopic organization. The Journal of Neuroscience 8 (5), 1531–1568.

Troyer, T., Krukowski, A., Priebe, N., Miller, K., 1998. Contrast-invariant orientation tuning in cat visual cortex: thalamocortical input tuning and correlation-based intracortical connectivity. The Journal of Neuroscience 18 (15), 5908–5927.

Truccolo, W., Ding, M., Knuth, K., Nakamura, R., Bressler, S., 2002. Trial-to-trial variability of cortical evoked responses: implications for the analysis of functional connectivity. Clinical Neurophysiology 113 (2), 206–226.

Ts'o, D., Frostig, R., Lieke, E., Grinvald, A., 1990. Functional organization of primate visual cortex revealed by high resolution optical imaging. Science 249 (4967), 417–420.

Tusa, R., Palmer, L., 1980. Retinotopic organization of areas 20 and 21 in the cat. The Journal of comparative neurology 193 (1), 147–164.

Tusa, R., Palmer, L., Rosenquist, A., 1978. The retinotopic organization of area 17 (striate cortex) in the cat. The Journal of comparative neurology 177 (2), 213–235.

Tusa, R., Rosenquist, A., Palmer, L., 1979. Retinotopic organization of areas 18 and 19 in the cat. The Journal of comparative neurology 185 (4), 657–678.

Usrey, W., Reid, R., 1999. Synchronous activity in the visual system. Annual Review of Physiology 61 (1), 435–456.

Vaadia, E., Haalman, I., Abeles, M., Bergman, H., Prut, Y., Slovin, H., Aertsen, A., 1995. Dynamics of neuronal interactions in monkey cortex in relation to behavioural events. Nature 373 (6514), 515–518.

Van Essen, D., Gallant, J., 1994. Neural mechanisms of form and motion processing in the primate visual system. NEURON-CAMBRIDGE MA- 13, 1–1.

van Hateren, J., Ruderman, D., 1998. Independent component analysis of natural image sequences yields spatio-temporal filters similar to simple cells in primary visual cortex. Proceedings of the Royal Society of London. Series B: Biological Sciences 265 (1412), 2315–2320.

van Hateren, J., van der Schaaf, A., 1998. Independent component filters of natural images compared with simple cells in primary visual cortex. Proceedings of the Royal Society of London. Series B: Biological Sciences 265 (1394), 359–366.

Vanzetta, I., Grinvald, A., 1999. Increased cortical oxidative metabolism due to sensory stimulation: implications for functional brain imaging. Science 286 (5444), 1555.

Vinje, W., Gallant, J., 2000. Sparse coding and decorrelation in primary visual cortex during natural vision. Science 287 (5456), 1273–1276.

Vogels, R., Spileers, W., Orban, G., 1989. The response variability of striate cortical neurons in the behaving monkey. Experimental Brain Research 77 (2), 432–436.

Vogels, T., Rajan, K., Abbott, L., 2005. Neural network dynamics. Annu. Rev. Neurosci. 28, 357–376.

Von Der Malsburg, C., 1981. The correlation theory of brain function. Internal Report 81-2Reprinted in Models of Neural Networks II, edited by E. Domany, J.L. van Hemmen, and K. Schulten (Springer, Berlin, 1994) Ch. 2, pp.95–119.

Wang, C., Huang, J., Bardy, C., FitzGibbon, T., Dreher, B., 2010. Influence of 'feedback' signals on spatial integration in receptive fields of cat area 17 neurons. Brain research 1328, 34–48.

Wang, C., Waleszczyk, W., Burke, W., Dreher, B., 2000. Modulatory influence of feedback projections from area 21a on neuronal activities in striate cortex of the cat. Cerebral Cortex 10 (12), 1217–1232.

Wang, X., Wei, Y., Vaingankar, V., Wang, Q., Koepsell, K., Sommer, F., Hirsch, J., 2007. Feedforward excitation and inhibition evoke dual modes of firing in the cat's visual thalamus during naturalistic viewing. Neuron 55 (3), 465–478.

Wang, Z., Roe, A., 2011. Columnar specificity of microvascular oxygenation and blood flow response in primary visual cortex: evaluation by local field potential and spiking activity. Journal of Cerebral Blood Flow & Metabolism.

Wehr, M., Laurent, G., 1996. Odour encoding by temporal sequences of firing in oscillating neural assemblies. Nature 384 (6605), 162–166.

Weliky, M., Bosking, W., Fitzpatrick, D., 1996. A systematic map of direction preference in primary visual cortex. Nature 379, 725–728.

Wiesenfeld, K., Moss, F., 1995. Stochastic resonance and the benefits of noise: from ice ages to crayfish and squids. Nature 373 (6509), 33–36.

Wolf, F., Geisel, T., 2003. Universality in visual cortical pattern formation. Journal of Physiology-Paris 97 (2-3), 253–264.

Woolrich, M., Behrens, T., Smith, S., 2004. Constrained linear basis sets for hrf modelling using variational bayes. NeuroImage 21 (4), 1748–1761.

Yabuta, N., Callaway, E., 1998. Cytochrome-oxidase blobs and intrinsic horizontal connections of layer 2/3 pyramidal neurons in primate v1. Visual neuroscience 15 (6), 1007–1027.

Yokoo, T., Knight, B., Sirovich, L., 2001. An optimization approach to signal extraction from noisy multivariate data. Neuroimage 14 (6), 1309–1326.

Yoshioka, T., Blasdel, G., Levitt, J., Lund, J., 1996. Relation between patterns of intrinsic lateral connectivity, ocular dominance, and cytochrome oxidase-reactive regions in macaque monkey striate cortex. Cerebral Cortex 6 (2), 297–310.

Yu, B., Cunningham, J., Santhanam, G., Ryu, S., Shenoy, K., Sahani, M., 2009. Gaussian-process factor analysis for low-dimensional single-trial analysis of neural population activity. Journal of neurophysiology 102 (1), 614–635.

Zhang, J., Rosenberg, A., Mallik, A., Husson, T., Issa, N., 2007. The representation of complex images in spatial frequency domains of primary visual cortex. The Journal of Neuroscience 27 (35), 9310–9318.

Zheng, D., LaMantia, A., Purves, D., 1991. Specialized vascularization of the primate visual cortex. The Journal of neuroscience 11 (8), 2622–2629.

Zheng, Y., Johnston, D., Berwick, J., Mayhew, J., 2001. Signal source separation in the analysis of neural activity in brain. NeuroImage 13 (3), 447–458.

Zohary, E., Shadlen, M., Newsome, W., 1994. Correlated neuronal discharge rate and its implications for psychophysical performance. Nature 370 (6485), 140–143.